SAPIENZA
UNIVERSITÀ DI ROMA

Control Methods for Safe and Efficient Cyber-Physical Systems

Faculty of Information Engineering, Informatics, and Statistics (I3S)
Department of Computer, Control, and Management Engineering Antonio Ruberti (DIAG)
Doctor of Philosophy in Automatica, Bioengineering and Operations Research, XXXII Cycle

Alessandro Giuseppi
Student ID: 1456856

Supervisor
Prof. Francesco Delli Priscoli

A.A. 2019-2020

Remember to look up at the stars
and not down at your feet.
Try to make sense of what you see
and wonder about what makes the
universe exist.
Be curious.
And however difficult life may seem,
there is always something you can do
and succeed at. It matters that you
don't just give up.

Stephen Hawkings, 2012

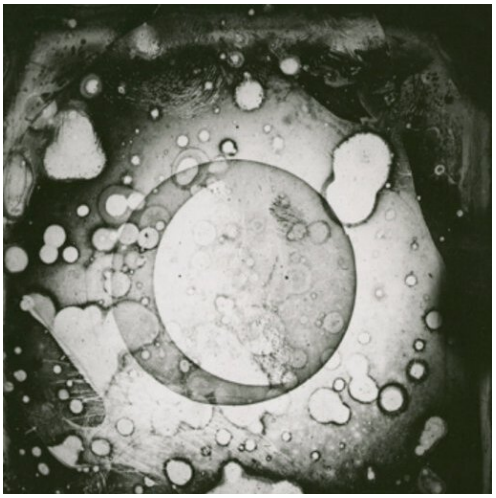

First photo of the Moon, John W. Draper, 1840

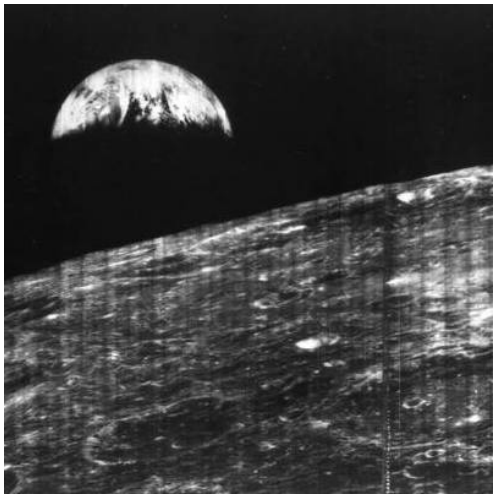

First view of Earth from a spacecraft orbiting the Moon, Lunar Orbiter I - NASA, 1966

First human-made photo on the Moon, Neil Armstrong - Apollo 11 - NASA, 1969

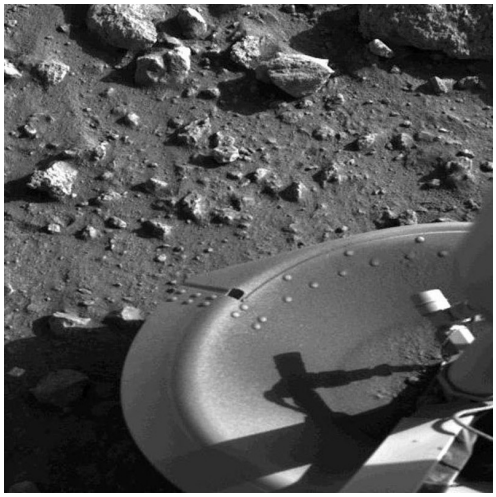

First photo on the surface of Mars, Viking 1 - NASA, 1976

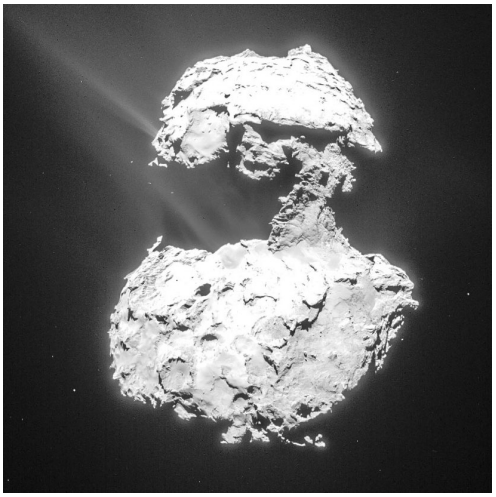

Comet Churyumov–Gerasimenko, Rosetta Spacecraft - ESA, 2015

First image of a Black Hole, Event Horizon Telescope, 2019

Acknowledgements

(intentionally left blank for the review process)

Abstract

The present manuscript represents a report of the main research activities done by the candidate during the three years of his PhD cursus studiorum.

The work revolves around the concept of Cyber-Physical Systems (CPS), a class of systems in which the interaction between their digital domain, constituted by connected devices capable of computing, and a physical process plays a fundamental role in their operation. The deep linkage between the cyber and the physical parts of a CPS makes their study appealing for several research fields as Automation and Computer Science, as properties such as stability and robustness are paired with concepts as information integrity and service availability.

Due to their very broad definition, CPS are studied and applied in the most heterogeneous domains, spacing from power systems and smart factories to healthcare and autonomous vehicles. The present work explores a total of four case studies that the candidate analysed during his PhD studies, covering energy & power management system, spacecraft control and selfish routing over dynamical networks.

The typical goal of a control system designed for a CPS is the one of attaining the desired, *optimal*, behaviour in the most *efficient* way possible, while also constraining the system evolution into a region considered to be *safe* for the system itself and the environment around it. This simple idea is behind the development of the first work presented, which was carried out by the candidate in the scope of the research project H2020 ATENA (regarding Critical Infrastructure Protection). The work develops a control solution for the Risk-Aware and Efficient operation of the Power Distribution Network, exploiting the presence of innovative devices as Electrical Storage Systems. In this application scenario, the candidate designed an Economic Model Predictive Controller (EMPC) for the purpose of increasing the resiliency of the service provision, by automatically reconfiguring the power network in response to, predicted or ongoing, adverse events, as malicious attacks or faults. The specifics of the case study were

refined during the project thanks to the continuous interaction with the Israel Electric Company (IEC), principal industrial end user of ATENA.

A more user-centric approach is taken for the development of the second controller proposed in this work, as it was designed to manage the heating and power appliances of a smart building, integrating also features as electric vehicles charging and demand side management capabilities. The methodology chosen for this second controller was still EMPC, as it offered the possibility of explicitly consider operational and logical constraints imposed by the specific case study, while also exploiting short-term prediction of the exogenous signals interacting with the system.

The third example of CPS studied by the candidate in this work was a multi-body satellite system. Thanks to a collaboration opportunity with the manufacturer Thales Alenia Space Italia, a real case study of interest for the company was analysed, leading to the development of a control scheme for a life-support system that could connect to orbiting satellites to extend their operative life and upgrade their capabilities. The control scheme developed is based on feedback linearization, under which it was proven that the two interconnected spacecraft may operate in parallel without requiring communication or information exchanges. The life-support is in fact able to remove its effects on the original satellite dynamics by applying a compensating control action that reconstructs the original system behaviour.

The fourth, and final, study presented was completed in the scope of the H2020 EU-Korea Project 5G-ALLSTAR (regarding the integration of satellite communications and 5G) and deals with the problem of selfish routing and load balancing in heterogeneous networks, to enable 5G Multi-Connectivity. The network studied was modeled as a discrete-time dynamical system, and the proposed control law was proven by Lyapunov arguments to drive the system state into an equilibrium condition that represents an approximation of the Wardrop user equilibrium. The limited availability of network resources was explicitly included in the control design, and the optimality of their usage was obtained in adversarial terms, as the various information flows compete with each other to maximise their connection performances.

All the researches included in this work covered different aspects and problems that arise when controlling a CPS. The common aspect that is shared among the four controllers is their focus on the safety and resiliency of the controlled systems, and the optimal usage of the limited available resources, in order to assure efficient and safe system operation and service provision.
In the first two researches this aspect is clear, since the optimal exploitation of the

available resources (energy) was obtained by a centralised controller capable of predictive optimisation, and it is worth noting that the adversarial load balancing considered in the fourth case study still leads the network in a state in which all of its users cannot utilise better the available resources without cooperating. Even if paying the so-called Price of Anarchy, the load balancing attained can still improve the connection resiliency by enabling Multi-Connectivity (i.e., the routing of a single information flow over multiple paths), a core feature of 5G.
Furthermore, the direct improvement of spacecraft resiliency brought by life-support systems as the one discussed in this work (in principle capable even of reactivating a non-operative satellite), is paired with the optimal usage of the limited actuating capabilities typical of spacecrafts, potentially lowering significantly space missions cost.

The control methods utilised in this work are taken from different fields of Control Theory, mostly due to the fact that the problems studied were defined starting from applied research projects characterised by very heterogeneous requirements and goals. The rationale behind the choice of the various methodologies utilised is justified for each controller, and the tailoring of their characteristics to the specific applications is discussed in depth in their corresponding chapters.

Table of contents

List of figures

List of tables

Chapter 1

General Introduction

This section introduces the concept of Cyber-Physical Systems and reports the rationale, contribution and structure of the thesis.

1.1 Cyber-Physical Systems

The first definition of Cyber-Physical Systems (CPS) was introduced during the 2006 National Science Foundation Workshop "Beyond SCADA: Networked Embedded Control for Cyber Physical Systems" [4] and classified CPS as systems in which computing capabilities and devices were strictly integrated with a physical process [5].

The concept of CPS rapidly gathered the attention of the scientific community, as the availability and affordability of distributed computing and sensing capabilities increased exponentially in the following years, thanks to diffusion of the paradigm of Internet of Things (IoT) and technological advancements. This proces eventually led to the integration of the concept of CPS into one of the basis of Industry 4.0 [2], [6].

Today, CPS are seen as systems in which a group of connected computing devices interact, and control, a set of physical processes. Such interaction is typically driven by feedback loops with which the physical processes influence computing and vice-versa. The focus on the connectivity capabilities of the computing devices, among themselves and with the external world, is what differentiates CPS from Embedded Systems and represents also the basis for the flexibility of the functionalities they can provide.
Due to their very broad definition, CPS find application in the most heterogeneous domains, spacing from contexts typical of Control and Automation Engineering, as

manufacturing (e.g., Smart Factories [7]), power systems (e.g., Smart Grids [8], Smart Homes [9]) and aerospace [10], [11] to areas such as healthcare [12], [13] and precision agriculture [14]. The only constant feature that characterises CPS in all of their application domains is the seamless integration of their cyber (i.e. the aspects related to the computing devices) and physical (i.e. the controlled processes) domains, enabler of extremely complex applications.

In fact, in order to correctly design, control or integrate a CPS, an in-depth knowledge of both its cyber and physical sub-systems is a required but not sufficient condition: a CPS shall always be seen as the *intersection* of its cyber and physical components and not their *union* [5], as the interaction between the two leads to phenomena that, if neglected, could compromise the functioning of the system itself.

A critical aspect that characterises CPS is the need of introducing thematics related to Cyber-Security directly into the control system. Other than assuring properties related to the system behaviour, such as stability and efficiency, modern control systems have to provide also features as confidentiality, integrity and system availability. The importance of these aspects comes from the fact that CPS, even when not related to a critical process, commonly utilise large amount of data, that, if maliciously exploited, could compromise the privacy, or even the security, of its source. An illustrative example of such a scenario are modern artificial pancreases, whose functional scheme is reported in Figure 1.1. A connected electronic device (potentially a smartphone) regulates the insulin intake of the patient, starting from the feedback it collects from a set of subcutaneous glucose sensors.

Thanks to the development of the so-called personalised medicine, the most recent solutions for artificial pancreases maintain a historical knowledge base containing the relevant biological signals of the patient. This knowledge base is then analysed, so that the controllers are able to adapt to their users by tuning some of their control parameters or structure. In general, the information discovery that enables the personalisation of the controller may benefit from cloud computing and from the study and correlation of other patient data. It is then evident that the information exchange with the remote servers rises numerous privacy concerns, and hence requires the compliance with strict regulations as the General Data Protection Regulation (GDPR) [15]. Additionally, the integrity of the control logic itself has to be assured, so that not only the injection of malicious control logic is theoretically prevented, but also several fail-safe measures shall be put in place to avoid the consequences of a successful attack on the controller, in the form of unwanted effects on the patients or the device inoperability.

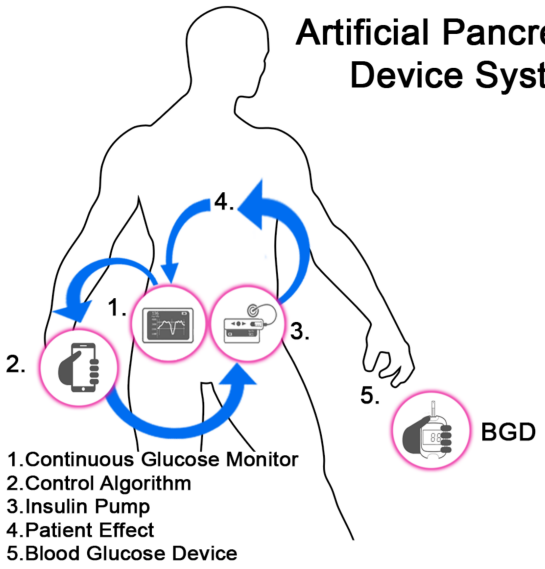

Fig. 1.1 Artificial Pancreas Functional Scheme from [1]

It is evident even in this simplified example that the increase of the complexity of the system benefits the control logic of the artificial pancreas, enabling the usage of more refined techniques particularly suited for the problem, as predictive and adaptive optimal control [16]. Nevertheless, a negative effect that shall not be neglected is that, at the same time, the presence of such powerful computing devices requires the integration of control solutions such as fault / attack / anomaly detection systems [17] and fault tolerant / robust control techniques to safely operate the system.

From a Cyber-Security point of view, the interaction between the cyber and the physical subsystems introduces into both new *vulnerabilities* that may be exploited by external agents to compromise the system or the service it provides. Addressing such vulnerabilities becomes of the utmost importance in applications in which the controlled system involves the safety of humans or is related to a Critical Infrastructure (CI), which is a system considered to be indispensable for the society (e.g., power, water and gas networks, healthcare systems / hospitals, transportation networks, financial markets, ...). It is not surprising then than a significant research effort was spent regarding security assurance and analysis in CPS [18], [19], with the European Union financing in the dedicated H2020 Workprogramme “Secure Societies” numerous research projects.

Other than security, another concept plays a fundamental role in the correct operation of CPS: safety. Even if the distinction between the two terms has been always been

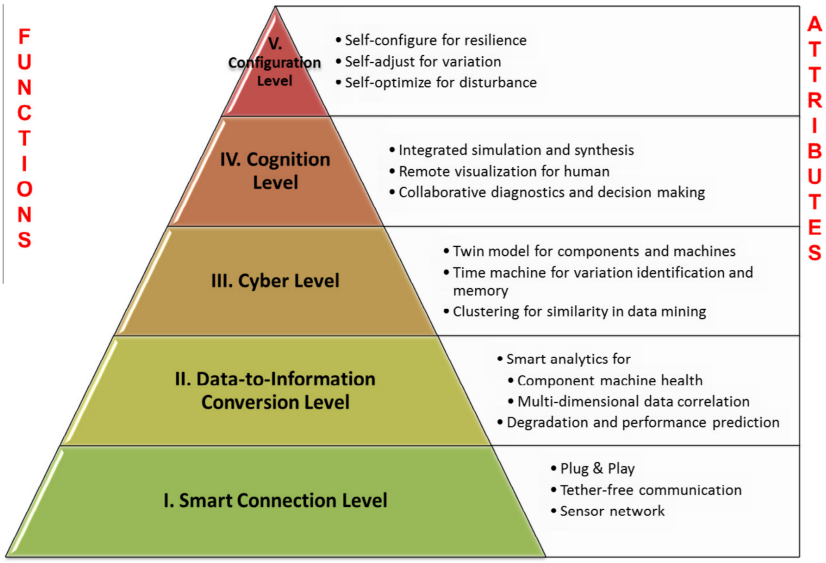

Fig. 1.2 CPS functional archetecture from [2]

a topic of discussion in the scientific community [20], we consider in this work the distinction between the two proposed in [21]:

- **safety** is the inability of the system to affect its environment in an undesirable way;
- **security** is the inability of the environment to affect the system in an undesirable way.

The definition given for security strictly relates it to the concepts of resiliency (i.e., the capability of a system to continuing its operation even after being damaged / losing actuators or sensors) and robustness (i.e., the property of the system to function correctly even in presence of uncertain factors in the design of its controller). On the other hand, safely operating a CPS means controlling it in such a way that the risk associated to a possible failure is minimised, while also containing, or mitigating, the consequences associated to an eventual adverse event. For this reason, Control Methods that directly integrate state and control constraints in their design, such as Model Predictive Control (MPC) [22], have proven to be a fundamental tool to address the challenges of CPS. In particular, the predictive nature at the basis of MPC also allows the system to be operated in a proactive way, meaning that the controller may drive the system along sub-optimal, in terms of performances, trajectories that are considered to be safer.

Ideally, a perfectly designed controller for a CPS would be able to autonomously manage any aspect of the system, and take the adequate decisions to attain the desired objectives in complete autonomy. In reality, in any application in which a critical process is involved, human supervision still plays a fundamental role and the controller assumes the role of a Decision Support System to guide the system operator in compliance with the Human-in-the-Loop paradigm. This aspect, together with several of the above mentioned characterising factors of CPS, has been mapped in the well known architecture of Figure 1.2 taken from [2], that summarises the role and features that CPS are going to have in Industry 4.0 and several other application scenarios in the vision of the authors.

As discussed, CPS are then systems that can be studied in a multi-disciplinary approach, as they present problems and characteristics that connect Information Science fields (as Big Data Analysis, Cyber Security, Intrusion and Anomaly Detection systems, ...) with classic topics of Control Theory (resiliency and robustness, optimal control, predictive operation, ...), making them an adequate topic in which to develop a PhD cursus studiorum.

1.2 Thesis Rationale and Structure

This thesis reports four researches [SJ2], [J2], [J3], [J1] that the candidate had the opportunity to complete over the three years of his PhD studies. Conceptually, the included works deal with various aspects of CPS, investigating the control problem incurred both from a methodological and from an application point of view.

In this regard, the candidate had the opportunity to work in two H2020 research projects founded by the European Union, allowing him to discuss with real industrial end-users their needs and requirements, while also being able to confront and complement his studies with other researchers, with different backgrounds, from internationally renowned Universities and research centres. The candidate carried out these activities as a researcher for the Consortium for the Research in Automation and Telecommunication (CRAT), a no profit research consortium constituted by the University of Rome “La Sapienza”, “Politecnico di Bari”, the University of Sannio and the companies Thales Alenia Space Italia and TopNetwork.

Fig. 1.3 H2020 ATENA, https://cordis.europa.eu/project/rcn/202699/

The first H2020 project in which the candidate participated from the first months of his PhD was **H2020 ATENA** (Advanced Tools to assEss and mitigate the criticality of ICT compoNents and their dependencies over Critical InfrAstructures, GA ID: 700581), a project dedicated to the protection of Critical Infrastructures, seen as CPS. The candidate was deeply involved in all the technical activities of the project, covering all of the three aspects in which the concept of security is often divided: protection, detection and mitigation. The focus of the research activities of the candidate was on the development of risk mitigation strategies for the secure, safe and efficient operation of power networks. This thesis reports one of the principal outputs [J1] of such activities. Nevertheless, of the candidate was also deeply involved in the managerial aspects of the project, as he covered the role of Work Package (WP) Leader for WP3 "Industrial Automation and Control Systems Design for Security" in which he produced the works [SJ5], [C6], [C1] not included in this work for their lower relevance to Control Theory.

Fig. 1.4 H2020 5G-ALLSTAR, https://cordis.europa.eu/project/rcn/217775

The second project in which the candidate participated, from the third year of his PhD, is **H2020 5G-ALLSTAR** (5G AgiLe and fLexible integration of SaTellite And cellulaR, GA ID: 815323) a joint EU-Korea research project that focuses on the integration of satellite-based communications into the 5G framework. In this project, the candidate focused his research in the WP he leads, namely WP4 "Multi Connectivity", studying aspects related to the control of information flows over telecommunication networks, by means of classical load balancing and networked system control methods. Among the algorithms and solutions under study, this thesis reports the most promising one that was recently submitted for publication [SJ2].

The rest of the thesis is structured as follows:

- **Chapter 2** reports a Risk-Aware Control Strategy based on Economic Model Predictive Control for the operation of the power distribution grid in presence of Electrical Storage Systems. This work was carried out in the context of the project H2020 ATENA and is currently in press as:

[J1] *F. Liberati, A. Di Giorgio, A. Giuseppi, A. Pietrabissa, and F. Delli Priscoli, "Efficient and Risk-Aware control of electricity distribution grids," in IEEE System Journal, in press.*

- **Chapter 3** contains a recently concluded study that the candidate investigated in collaboration with the Department of Astronautical, Electrical and Energy Engineering (DIAEE), of the University of Rome "La Sapienza". The work consists in an application of Economic Model Predictive Control to the problem of Electric and Heating Resources Management in Smart Building, modeled utilising Mixed Integer Programming to include the numerous operative constraints considered. The research object of this chapter produced the following publication:

[J3] *F. Liberati, A. Di Giorgio, A. Giuseppi, A. Pietrabissa, E. Habib, and L.Martirano, "Joint model predictive control of electric and heating resources in a smart building,"IEEE Transactions on Industry Applications, 2019.*

- **Chapter 4** covers the results of a research collaboration with the Department of Guidance Navigation & Control Engineering of Thales Alenia Space Italia. The work is related to the design and development of a control scheme to operate a support device to prolong the operational life of orbiting satellites. The proposed scheme is based on feedback linearization and employs the support device to provide additional fault-tolerance and resiliency capabilities to legacy satellites. The associated publication is:

[J2] *Giuseppi, A. Pietrabissa, S. Cilione, and L. Galvagni, "Feedback linearization-based satellite attitude control with a life-support device without communications,"Control Engineering Practice, vol. 90, pp. 221–230, 2019.*

- **Chapter 5** reports a distributed control law for adversarial routing and load balancing in capacitated networks, with application to 5G multi-connectivity scenarios. The proposed control law is proven, by Lyapunov arguments, to steer the system into equilibrium states that are approximated Wardrop Equilibria.

This work was developed in the context of the project H2020 5G-ALLSTAR and led to submission of the paper:

[SJ2] *F. Delli Priscoli, A. Giuseppi, and A. Pietrabissa, "Capacity-constrained Wardrop equilibria and application to multi-connectivity in 5G networks,"in Journal of the Franklin Institute, under review*

- **Chapter 6** draws the overall conclusions of the thesis, summarising also the future works identified in the previous chapters.
- **The Bibliography** Concludes the work and contains the publication list of the candidate and the thesis references.

From a conceptual point of view, chapters 2 and 3 deal with the problem of energy management in two different application scenarios. The selected methodology of Economic Model Predictive Control (EMPC) allows the controlled systems to exploit the knowledge of short term predictions of the exogenous signals that enter in the system (e.g., power generation profiles from distributed renewable sources, heating requests...). Furthermore, EMPC perfectly copes with the natural multi-objective nature that characterise the operation of CPS, allowing the explicit inclusion in the formulation of several different aspects and goals dictated from the specific application. Being CPS extremely complex systems that consider numerous aspects that often go beyond the main physical process (e.g., associated risk level, user satisfaction, security, control efficiency, ...), their "optimal" and "efficient" operation is often related to several different criteria that may, in general, be in conflict. Other than capturing all the objectives and Key Performance Indicators relevant to the system end users, the design process of the two controllers also took into account the specific requirements (derived from safety / security concerns, regulations and operative needs) imposed by the two applications considered. The control developed in the first chapter is heavily linked to the concept of operational risk level and adverse event mitigation, while the one of the second chapter accommodates a broader class of user-specified requests.

Chapter 4, while still dealing with an optimal control problem (optimal spacecraft / satellite attitude tracking and regulation) by proposing two controllers based respectively on Linear Quadratic Regulator (LQR) and MPC, focuses more on resiliency. The aim of the case study was the provision of resiliency capabilities to already orbiting satellites that are approaching the end of their operative life due to the aging of the equipment (actuators and sensors) and fuel depletion. One of the most interesting results of the chapter is the fact that the proposed control scheme does not require

explicit information exchange between the original satellite and the support device that attaches to it, under the hypothesis of controlling the two with feedback linearization-based laws, significantly reducing the complexity and cost of the system while also improving its security by removing a potential vulnerability.

Finally, Chapter 5 considers a complementary aspect of "optimal" and "efficient" operations, being the need of operating certain distributed CPS in an adversarial framework in which various networked agents and systems compete. The scenario considered consists in a capacitated telecommunication network, described as a discrete-time dynamical system, in which various information flows (commodities) decide their routing unilaterally to minimise their own power consumption, up to a situation in which no commodity can improve its routing without the cooperation of the others. The network state to which the proposed control law converges to is in general, less efficient than a system-optimal state, and this performance gap is often referred to as the "Price of Anarchy" [23]. Nevertheless, properly routing information flows, in both cooperative and adversarial scenarios, is a fundamental process for both the security and the efficient operation of CPS that, at the same time, can be seen as a feedback-based operation of a networked system itself.

Chapter 2

Efficient and Risk-aware Control of Electricity Distribution Grids

This chapter contains the reults of the research activites of the candidate in the framework of the H2020 project ATENA related to the Risk-Aware and Efficient operation of power distribution networks. The case study was defined following the requirements and interests of the main end user of the project, the Israel Electric Company (IEC). The work of this chapter led to the production of the recently accepted paper

[J1] *F. Liberati, A. Di Giorgio, A. Giuseppi, A. Pietrabissa, and F. Delli Priscoli, "Efficient and Risk-Aware control of electricity distribution grids," in IEEE System Journal, in press.*

2.1 Dynamic Network Reconfiguration

This work presents an Economic Model Predictive Control (EMPC) algorithm for reducing losses and increasing the resilience of medium voltage electricity distribution grids characterized by high penetration of renewable energy sources and possibly subject to natural or malicious adverse events. The proposed control system optimizes grid operations through network reconfiguration, control of distributed Energy Storage Systems (ESSs) and on-load tap changers. The core of the EMPC algorithm is a non-convex optimization problem integrating the ESSs dynamics, the topological and power technical constraints of the grid and the modelling of the cascading effects

of potential adverse events. An equivalent (i.e., having the same optimal solution) proxy of the non-convex problem is proposed to make the solution more tractable. Simulations performed on a 16-bus test distribution network validate the proposed control strategy.

Nomenclature of the chapter

Indices and Sets	
k	Current time
h	Time index in the control window $h \in [k, k+N-1]$
i, j	Bus indices
$\mathcal{V}^{ESS}$	Set of network nodes hosting ESSs
$\mathcal{V}^{DG}$	Set of network nodes hosting DGs
$\mathcal{V}^{SB}$	Set of HV/MV substations
$\mathcal{A}, \mathcal{V}$	Set of network lines and set of network nodes
Parameters	
B_{ij}, G_{ij}	Susceptance and Conductance of line (i, j)
C_i^{ESS}	Capacity (kWh) of the ESSs at bus i
N	Length of the prediction horizon
r_i,r_{ij}	Risk values associated to bus i and line (i, j)
SOC_i^{ref}	Reference state of charge of the ESS at bus i
S, Z	Auxiliary super source and super sink nodes
T	Sampling period
V_{ij}^{OLTC}	OLTC voltage level at node i for turn ratio j
$\mathbf{x_k}$	Vector gathering the state feedback at time k (current grid topology and ESS SOC)
$\alpha, \beta, \gamma, \delta, \epsilon$	Weight parameters of the objective function
Control Variables	
$a_{ij}(h)$	Connection status of line (i, j) at time h
P_i^{ESS}, Q_i^{ESS}	Active/reactive power of the ESS at bus i
$\mathbf{u_k}$	Vector of the control variables over the control window
δ_{ij}	Boolean variable indicating the OLTC level selected at bus i
σ	Load shedding factor

Other Variables	
$\mathcal{F}$	Target function
C_i	Centrality of node i
$f_{i,j}$	Radiality flux in line (i,j)
$f^c_{i,j}$	Centrality flux in line (i,j)
$I_{i,j}$	Current flowing in line (i,j)
P_i, Q_i	Active/reactive power injected at bus i
P_{ij}, Q_{ij}	Active/reactive power injected into line (i,j)
P_i^{DG}, Q_i^{DG}	Active/reactive power generated by the DG at bus i
P_i^{load}, Q_i^{load}	Active/reactive load at bus i
R_{ij}	Auxiliary variable
SOC_i	State of charge of the ESS at bus i
T_{ij}	Auxiliary variable
u_i	Auxiliary variable
V_i	Voltage magnitude at bus i
θ_i	Voltage angle at bus i
θ_{ij}	$\theta_{ij} = \theta_i - \theta_j$

2.2 Introduction

2.2.1 Background and aim

Electricity distribution networks are cyber-physical systems that work based on the interplay of the physical grid, characterized by its constraints and dynamics, and dedicated information and communication technology (ICT) systems (supervisory control and data acquisition (SCADA), Energy Management System (EMS), etc.). The transition towards distributed generation and electro-mobility is making the operation of the electricity network more complex [24], [25]; at the same time, innovations in the ICT systems potentially introduce new vulnerabilities and raise concerns for cyber security [26]. This work proposes a Model Predictive Control (MPC) strategy for minimizing network losses and the impact of adverse events in Medium Voltage (MV) distribution grids characterized by high Renewable Energy Sources (RES) penetration. This is achieved by coordinating the control of line switches (which allow to reconfigure the topology of the grid), the on-load tap changers (OLTCs) deployed at the level

of high voltage (HV) to MV substations (which enable voltage control), and the distributed electric storage systems (ESSs).

Three main use cases are discussed (see Section 2.3): i) power losses minimization during normal grid operation; ii) risk-aware grid operation, in case information about the operative level of the different subsystems of the grid is available; iii) resilient grid control in case of loss of power at the HV/MV substations (also called primary substations).

2.2.2 Related Works

Though the problem of ensuring an adequate level of security against cyber-physical attacks is relatively recent, the one of efficiently operating the electricity distribution grid has been largely studied in the technical literature, typically considering the computation of *optimal network configurations* minimizing the network power losses. Recent relevant papers dealing with network reconfiguration and at the base of this work are [27]–[35]. In [27] and [28], a network reconfiguration algorithm is presented to minimize power losses in a scenario foreseeing high penetration of distributed generations (DGs). In particular, the authors of [27] present an exact, non convex and non linear formulation of the problem and show how, based on a load-flow technique introduced in [29], the non convex formulation can be turned into an equivalent convex one, easier to be tackled by the available solvers and hence more suitable for online applications, such as the one in this work. A similar convexification procedure presented in [36] is used in [28] for the quadratic relaxation of the reconfiguration problem nonlinearities arising from the power flow equations. In [30] instead, a coordinated control for voltage regulation and network reconfiguration is proposed. The present work extends the contributions in [27],[28] and [30] by introducing the ESS control in combination with the network reconfiguration and OLTC control, and by extending the formulation to the multi-time slot case, utilizing the MPC approach and thus providing predictive capabilities to the control strategy employed.

In [31], the authors jointly consider network reconfiguration and optimal placement and sizing of DGs and capacitors, via an artificial bee colony optimization approach. A similar placement and sizing optimization problem is solved for ESSs and DGs in [37], which proposes yearly reconfiguration to increase the network efficiency and optimally plan upgrading interventions. The minimization of operative costs and power losses is proposed in [37], by defining a stochastic mixed integer linear programming problem

that clusters demand-generation patterns into so-called snapshots. Another recent work that deals with both optimal ESSs placement and efficient network operation is [32], where the authors combine the problem of planning ESSs placement and sizing with an hourly network reconfiguration in order to minimize power losses.

Differentiating from the above works, this work deals with online optimization (every 15 minutes) of network operation, to increase both the efficiency and the resiliency of the network in response to real-time forecasts of load and generation profiles.

Another key reference for the present work is [38], which shows that the network radiality and the connectivity of loads to HV/MV substations - two typical requirements in the operation of distribution grids - can be guaranteed, in passive networks, by combining a topological constraint on the number of active lines with the power flow equations (as explained more in details in Section 2.4). This is however not sufficient to guarantee radiality in active networks, i.e. in networks hosting controllable energy sources, such as ESSs and DGs [39]. A workaround in [38] is to add fictitious loads at the DG nodes, and impose their connection to the substation via additional constraints. The present work extends [38] by introducing a first set of conditions to enforce radiality, and a second set of conditions to capture specific topological properties of the network configuration, such as hop distance from the substation, which allows to model aspects such as cascading effects and interdependencies in the optimization problem. As a result, the proposed control strategy will not give rise to loops in the network and/or islanded configurations during normal operation, unless explicitly allowed via selection of specific control parameters, as explained in Section 2.3.1.

Also heuristic methods have been proposed for network reconfiguration. In [40], the authors employ colored Petri networks to develop a set of reconfiguration rules; in [41], a runner-root algorithm is developed to reduce power losses and balance the loads in the network; in [42], a genetic algorithm is presented to solve the optimal allocation of DGs and the network reconfiguration problem.

Finally, two other relevant works related to the present work are [34] and [35], which propose network reconfiguration to minimize grid losses and optimize grid reliability. Specifically, the latter is achieved via the optimization of network reliability indicators such as the system average interruption duration index (SAIDI) and the system average interruption frequency index (SAIFI) [43], based on the knowledge of grid reliability historical data. The present work extends the approach in [34] to the real-time optimization of network risk, by introducing the reaction to notification alerts coming from a risk predictor system, as explained in Section 2.3, without having to rely on

genetic algorithms or heuristic solutions, while coordinating the reconfiguration with ESS control.

2.2.3 Main Contributions

The main contributions and the distinctive features of this work are:

1. The formulation of a *joint network reconfiguration, ESS and OLTC control problem*, for secure and efficient operation of the grid;
2. The introduction of a *multi-time slot control horizon*, which allows to tackle dynamic scenarios characterized by variable power injections from RES and variable operative levels of network components;
3. The use of the MPC concept, which enables real-time reaction to updates of short-term RES forecasts and notifications of adverse events, while taking into account economic aspects of the network operation and keeping the ESS operation feasible.
4. The application of the method presented in [29] for building a *conified proxy* of the non-convex optimization problem at the basis of MPC, raising from the inclusion of the hybrid power flow equations in the reconfiguration problem;
5. The introduction of a set of *fully topological constraints* to guarantee *network radiality* and avoid network islanding, in networks with distributed generation and ESSs;
6. The integration (in addition to the "classical" power losses minimization terms) of specific terms related to the minimization of the impact arising from malicious/adverse events and/or the degraded operative level of grid components. This establishes a real-time trade-off between the requirement of efficient operation and that of risk minimization (the topological constraints allows to model cascading effects and hence to compute risk metrics associated to the network configuration);
7. The support of grid *islanding* operation in absence of main supply from the transmission network. The characterizing aspect is the efficient use of the ESSs to maximize grid survivability. This is achieved by dynamically changing the net load sustained by the ESSs, through the proper shift of load and distributed generation among network trees via reconfiguration and load shedding.

2.2.4 Chapter Organization

Section 2.3 presents the reference scenario, the addressed use cases and the logic underlying the proposed control system. Section 2.4 details the mathematical formulation of the proposed control problem. Section 2.5 discusses simulation results. Section 2.6 presents conclusions and future research.

2.3 Reference Scenario and Control Logic

2.3.1 Reference Scenario and Use Cases

The reference scenario discussed in this work considers the control of a reconfigurable MV grid equipped with storage and DG units. The controlled elements include: the ESS (to inject/adsorb power for balancing purposes), the OLTC (with effect on voltage control), the switches (for grid topology reconfiguration), sheddable loads (in case of islanding operations). The control system proposed in the following is designed focusing particularly on the following use cases.

Minimization of Power Losses against RES fluctuations

This is the base use case aimed at mitigating the impact of time-varying and potentially volatile generation and consumption patterns on the grid in terms of network power losses. Day-ahead and short-term predictions of DG are supposed to be available to the control system, which reconfigures the grid and controls ESSs/OLTC in real-time to achieve the objective.

Preventive Mitigation of Adverse Events in the Distribution Grid

This use case focuses on risk-aware grid operation, in which the grid is operated taking into account current and future estimated risk levels of its components. In details, the current and predicted risk levels related to network nodes and lines are assumed to be available to the controller from a risk predictor system, which correlates heterogeneous information (e.g., ongoing anomalies, cyber-attacks detected, meteorological conditions) regarding the state of the infrastructure, and computes a short-term prediction of the risk level associated with the various system components (see [44] and [J4] for details

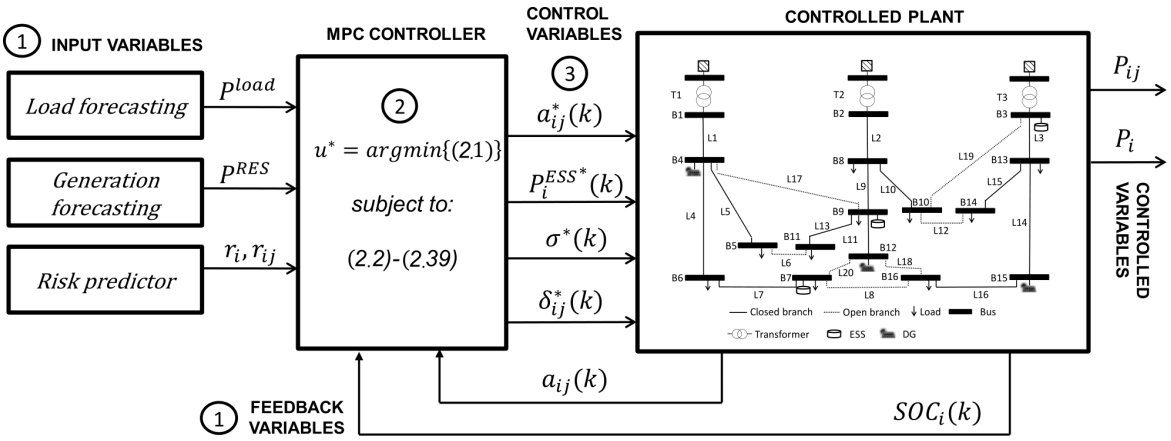

Fig. 2.1 Block diagram of the proposed control system.

on the functioning of the risk predictor, which has been developed and demonstrated in the context of the European project ATENA). Risk levels are associated to both lines and nodes of the grid, in order to capture different kinds of adverse events or cyber attacks.

Preventive Mitigation of Adverse Events at Transmission/Distribution Interface

This use case concerns adverse events impacting on the transmission network and propagating to the distribution side, like cyber attacks against large power plants and HV/MV substations, which can lead to the disconnection of the distribution side from the transmission network and give rise to islanded operation. In this case, grid loading, voltage and frequency control [45] are sustained by the distributed generation and the ESSs. The control objective is to maximize the survivability of the distribution grid by properly operating DG resources and the ESS, and resorting to load shedding only to increase the survival time of the network.

The proposed control logic is presented next.

2.3.2 Control Methodology and Application Logic

The block diagram of the controlled system is presented in Figure 2.1 and explained in details in this and the next section. Dealing at the same time with efficiency and security related aspects, the most natural choice to address the problem is the

implementation of a predictive controller, that shall take its control actions considering also the future effects that these will have on the system, in order to prevent unsafe operations and optimize efficiency in the long-term. A promising solution is represented by Economic Model Predictive Control (EMPC), a variant of MPC that explicitly takes into account the optimization of system performance and efficiency metrics (see e.g. [46], [47]). In MPC [22], at the generic time k, input data (short term load/generation forecasts and predicted risk values in the present case) and the feedback of the state of the plant (step 1 in Figure 2.1) are retrieved, and the control signals are computed by solving a constrained optimization problem defined over a time window N steps in the future (step 2); the first sample of the computed control signals is applied to the plant (step 3) and then the process is reiterated at time $k+1$.

The iterative repetition of the optimization procedure, referred to in the literature as "receding horizon paradigm", is the fundamental characteristic of MPC control, and represents its main advantage over other control schemes. Taking, at every time step k, a state feedback from the system, and consequently updating the optimal control trajectory, may be seen as bringing the intrinsic properties of robustness that characterize closed-loop control into the optimization domain that often characterizes open-loop controllers. Being the system considered in this work characterized by significant uncertainties on the long-term behaviour of some of its components (e.g., photovoltaic (PV) plants, load profiles), applying such a scheme represents an ideal solution with respect to other optimization approaches that assume a perfect knowledge of the system, or at least of its stochastic behaviour.

In EMPC, the objective function is selected to optimize the performance of the system. In this work it is used to jointly account for economic, security and stability requirements. The computed control signals are the state of the switches, the ESSs charging/discharging power and the position of the OLTCs. The feedback acquired at k is given by the state of the controlled switches and the State of Charge (SOC) of the ESSs.

2.4 Formulation of the Control Problem

We discuss in the following the optimization problem that is solved at each time k by the MPC controller (step 2 in Figure 2.1). The problem is defined over the time interval $[k, k+N-1]$, referred to as *control horizon*. In the following, a second

time index $h \in [k, k+N-1]$ is used to denote the generic time instant within the control horizon. Regarding the main nomenclature used, as customary in network reconfiguration studies, the topological aspect of the distribution network is modelled by a graph $\mathcal{G} = \{\mathcal{V}, \mathcal{A}\}$, where $\mathcal{V}$ is the set of network buses and $\mathcal{A}$ is an adjacency matrix specifying the physical connections, i.e., $a_{ij} = a_{ji} = 1$ if there exists a line between buses i and j, zero otherwise. The Boolean control variable $a_{ij}(h)$ captures the status (connected/disconnected) of line (i, j) at time h (the status can change over time only for the subset of lines that can be switched). In the following the standard notation adopted in power system studies is used: P_i is the bus power injection (positive) or withdrawal, P_{ij} and Q_{ij} denote, respectively, the active and reactive line flows, V_i is the bus voltage, θ_i is the bus voltage angle, θ_{ij} is the difference between voltage angles at buses i and j. Power injection and withdrawal at the different bus types is specialised by the use of acronyms in superscript (P_i^{DG}, P_i^{ESS}, P_i^{load}, etc.). Finally, additional specific notation is defined in the following in the place where it is introduced (all symbols are as well defined in the nomenclature section). The objective function and the constraints are presented and discussed in the following.

Objective Function

The objective function is designed to jointly optimize the performance of the system and its resilience to faults/attacks, in a multi-objective sense. It is given by five main terms, each weighed by the coefficients $\alpha, \beta, \gamma, \delta, \epsilon$.

$$\begin{aligned}
&\mathcal{F}_N(k, \mathbf{x}_k, \mathbf{u}_k) = \\
&\sum_{h=k}^{k+N-1} \Big\{ \alpha(h) \sum_{i \in \mathcal{V}} P_i(h) + \beta(h) \sum_{i,j \in \mathcal{V}, j>i} [a_{ij}(h)(1-a_{ij}(h-1)) + a_{ij}(h-1)(1-a_{ij}(h))] + \\
&+ \gamma(h) \sum_{i \in \mathcal{V}} \Big[C_i(h) r_i(h) + \sum_{j \in \mathcal{V}: j>i} a_{ij}(h) r_{ij}(h) \Big] + \delta(h) \sum_{i \in \mathcal{V}^{ESS}} \Big[SOC_i(h) - SOC_i^{ref} \Big]^2 + \\
&+ \epsilon(h) \sigma(h) \Big\}
\end{aligned} \tag{2.1}$$

The subscript N in $\mathcal{F}_N(k, \mathbf{x}_k, \mathbf{u}_k)$ is to denote that the optimal control problem is defined over N time intervals, $\mathbf{x}_k$ denotes the state of the controlled elements at time k, as acquired via feedback from the controlled devices. It is given by the state of the switches and the SOC of the ESS, i.e. $\mathbf{x}_k := \{a_{ij}(k), (i,j) \in \mathcal{A}\} \cup \{SOC_i(k), i \in \mathcal{V}^{ESS}\}$. $\mathbf{u}_k$ is the set of decision variables, i.e. the switching actions, the position of the tap

changers, the ESS power injections and the load shedding (only in the islanded case), i.e., $\mathbf{u}_k := \{a_{ij}(h), (i,j) \in \mathcal{A}, h \in [k, k+N-1]\} \cup \{P_i^{ESS}(h), i \in \mathcal{V}^{ESS}, h \in [k, k+N-1]\} \cup \{\sigma(h), h \in [k, k+N-1]\}$. Each term of the target function is explained in the following.

The term $\mathcal{F}_1 := \sum_{i \in \mathcal{V}} P_i(h)$ represents the network power losses foreseen at time h (given by the sum of the power injected/withdrawn at the grid buses).

The term $\mathcal{F}_2 := \sum_{i \in \mathcal{V}} \sum_{j \in \mathcal{V}: j>i} [a_{ij}(h)(1 - a_{ij}(h-1)) + a_{ij}(h-1)(1 - a_{ij}(h))]$ is the number of switching operations at h. Minimizing $\mathcal{F}_2(k)$ avoids unnecessary switching actions.

The term $\mathcal{F}_3 := \sum_{i \in \mathcal{V}} [C_i(h) r_i(h) + \sum_{j \in \mathcal{V}: j>i} a_{ij}(h) r_{ij}(h)]$ enables risk-aware optimization by including the risk levels of nodes and lines (available from the risk predictor). This is particularly relevant in scenarios in which components' operative levels are impacted by adverse events. Parameters $r_{ij}(h), r_i(h) \in [0,1]$ are the predicted "risk levels" for the generic line (i,j) and for node i at h, respectively. They can be understood as the 1-complement of the operative level or the availability of a given subsystem, so that the higher $r_{ij}(h), r_i(h)$, the higher is the probability that the given system will experience a malfunctioning at time h. The role of variable $C_i(h)$ is to capture a *centrality measure* of the generic node i, i.e., the number of nodes that would lose their connection to their primary substation in the case of node i failure. The product $C_i(h) r_i(h)$ hence provides a measure of that is proportional to the expected number of nodes that will be disconnected after a failure of i, given the network configuration at time h. It is worth remarking that, even if $C_i(h)$ should be proportional the number of descendant nodes of i in the tree that spans from the primary substation, due to the dynamical nature of the network topology, this information is not known a priori to the controller, and consequently it has to be computed during the optimization utilising a set of constraints that will be detailed in the following. The second term in $\mathcal{F}_3$ is included in order to penalise the usage of links characterized by high risk levels.

The term $\mathcal{F}_4 := \sum_{i \in \mathcal{V}^{ESS}} [SOC_i(h) - SOC_i^{ref}]^2$ is a regulation term which ensures that the ESSs are operated near a reference SOC, in order to maintain absorption/injection control margins.

The term $\mathcal{F}_5 := \sigma(h)$ is a load shedding factor, which is considered only in the islanded operation, when load is potentially shed in order to further prolong the operation of the network (a uniform shedding factor $\sigma(h) \in [0,1]$ is considered for all the nodes so

to keep simple the illustration of the problem; more refined shedding criteria available from literature can be easily integrated).

The weights $\alpha(h), \beta(h), \gamma(h), \delta(h), \epsilon(h)$ determine the trade-off among the various objectives (i.e., economic performances and security/resiliency related aspects). Their time dependence is due to the fact that they may also weight differently short-term and long-term performances: due to the uncertain prediction on the system exogenous signals (e.g., renewable source power profiles, risk level due to unexpected adverse events, load profiles) it may be reasonable to give priority to objective closer in the prediction window, as the controller can assume an higher confidence level on its predictions. The weights can also be used to bring the objective function terms to comparable scales and homogeneous measuring units (for example, by quantifying the economic losses associated to risk levels and potential faults.

The other fundamental parameter that defines the overall controller is the length of the prediction horizon N, that should never be longer than the confidence interval over which the predictions provided to the control system can be assumed to be reasonably accurate. For this reason, in the testing reported, it was set the window to be 3 hours long.

Constraints

The following constraints are included, defined for $h \in [k, k+N-1]$.

Power Flow Constraints: The real and reactive power flows from node i to node j are (see e.g. [29])

$$P_{ij}(h) = a_{ij}(h)[-G_{ij}V_i(h)V_j(h)\cos(\theta_{ij}(h)) - B_{ij}V_i(h)V_j(h)\sin(\theta_{ij}(h)) + G_{ij}V_i^2(h)], \tag{2.2}$$

$$Q_{ij}(h) = a_{ij}(h)[+B_{ij}V_i(h)V_j(h)\cos(\theta_{ij}(h)) - G_{ij}V_i(h)V_j(h)\sin(\theta_{ij}(h)) - B_{ij}V_i^2(h)], \tag{2.3}$$

where $\theta_{ij}(h) = \theta_i(h) - \theta_j(h)$. Equations (2.2) and (2.3) are defined for $(i,j) : a_{ij} = 1$. G_{ij} and B_{ij} are, respectively, the line series conductance and susceptance, i.e., the real and the imaginary part of the (i,j) line series admittance Y_{ij}. Lines' shunt elements are neglected (a reasonable assumption in distribution networks [48]).

Power Balance Equations: For all $i \in \mathcal{V}$

$$P_i(h) = P_i^{SB}(h) + P_i^{DG}(h) + P_i^{ESS}(h) - P_i^{load}(h) = \sum_j P_{ij}(h) + G_{ii}(V_i(h))^2 \tag{2.4}$$

$$Q_i(h) = Q_i^{SB}(h) + Q_i^{DG}(h) + Q_i^{ESS}(h) - Q_i^{load}(h) = \sum_j Q_{ij}(h) - B_{ii}(V_i(h))^2 \tag{2.5}$$

Depending on the bus type (load, generation, storage bus), one or more terms might be zero. The load shedding factor, if enabled, scales the load-related power profiles that appear in (2.4) and (2.5).

Radiality Constraints: In the far majority of cases, distribution networks are radially operated. Both heuristic and exact radiality constraints have been proposed in literature, but, as discussed, most of them work only in case of passive networks [33]. References [38] and [39] have recently proposed conditions to ensure radiality in active distribution grids. Based on [38], the following constraint is included

$$\sum_{\{ij:a_{ij}=1, j>i\}} a_{ij}(h) = |\mathcal{V}| - |\mathcal{V}^{SB}|, \tag{2.6}$$

which states that the number of connected lines in the network shall equal the number of nodes minus the number of primary substations. In passive networks, (2.6) combined with (2.4)-(2.5) guarantees radiality [39]. In active networks with ESSs, (2.6) ensures radiality only if the ESSs are hosted at primary substation level (otherwise the formation of islands powered by the ESSs is possible), as shown in [39]. In general, this kind of constraints avoid the presence of islanded portions of the network exploiting the unfeasibility of their power flow, which in active networks, due to the presence of devices such as ESSs, is no longer a correct assumption. In the following, (2.6) is extended in order to guarantee radiality in the general active networks case. An *auxiliary flux* is introduced to ensure that each ESS is connected to a HV/MV substation, similarly to what presented in [38]. This connectivity flux goes from the transmission network into the distribution network, and is forced to reach all the ESSs, assuring hence the connectivity sought. To formalise this auxiliary flux, two auxiliary nodes are added: a *super source* S, representing the transmission network, connected to each HV/MV substation through outgoing edges, and a *super sink* Z, connected to each ESS through incoming edges. In addition, two auxiliary flux variables f_{ij} and f_{ji} are associated to each link in the augmented network, representing the link flows in the two opposite directions. The following set of constraints, modelling flux conservation for nodes and

capacity limits for links, guarantee the connectivity desired for the ESSs:

$$f_{ij}(h) \in \{0, 1, ..., |\mathcal{V}^{ESS}|\} \quad \forall i, j \in \mathcal{V} \cup \{S, Z\} \tag{2.7}$$

$$a_{ij}(h) \geq \frac{f_{ij}(h) + f_{ji}(h)}{|\mathcal{V}^{ESS}|} \quad \forall i, j \in \mathcal{V} \cup \{S, Z\} \tag{2.8}$$

$$f_{ij}(h) f_{ji}(h) = 0 \quad \forall i, j \in \mathcal{V} \cup \{S, Z\} \tag{2.9}$$

$$\sum_{j \in \mathcal{N}_i(h)} f_{ij}(h) - \sum_{j \in \mathcal{N}_i(h)} f_{ji}(h) = 0, \quad \forall i \in \mathcal{V} \tag{2.10}$$

$$\sum_{j \in \mathcal{N}_S(h)} f_{Sj}(h) = |\mathcal{V}^{ESS}| \tag{2.11}$$

$$f_{jZ}(h) = 1 \quad \forall j \in \mathcal{N}_Z \tag{2.12}$$

where $|\mathcal{V}^{ESS}|$ is the number of buses hosting ESSs and $\mathcal{N}_i$ represents the neighbours of the node i (i.e. $\mathcal{N}_S$ are the HV/MV substations and $\mathcal{N}_Z$ the buses hosting ESSs). Constraint (2.9) prevents from having flows in both directions on each link. Constraint (2.11) states that the flow from the super source has to be equal to $|\mathcal{V}^{ESS}|$, while (2.12) forces the connection with a primary substation for all the ESS and (2.10) models the flux conservation. Constraint (2.8) forces $a_{ij} = 1$ if any flux passes through branch (i, j) in either direction.

A possible interpretation of constraints (7)-(12) is that they force the existence of a path between the HV/MV substations and the ESSs by the mass/flux conservation law, ensuring their connection. Since the ESSs are now always connected to the transmission line, they cannot act as a slack node for an independent island, whose presence could imply the non-radiality of the network [39], and constraint (6) returns a valid mean to impose radiality.

Definition of $C_i(h)$ in (2.1): Variable $C_i(h)$ should be informative of the number of nodes that are the descendants of a given node i at time h from a topological point of view. In general, this variable can be computed in polynomial time on a fixed network configuration, but in order to be included in the optimization process, it has to be computed by the optimization solver for each of the topologies it evaluates. For this reason, a second auxiliary flow is introduced in the following. This new flux is assumed to be produced by the super source node S, and absorbed by the super sink node Z. The idea is that each node shall feed exactly one unit of flow to Z, meaning that the intake of flux that the node i receives is exactly the number of its topological descendants, increased by one. To attain this result, all the nodes in the network are connected to the super sink through outgoing edges with unitary

capacity. S feeds the HV/MV substations with a total quantity of flux equal to the number of buses. Let $f_{ij}^c(h)$ represent the flow in the link connecting the nodes i and j: $f_{ij}^c(h) \in \{-|\mathcal{V}^{SB}|, ..., 0, ..., |\mathcal{V}^{SB}|\} \quad \forall i, j \in V \cup \{S, Z\}$. The following constraints are then included.

$$\sum_{j \in \mathcal{N}(S)} f_{Sj}^c(h) = |\mathcal{V}^{SB}| \tag{2.13}$$

$$f_{jZ}^c(h) = 1 \quad \forall j \in \mathcal{N}(Z) \tag{2.14}$$

$$a_{ij}(h) \geq \left(\frac{f_{ij}^c(h)}{|\mathcal{V}^{SB}|}\right)^2 \qquad \forall i, j \in V \cup \{S, Z\} \tag{2.15}$$

$$\sum_{j \in \mathcal{N}(i)} f_{ij}^c(h) - \sum_{j | i \in \mathcal{N}(j)} f_{ji}^c(h) = 0 \quad \forall i \in \mathcal{V} \tag{2.16}$$

$$C_i(h) \geq \sum_{j \in \mathcal{N}(j)} f_{i,j}^c(h)^2 + \sum_{j | i \in \mathcal{N}(j)} f_{j,i}^c(h)^2 \quad \forall i \in \mathcal{V} \tag{2.17}$$

Notice that in this case the physical links are given an arbitrary direction on the flow graph, as there is no equivalent constraint to (2.9) and f_{ij}^c can assume also negative values. To address this change, (2.8) has been replaced with (2.15), and its interpretation is that the only network edges on which the functional flux may flow are the ones on which power is flowing (i.e., $a_{ij}(h) = 1$). Constraint (2.17) defines the centrality when active, and its activation is guaranteed by the minimization of $\mathcal{F}_3$, which in turn steers the system to select configurations in which nodes with high risk levels have low centrality, as a measure to avoid cascading failures. The considered centrality index is then proportional to the square of the number of descendant nodes that depend on node i, as it is proportional to the square of the amount of auxiliary flux that goes through it, to further penalise configurations that associate nodes subject to high risk levels to central positions.

It is worth noting that in this work it was decided to capture the topological centrality, as by design the number of descendant nodes at risk was considered to be more relevant than the amount of load. With trivial modifications this functional flux can be adapted to use cases in which the priority is given to configurations that consider the quantity of supported load as a centrality index.

Voltage and Current Limits:

$$V_i^{min} \leq V_i(h) \leq V_i^{max}, \forall i \in \mathcal{V} \tag{2.18}$$

$$I_{ij}(h) \leq I_{ij}^{max}, \forall (i, j), i \geq j, \tag{2.19}$$

where $I_{ij}(h)$ is the line current magnitude, which can be written in function of voltages as shown in [27] (see (5)-(9) therein).

Step-voltage Regulation at Primary Substations: The voltage level at the substation buses can be controlled by acting on the transformers' OLTC (see e.g. [49]), which can be used to select different voltage levels

$$V_i(h) = \sum_{j=1}^{l_i} \delta_{ij}(h) V_{ij}^{OLTC}, \quad \forall i \in \mathcal{V}^{SB} \tag{2.20}$$

$$\sum_{j=1}^{l_i} \delta_{ij}(h) = 1, \quad \forall i \in \mathcal{V}^{SB} \tag{2.21}$$

where l_i is the number of the voltage levels V_{ij}^{OLTC} that can be selected at substation bus i. $\delta_{ij}(h)$ is a Boolean control variable used to select the voltage level. The second constraint assures that only one voltage level is selected at time h.

ESS Constraints and Dynamics: ESS constraints are introduced in order to model the ESS power rating, battery capacity, SOC dynamics; also a terminal constraint is introduced to guarantee system stability.

$$P_i^{ESS,min} \leq P_i^{ESS}(h) \leq P_i^{ESS,max}, \tag{2.22}$$

$$Q_i^{ESS,min} \leq Q_i^{ESS}(h) \leq Q_i^{ESS,max}, \tag{2.23}$$

$$SOC_i^{min} \leq SOC_i(h) \leq SOC_i^{max}, \forall i \in \mathcal{V}^{ESS} \tag{2.24}$$

$$SOC_i(h+1) = SOC_i(h) - TP_i^{ESS}(h)\frac{100}{C_i^{ESS}} \tag{2.25}$$

$$SOC_i(k+N) \geq SOC_i^{ref} \tag{2.26}$$

$T \in \mathbb{R}$ the discretization time step. In relation to (2.23), notice that it is possible to act on the ESS inverter to control the reactive power. The reader is referred to the literature (see e.g. [50]) for details on ESS reactive power control. Note that in (2.25) it was assumed, for simplicity, that the storage was operated with 100% efficiency.

Initial Conditions: The EMPC problem is solved at each time k based on the following initial conditions

$$SOC_i(k) = SOC_i^k, \forall i \tag{2.27}$$

$$a_{ij}(k) = a_{ij}^k, \forall i \tag{2.28}$$

where SOC_i^k and a_{ij}^k are, respectively, the measured ESS SOC level and the known network configuration at k.

The above problem is a non-convex mixed-integer nonlinear programming (MINLP) problem.

2.4.1 Conification of the Problem Constraints

Based on the procedure in [29], the above problem can be transformed into an equivalent, conified, quadratic programming problem having the same optimal solution. The constraints involved in this transformation are the ones related to power flow, in particular (2.2)-(2.3), that due to their nonlinearity increase the complexity of the problem. The transformation is outlined in the following; full details are in [29].

The following substitutions are made through the inclusion of the new auxiliary variables $u_i(h)$ for $i \in \mathcal{V}$ and $R_{ij}(h)$, $T_{ij}(h)$ for $(i,j) : a_{ij} = 1$

$$u_i(h) \leftarrow V_i(h)^2/\sqrt{2} \tag{2.29}$$

$$R_{ij}(h) \leftarrow V_i(h)V_j(h)\cos\theta_{ij} \tag{2.30}$$

$$T_{ij}(h) \leftarrow V_i(h)V_j(h)\sin\theta_{ij} \tag{2.31}$$

With these positions, the power flow equations (2.2)-(2.3) become

$$P_{ij}(h) = a_{ij}(h)[-G_{ij}R_{ij}(h) + B_{ij}T_{ij}(h) + G_{ij}\sqrt{2}u_i(h)] \tag{2.32}$$

$$Q_{ij}(h) = a_{ij}(h)[B_{ij}R_{ij}(h) + G_{ij}T_{ij}(h) - B_{ij}\sqrt{2}u_i(h)] \tag{2.33}$$

As explained in [27], (2.32)-(2.33) can be exactly linearised by introducing new Boolean variables $u_i^{ij}(h)$ for each line (i,j) connected to the generic bus i (in particular, variables $u_i^{ij}(h)$ are defined for $i \in \mathcal{V}$, $j \in \mathcal{V}$ and $(i,j) : a_{ij} = 1$). The following additional auxiliary constraints are introduced to force variables $u_i^{ij}(h)$ to be equal to zero when the line is

disconnected and equal to $u_i(h)$ otherwise.

$$0 \leq u_i^{ij}(h) \leq \frac{(V_i^{max})^2}{\sqrt{2}} a_{ij}(h) \tag{2.34}$$

$$0 \leq u_i(h) - u_i^{ij}(h) \leq \frac{(V_i^{max})^2}{\sqrt{2}} (1 - a_{ij}(h)) \tag{2.35}$$

$$2u_i^{ij}(h)u_j^{ji}(h) \geq R_{ij}(h)^2 + T_{ij}(h)^2, R_{ij}(h) \geq 0 \tag{2.36}$$

Then, with the above positions it can be verified that (2.32)-(2.33) can be written in a linear form as

$$P_{ij}(h) = -G_{ij}R_{ij}(h) + B_{ij}T_{ij}(h) + G_{ij}\sqrt{(2)}u_i(h) \tag{2.37}$$

$$Q_{ij}(h) = B_{ij}R_{ij}(h) + G_{ij}T_{ij}(h) - B_{ij}\sqrt{(2)}u_i(h) \tag{2.38}$$

In fact, the reader can check that, when $a_{ij}(h) = 1$, (2.37)-(2.38) coincide with (2.32)-(2.33), because $u_i^{ij}(h) = u_i(h)$ due to (2.35). When $a_{ij}(h) = 0$, then $u_i^{ij}(h) = 0$ due to (2.34), and also $R_{ij}(h)$ and $T_{ij}(h)$ are equal to zero, because of (2.36); hence it is recovered that $P_{ij}(h) = 0$ and $Q_{ij}(h) = 0$, as expected.

Departing from [29] and [27], further attention is needed to manage variables u_i and V_i for $i \in \mathcal{V}^{\mathcal{SB}}$, since voltages at substation buses are control variables that can assume only discrete values, as modelled in (2.20). Considering (2.29) and (2.20),

$$u_i(h) = \frac{\left(\sum_{j=1}^{l_i} \delta_{ij}(h) V_{ij}^{OLTC}\right)^2}{\sqrt{2}}. \tag{2.39}$$

Considering that $\delta_{ij}(h)^2 = \delta_{ij}(h)$, and that $\delta_{ij}(h)\delta_{ik}(h) = 0$ for $j \neq k$, because of (2.21), then (2.39) finally becomes

$$u_i(h) = \frac{\sum_{j=1}^{l_i} \delta_{ij}(h)(V_{ij}^{OLTC})^2}{\sqrt{2}} \tag{2.40}$$

The next section summarizes the proposed control algorithm.

2.4.2 Overall Formulation

Algorithm 1 (EMPC risk-aware optimization of distribution grid). At each time $k = 1, 2, ...$ do (see Figure 2.1):

1. Measure $\mathbf{x}_k$, the current state of the controlled elements in the grid (open/close state of each switch and SOC of each ESS). Acquire external input values (load and generation forecasts, predicted risk values);
2. Solve $\mathbf{u}_k^* = argmin\{\mathcal{F}_N(k, \mathbf{x}_k, \mathbf{u}_k)\}$ in (2.1) subject to: (2.2)-(2.40). (Find the optimal topology configuration, the optimal position of the tap changers and the optimal ESS power injections over the time interval $[k, k+N-1]$.)
3. Apply to the system the first sample of the optimal control sequence $\mathbf{u}_k^*$;
4. Wait for the next sampling time and go to step 1).

2.4.3 Problem Complexity

The resulting problem is characterized by the presence of conic constraints and binary decision variables. Commercial solvers typically deal with such problems with variations of the branch and cut algorithm, meaning that the computational time required to find the optimal solution has an exponential dependence to the number of binary variables. Furthermore, it is shown in [29] that the solving time for the conified power flow problem on a fixed topology remains compatible with the application considered even in large networks (with a network of 88 nodes requiring less than twice the time of a 12 nodes one), supporting the fact that the main limiting factor of the proposed controller for scaling is related to the number of binary variables (i.e., to the number of controllable switches). In the proposed formulation, each remote operable switch is associated with a decision variable for each time slot in the prediction, but in larger networks one may assume to let the control variables $a_{ij}(h)$ change value only a given number of times in the prediction window, significantly reducing the number of binary variables of the problem (e.g., one reconfiguration allowed every hour). Furthermore, for testing purposes it was considered in the following a network whose links are all equipped with a controllable switch, while in real scenarios the degree of freedom available to the controller is expected to be smaller, as only a portion of the network switches is remotely controllable. To control networks with a high number of controllable switches, a possible approach is that of computing off-line the set of admissible configurations

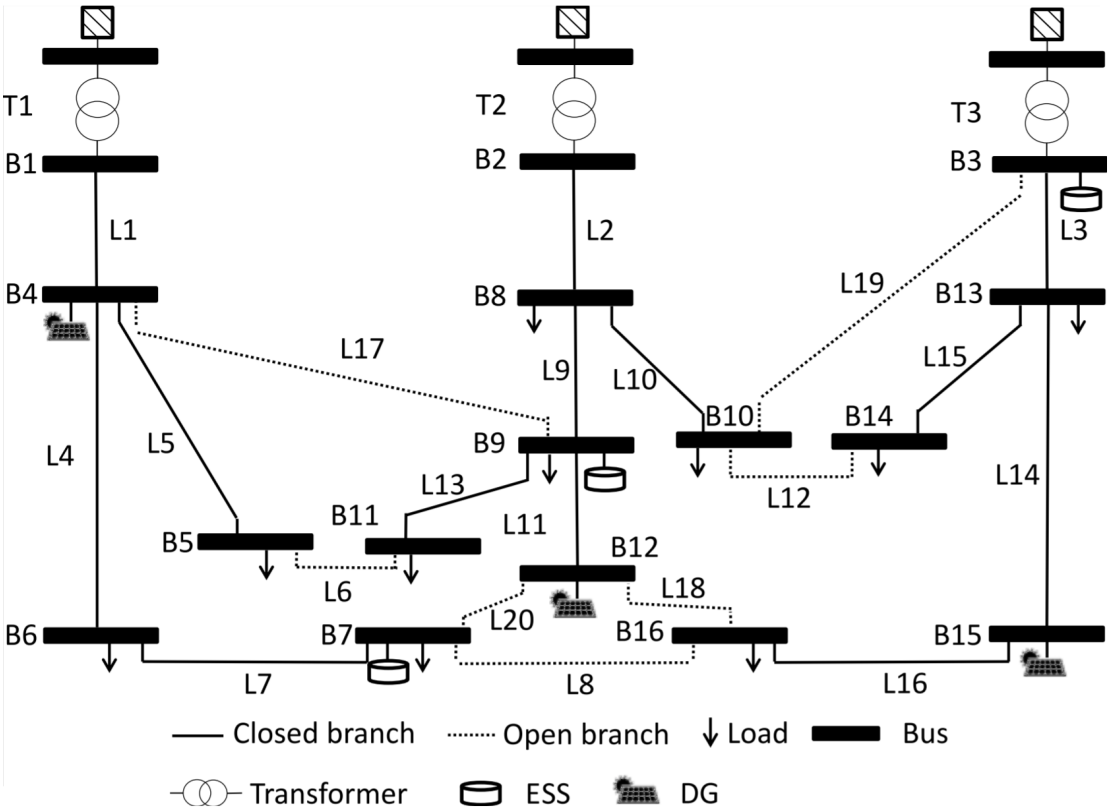

Fig. 2.2 Test distribution network (figure adapted from [51]). The benchmark configuration is the one with solid black lines.

(which, for radiality, operative and power-quality concerns has a cardinality significantly lower than total number of possible configurations) and let the EMPC controller select a configuration only in this set. Doing so would significantly reduce complexity, since the number of binary variables would be significantly reduced and the constraints for radiality assurance could be removed. This option, combined with limiting the number of allowed switching in the prediction window allows the solving time to be adequate to use cases of a larger scale than the ones considered in this work and in the H2020 Atena project.

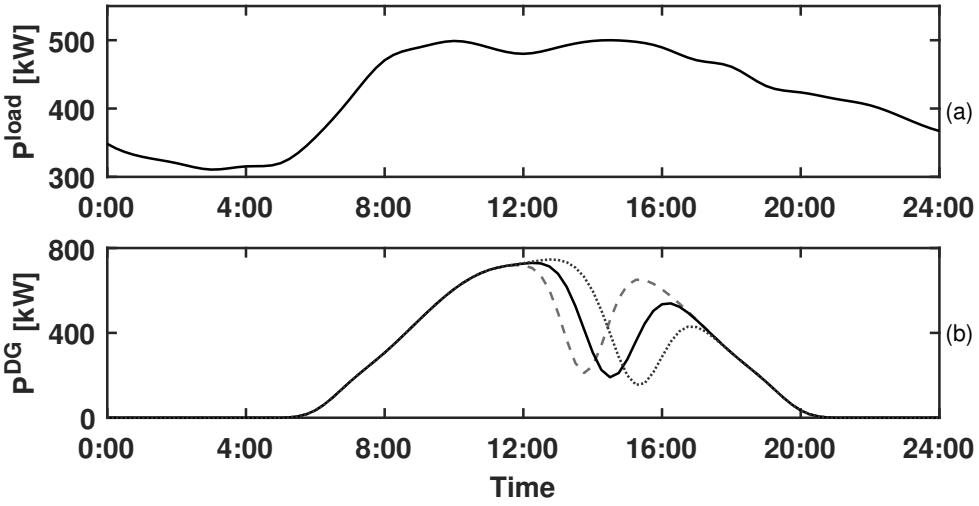

Fig. 2.3 (a) Power consumption at MV/LV substations and (b) power generation at node 4 (dashed line), 12 (solid line) and 15 (dotted line). Notice the humps in the generation profiles, which are shifted in time in order to simulate a cloudy condition moving from the upper left portion of the network to the lower right one.

2.5 Simulation Results

2.5.1 Simulation Setup

The proposed algorithm has been tested on a 16-bus three-feeder distribution network commonly employed in literature (see Figure 2.2); network data are taken from [52]. The network was chosen so that it presents a high number of potential configurations that differ significantly, allowing a clearer interpretation of the results.

In order to provide a proof of concept, common input data to all the use cases are as follows. MV/LV substations placed along the feeders and serving end users are characterized by a typical summer load pattern [53], as reported in Figure 2.3, while the MV busbars of the HV/MV substations are characterized by a small constant consumption of 10 kW related to the auxiliary devices; prediction and actual consumption patterns are assumed to be the same in the following. Three large-scale PV plants with 750 kW peak capacity are placed at nodes 4, 12 and 15; a typical clear sky pattern is initially considered as common day-ahead power prediction, and then perturbed in real-time to build short-term power predictions that reconstruct the three actual generation patterns reported in Figure 2.3b. Three 2 MW/1 MVAr/2 MWh ESSs are placed at nodes 3, 7 and 9 to assess the effect of energy storing at different distances from the HV/MV substations; reference SOC levels have been set to 70% to give to the

controller enough operational margin while storing enough energy to properly support the islanded operation of the system. The power factor is 0.98 for all the load and generation nodes, lagging or leading respectively. The considered OLTCs possess 11 taps allowing ±5% voltage variation with respect to the typical 20 kV nominal level (the same range is imposed to all the nodes in the network). The problem was solved in per-unit to avoid numerical issues (solving optimization problems in which the variables can assume values over several different orders of magnitude may lead to numerical precision loss).
The sampling time T and control horizon N have been set to 15 minutes and 3 hours respectively. The rationale behind N in particular is to take it large enough to provide flexibility to the system, while resulting in compatible solving times. Also, a value of N too large would introduce into the problem the high uncertainties associated with the predictions of the solar plant profiles and the risk levels far from the current time. Finally the weights appearing in the target function have been empirically selected as $\alpha(h) = 10, \gamma(h) = 1, \beta(h) = 10^{-4}, \delta(h) = 10^{-4}, \forall h$ in order to guarantee a good performance of the system in the various simulations. The parameter α was given the highest value in order to have the control focus more on power loss reduction, also taking care of the activation of constraint (2.36) and consequently assuring the correctness of the conification procedure. The weight γ was given a secondary priority level. The weights relative to the control actions, namely, β and δ, were given a lower value in order to let the control system have a significant degree of freedom. More in general, the operator can carry-out a detailed parameter selection study in order to best tune the system behaviour according to its preferences and the weights themselves can be time-varying depending, for example, on the short-term forecasted risk-level associated to the overall network or its current state.

To establish a benchmark, Figure 2.2 reports a configuration of the network with an approximately equal distribution of the load among the HV/MV substations, which reflects a typical practice adopted by distribution system operators for configuring the grid in absence of methods like the one here presented.

Simulations have been performed using the Julia v0.7 technical computing language, on an Intel I7, 8GB RAM machine running Windows 10. The optimization problem has been solved using Gurobi [54]. The average time for an EMPC iteration is approximately one minute, under the condition that the solution of the previous step is provided to the solver as initial guess to speed up the convergence. For large networks constraints

limiting the number of reconfigurations in the prediction horizon can be added to speed up the computation.

2.5.2 Simulation 1: Minimization of power losses

This simulation is aimed at assessing how the proposed control system manages the network losses, also taking into account RES fluctuations, assuming null risk level for all network components. Figure 2.6a reports the comparison among the losses in the uncontrolled case (which considers the benchmark configuration) and according to the proposed EMPC. The losses in the controlled case always remain below the benchmark, with an energy saving at the end of the day of 23%. Figure 2.5 shows a significant subset of the 23 configurations taking place during the simulation. The configuration is the same during the hours when the generation is absent, while loads are connected as close as possible to the sources during the generation peak. At 14:30, the lowest point in bus 12 generation valley, the storage in bus 7 discharges feeding the largest tree, which is connected to the first HV/MV substation.

The ESSs at bus 7 and 9 basically behave as generators over the period in which the net load in the network has its peaks, and recharge in the valleys; the ESS at bus 3 is not activated, as expected, due to its placement in the HV/MV substation (Figure 2.6b). The ESSs' SOC remains close to the reference, showing the feasibility of the ESSs contribution in the long term (Figure 2.6c). Finally, Figure 2.7 reports the voltages of the network buses over time. It can be seen that in the controlled scenario the profiles remain similar to the uncontrolled one, with the voltages remaining in a slightly more contained region and the sudden changes in their profile caused by the reconfigurations. It can be noted that the OLTCs select the tap guaranteeing the maximum allowed voltage level (21 kV) in all HV/MV substations, this allows to minimise power losses and was possible for the absence of significant voltage increases over the other buses, as the power flow remained feasible for all times. Similar behaviour is observed in the remaining simulations.

2.5.3 Simulation 2: Preventive Mitigation of Adverse Events in the Distribution Grid

In the following it is shown the reaction of the proposed controller to the notification of updated risk levels for network components, to simulate e.g. attempts of attacks

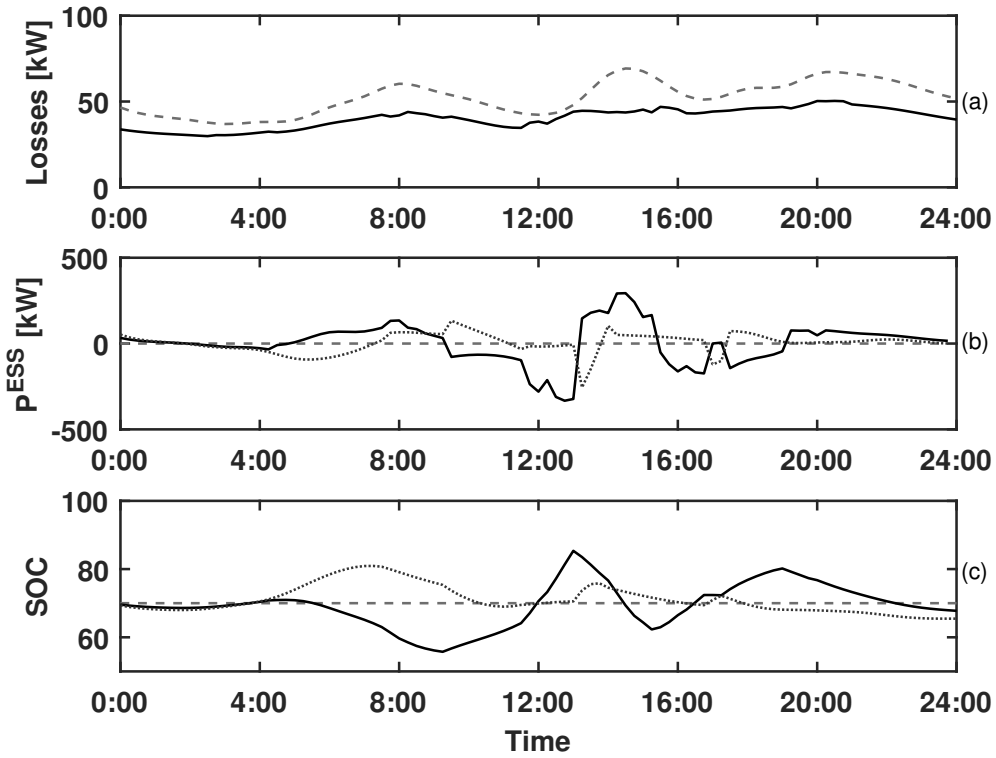

Fig. 2.4 Simulation 1 - (a) Evolution of network power losses in the uncontrolled case (dashed line) and according to the proposed EMPC strategy (solid line), (b,c) power and SOC of the ESSs installed at node 3 (dashed line), 7 (solid line), and 9 (dotted line).

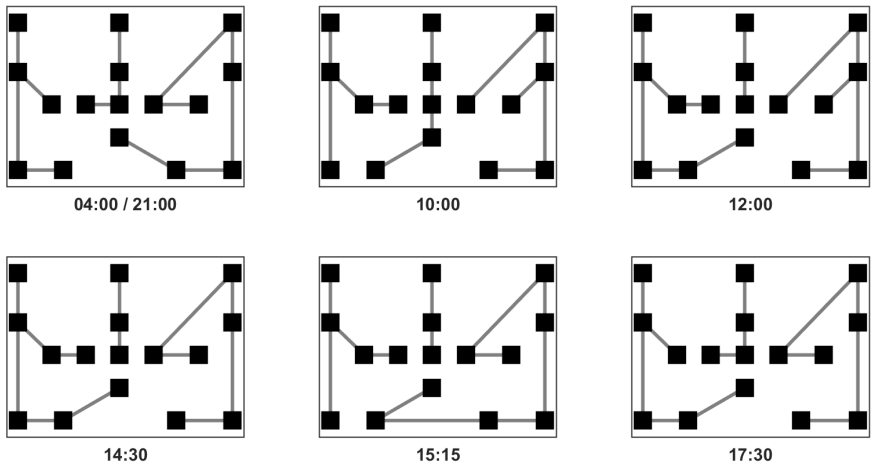

Fig. 2.5 Simulation 1 - Network configurations at different times.

to switches or adverse natural events; the risk levels notified by the risk predictor are reported in Table 2.1.

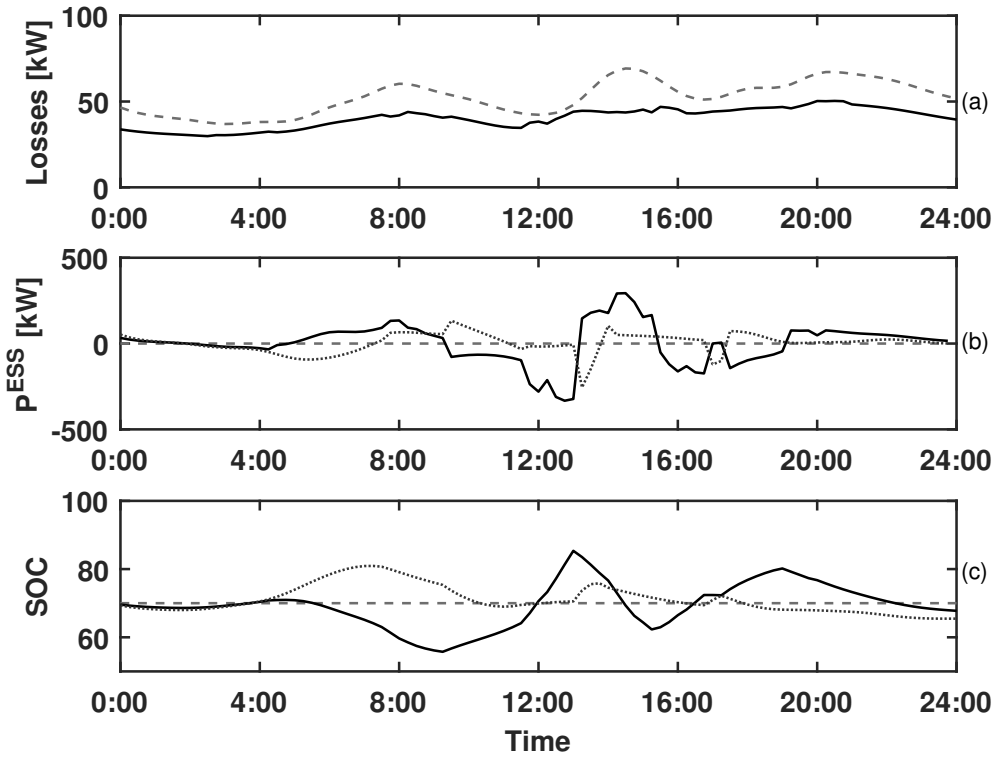

Fig. 2.6 Simulation 1 - (a) Evolution of network power losses in the uncontrolled case (dashed line) and according to the proposed EMPC strategy (solid line), (b,c) power and SOC of the ESSs installed at node 3 (dashed line), 7 (solid line), and 9 (dotted line).

Figures 2.8a and 2.8b report the aggregated risk index, defined as $\mathcal{F}_3$ in Section 2.4, and the power losses computed in the uncontrolled case and according to the proposed control. As expected, the overall risk level is mitigated, by 93%, at the cost of reducing the performance in terms of energy saving (19% reduction of losses, compared to previous 23%).

Figure 2.9 presents configurations of the network computed respectively in instants in which the risk prediction is high on both nodes and links (12:00), only on links (14:30), and on neither (17:30). It can be seen that at 12:00, during the high risk time frame, the network is configured in such a way as to avoid the usage of both lines 10 and 20; also, the controller selects a configuration in which the buses 9 and 13 are at the end of the respective feeders, hence guaranteeing the power supply to consumers connected to those buses, while also avoiding cascading effects of a potential successful cyber attack. Due to the asymmetric configuration characterized by a highly loaded tree departing from bus 1, all the generators are connected to that tree in order to mitigate the power losses; also the ESSs provide their additional contribution, see Figure 2.8c,

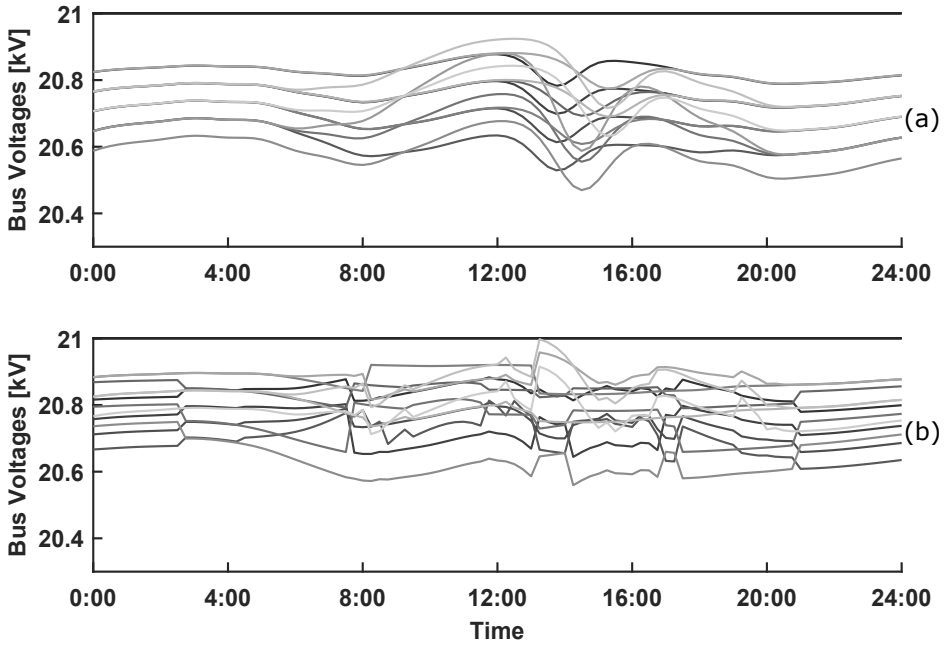

Fig. 2.7 Simulation 1 - (a) Evolution of bus voltages in the uncontrolled case, (b) Evolution of bus voltages in the controlled case

Table 2.1 Simulation 2 - Predicted components risk levels

Components	Risk Level	Start time	End Time
Lines 10, 20	0.2; 0.2	10:45	14:45
Buses 9, 13	0.9; 0.8	11:45	13:45

basically amplifying the same behavior seen in Figure 2.6b. At 14:30, while still being provided with a high risk level for lines 10 and 20, the controller selects a configuration more similar to the ones of the first simulation (Section 2.5.2), since the risk prediction for the nodes is now set to zero. Finally, after the end of the alerting period, the configuration gradually returns the same one computed in absence of risk in Section 2.5.2 (see the configuration at 17:30 in Figure 2.9).

2.5.4 Simulation 3: Preventive Mitigation of Adverse Events at Transmission/Distribution Interface

The last simulation considers the opening of breakers in the HV/MV substations and the consequent disconnection of the distribution grid from the transmission network, which gives rise to controlled islanded operation starting from 11:30, a conditions in

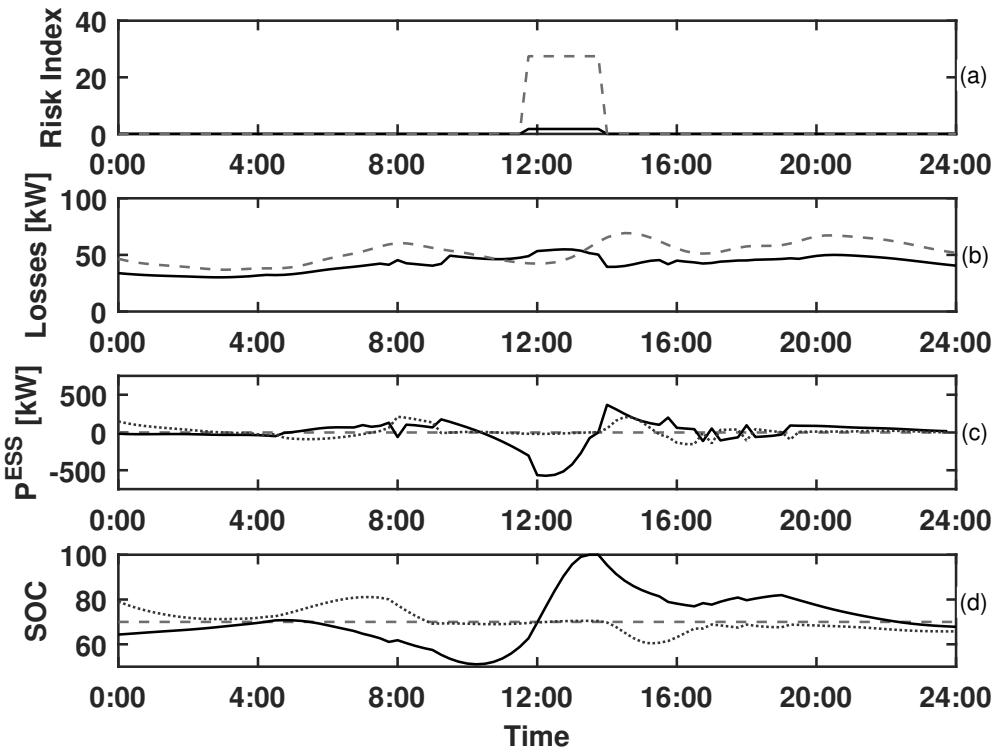

Fig. 2.8 Simulation 2 - (a,b) Evolution of network aggregated risk and power losses in the uncontrolled case (dashed line) and according to the proposed EMPC strategy (solid line), (c,d) power and SOC of the ESSs installed at node 3 (dashed line), 7 (solid line), and 9 (dotted line).

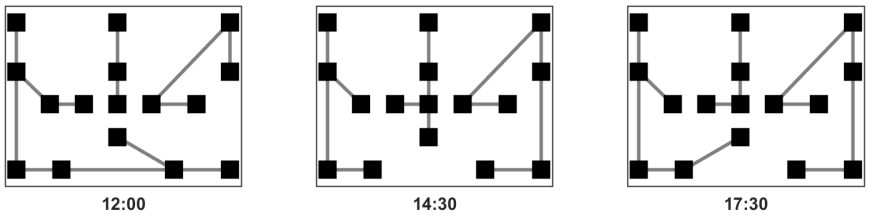

Fig. 2.9 Simulation 2 - Network configurations at different times.

which the balance between demand and supply is guaranteed by the ESSs. During islanding, the prediction window was shortened to 1 hour, to allow faster response of the system, and the network radiality was assured by constraint (2.6) and the power flow, as constraints (2.7)-(2.12) were no longer needed to guarantee the connection of the, now inactive, HV/MV substations to the storage devices. Also, the reference level for the SOC was lowered to 20% to encourage ESSs discharge at the beginning of the disconnection period to sustain the network, and consequently delay the shedding intervention. Figure 2.10 shows how the proposed strategy keeps the most loads

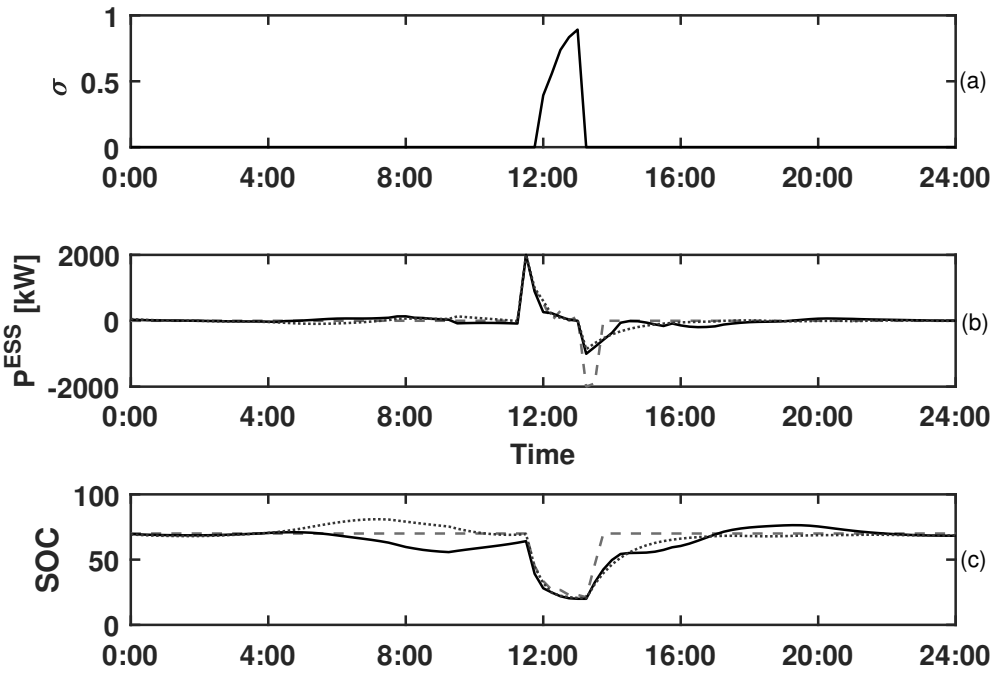

Fig. 2.10 Simulation 3 - (a) Load shedding factor, (b,c) power and SOC of the ESSs installed at node 3 (dashed line), 7 (solid line), and 9 (dotted line).

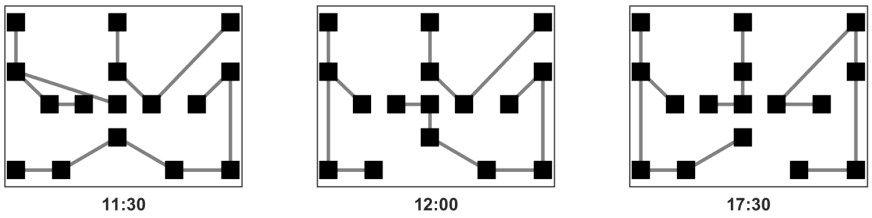

Fig. 2.11 Simulation 3 - Network configurations at different sampling times during islanded operation.

connected when the ESSs SOC is high, and then gradually increases the load shedding factor to prolong the survival time of the system. After 13:00, when the connection to the transmission is re-established, the ESSs recover their SOC at different speeds, according to their topological position, in order to keep minimizing the network losses. Figure 2.11 shows two configurations during the islanded operation, where the controller tries to balance the discharge of the ESSs by connecting most loads to the storage with the highest SOC, utilizing the generators to sustain the bigger trees. The third configuration reported shows that the same network configurations as the one in Section 2.5.2 (normal operation) is recovered, after a transitory period during which the SOCs return close to their reference of 70%.

2.6 Conclusions

This work has presented a coordinated network reconfiguration and energy storage system (ESS) control strategy for the efficient and secure operation of electricity distribution grids. The proposed approach enables the real-time reaction to the predictions of future fluctuations of power production from renewable and malicious/natural adverse events, with the aim of minimizing the network losses, the aggregated risk indicator and allowing preventive or post-attack grid operation.

The non-convex optimization problem at the basis of the adopted model predictive control (MPC) methodology incorporates the ESSs dynamics, the hybrid power flow equations and ad-hoc topological constraints; this allows to compute a control action taking into account future feasible operative conditions of the ESSs and the network in presence of distributed generation, and also the cascading effects on the nodes downstream of the vulnerable ones. The optimal solution of this problem is achieved at each sampling time by solving a conified proxy of the original problem, having the same optimal solution. The proposed method has been shown to be effective when applied to a 16-bus test distribution grid. Future works will regard the investigation of the theoretical properties of the MPC algorithm, and a heuristic procedure for the identification of optimal values for the weighting terms in the objective function, starting from a high level description of the operator preferences.

Chapter 3

Joint Model Predictive Control of Electric and Heating Resources in a Smart Building

The new challenge in power systems design and operation is to organize and control smart micro grids supplying aggregation of users and special loads as electric vehicles charging stations. The presence of renewable and storage can help the optimal operation only if a good control manages all the elements of the grid. New models of green buildings and energy communities are proposed. For a real application they need an appropriate and advanced power system equipped with a building automation control system. This work presents an economic model predictive control approach to the problem of managing in a coordinated way the electric and heating resources in a smart building, for the purpose of achieving in real time nearly zero energy consumption and automated participation to demand response programs. The proposed control, leveraging a mixed integer quadratic programming problem, allows to meet manifold thermal and electric users' requirements and react to inbound demand response signals, while still guaranteeing stable operation of the building's electric and thermal storage equipment. The simulation results, performed for a real case study in Italy, highlight the peculiarities of the proposed approach in the joint handling of electric and thermal building flexibility. The results of this chapter have been published in

[J3] *F. Liberati, A. Di Giorgio, A. Giuseppi, A. Pietrabissa, E. Habib, and L.Martirano, "Joint model predictive control of electric and heating resources in a smart building,"IEEE Transactions on Industry Applications, 2019.*

Nomenclature of the chapter

Indices	
e	Index of the generic electric vehicle EV
i	Time index in the MPC window
k	Absolute time index
l	Index of the generic plannable load
u	Index of the generic housing unit
Parameters	
C^{floor}, C^{wall}	Heat capacity of the floor and walls $[kJ/K]$
C_i, c_i	Electricity tariff and cost of energy at time i $[EUR/kWh]$
E^{ess}, E_e^{ev}	Capacity of the ESS and of the eth EV$[kWh]$
c_{air}, c_w	Specific heat of the air and water $[kJ/(kg \cdot K)]$
F_l	Latest allowed finish time of appliance l $[s]$
F_e	End time of recharging session of EV e $[s]$
γ	Heat pump coefficient of performance
L_i	Set of plannable loads active at time i
M	Boiler water mass $[kg]$
N	Length of the MPC time window $[s]$
N_l	Duration of appliance program l $[s]$
$P_e^{ev,max}$	Maximum charging/discharging power of EV e $[kW]$
P_i^{npl}	Non plannable loads power absorption at time i $[kW]$
P_i^{pl}	Power absorbed by the plannable loads at time i $[kW]$
P_i^{pv}	Power produced by the PV panel at time i $[kW]$
ρ_{air}	Air density $[kg/m^3]$
$R_{wall}^{ext}, R_{air}^{walls}, R_{floor}^{air}$	Thermal resistance of the external walls; between the walls and the floor with the air $[K/kW]$
R_{floor}^{pipes}	between the floor and the pipes $[K/kW]$
S_l	Earliest allowed start time for the program of appliance lth $[s]$
S_e	Start time of recharging session of EV e $[s]$
U	Set of building's units
$\mathcal{T}$	Sampling period $[s]$
V_u	Air volume in building's unit u $[m^3]$
ξ^{ess}, ξ_e^{ess}	Loss factor of the ESS and of the eth EV battery pack

Variables	
P_i^{poc}	Power flow at the grid point of connection at i $[kW]$
P_i^{ess}	Power injected or absorbed by the ESS at time i $[kW]$
P_i^{ev}	Aggregated power injected/absorbed by EVs at i $[kW]$
P_i^{hp}	Power absorbed by the heat pump at time i $[kW]$
$S\tilde{O}C_i^{ess}$	Reference state of charge of the ESS at time i [%]
SOC_i^{ess}	State of charge of the ESS at time i [%]
$T_{u,i}^{air}$	Air temperature in unit u at time i $[°C]$
$T_{u,i}^{pipes}, T_{u,i}^{floor}, T_{u,i}^{walls}$	Pipes, floor and Walls temperature in unit u at time i $[°C]$
T_i^{ext}	External air temperature at time i $[°C]$
$\tilde{T}_{u,i}^{air}$	Reference air temperature in unit u at time i $[°C]$
T_i^{boiler}	Boiler water temperature at time i $[°C]$
$\tilde{T}_i^{boiler}$	Reference boiler water temperature at time i $[°C]$
Control Variables	
c_i^{ess}	$c_i^{ess} \in \{0,1\}$, $c_i^{ess} = 1$ if the ESS recharges at i
$c_{e,i}^{ev}$	$c_{e,i}^{ev} \in \{0,1\}$, $c_{e,i}^{ev} = 1$ if EV e recharges at i
d_i^{ess}	$d_i^{ess} \in \{0,1\}$, $d_i^{ess} = 1$ if the ESS discharges at i
$d_{i,e}^{ev}$	$d_{i,e}^{ev} \in \{0,1\}$, $d_{i,e}^{ev} = 1$ if EV e discharges at i
$G_{u,i}$	Water mass flow intake of housing unit u at i kg/s
$P_i^{ess,c}, P_i^{ess,d}$	Charging/discharging ESS power at i kW
$P_{i,e}^{ev}$	Power injected or absorbed by the EV e at i kW
$P_{e,i}^{ev,c}, P_{e,i}^{ev,d}$	Charging/discharging power of EV e at i kW
$s_{l,j}$	$s_{l,j} \in \{0,1\}$, $s_{l,j} = 1$ if the plannable program l is set to start at time j

3.1 Introduction

3.1.1 Motivation of the Work

Buildings and the construction sector are responsible, according to [55], for 30% of the final energy consumption, for more than 55% of the global electricity demand and for around 40% of the CO_2 emissions. Increasing efficiency and smartness of the building

stock is therefore fundamental to reduce greenhouse gas emissions, energy consumption and increase the share of RES.

In Europe, the Energy Performance of Buildings Directive (2010/31/EU) [56], as amended in 2018 by the Directive (EU) 2018/844 [57], has established key principles, measures and binding targets, such as the introduction of minimum energy performance requirements for buildings, energy certification, mandates for nearly zero-energy performance in new buildings, for the installation of recharging points for Plug-in Electric Vehicles (PEVs), etc. The Directive also envisages separate regulation of the temperature in each room, vehicle to grid, deployment of high-capacity communication networks, building automation and control system to "support energy efficient, economical and safe operation of technical building systems through automatic controls..." [57] and introduces "the smart readiness indicator" for buildings, which "should be used to measure the capacity of buildings to use information and communication technologies and electronic systems to adapt the operation of buildings to the needs of the occupants and the grid and to improve the energy efficiency and overall performance of buildings" [57]. The aggregation of small and medium users in a cluster or community is one of the most exciting challenges in the field of power systems, in which the building automation and the controls play a fundamental role.

3.1.2 Purpose of the work

This work proposes a MPC approach to the problem of managing, in a coordinated and synergic way, the electric and heating resources in a smart building, for the purpose of achieving, in real time, nearly zero energy consumption and automated participation to Demand Response (DR) programs, while satisfying users comfort. The reference scenario (Fig. 3.1) considers a mixed-use building consisting of several units (e.g. shops, common areas, residential units, etc.), equipped with centralized local energy resources, such as: PV panels, ESS, heating system, ground-source heat pump, and individual electricity smart (controllable/plannable) loads such as appliances and PEVs charging stations. A centralized hot water storage provides heating to each unit and can be used as a controllable thermal storage.

The controllable variables of the system (i.e., the variables manipulated in order to control the behavior of the system) include the power absorption of the heat pump and the opening of the hot water flow valves at the single building units (which affect both the temperature of the water in the boiler and the air temperature in the single units

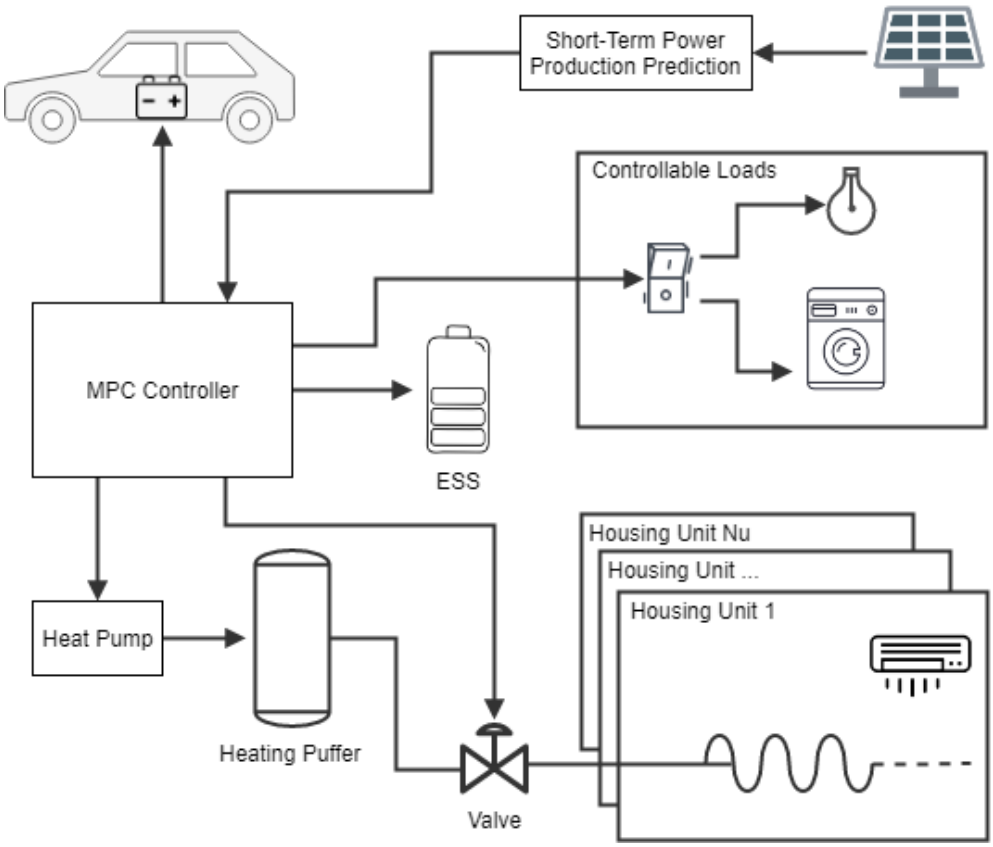

Fig. 3.1 Reference architecture of a smart building, consisting of several units heated by a centralized controlled system.

of the building), the start times of smart appliances, the charging and discharging power of the ESS and the PEVs (which, together with the heat pump control and the local power generation, affect the overall net power withdrawal of the building). The controlled variables of the system are the temperature of the hot water storage, the air temperature in the building's units, the SOC of the ESS, the PEVs' SOC and the overall building net power withdrawn from the grid. More in particular, the control objectives include: 1) to ensure comfort of the building occupants, in particular, to ensure that the set temperature in each unit (possibly different from unit to unit) is tracked when the inhabitant desires; 2) to minimize the electricity bill of the building, also in presence of complex electricity tariff models; 3) to minimize the power flow at the point of coupling of the building with the grid; 4) more in general, to be able to control the power flow at the point of connection with the grid, thus enabling the building e.g. to participate in DR programs; 5) to control the ESS SOC and the temperature of the hot water storage (which, together with the air temperature in the units, are

the state variables of the overall controlled system), so that they remain close to an appropriate reference value to guarantee sufficient upside and downside control margins for the system. The overall control problem formulation includes terms accounting for all of the above objectives, so that the resulting system will be able to work in all of the use cases resulting from prioritizing one or more of the control objectives over the remaining ones. The proposed problem falls into the category of EMPC, which is an optimization-based control technique in which the objective function has an economic or general performance based meaning (rather than a stabilizing meaning, as in classical MPC [58]). The objective function is quadratic (to penalize deviations of the controlled temperatures and SOC from the reference setpoints) and includes mixed-integer terms, also to be able to model and correctly price power flows from/to the grid. Constraints include user comfort and systems' technical constraints, and the dynamics equations of the system, which model the evolution of air temperature in the building's units, water temperature in the boiler, and SOC of the ESS and PEVs.

A real case study of a building with a micro grid in Italy is taken into account for the modelling, dimensioning and calibration of the system's equations. Simulation results are proposed to show how the performance of the building (in terms of the control objectives proposed above) can be optimized by leveraging synergies of the heat and electric resources available, by maximizing self-consumption of locally generated power, (heat and electric) storage (also including building's thermal inertia), modulation and shifting of loads to exploit tariff valleys, etc.

3.1.3 Chapter Organisation

The remainder of the chapter is organised as follows. Section 3.2 discusses the state of the art, providing an overview about the factors influencing the design of EMSs in buildings and the main approaches used to address the electric and thermal load management problem. Section 3.3 presents the control problem formalization. Section 3.4 presents the case study and reports the simulation results. Finally, Section 3.5 concludes the work.

3.2 State of the art and proposed contribution

In recent years, the topic of load control as a mean for enabling smart households and buildings to nearly zero energy consumption and DR functionalities has been the subject of intense research. Reviews of the many concepts and methods in EMSs design and DR problems can be found, e.g., in [59], [60] and [61]. For the sake of what follows, it is instrumental to remark that the load control problem is influenced by several factors, such as the type of loads [62] and generation [63], the pricing scheme [64], the occupancy of the household [65] and the weather [66]. All these factors result in a variability of performances, as testified by a variety of pilot projects running in Germany [67], Belgium [68], the Netherlands [69], etc.

As a matter of fact, the use of an EMS for automated participation in DR programs is largely recognized as fundamental in challenging scenarios, in which multiple sources of energy like local generators from RES and an ESS have to be managed, in combination with several classes of loads, such as smart appliances, PEVs, and in presence of complex electricity price structures such as Time Of Use (TOU), Day Ahead Pricing (DAP), Critical Peak Pricing (CPP), Real Time Pricing (RTP) [70], Multi-TOU and Multi-CPP [71]; such pricing schemes are introduced by retailers to achieve responsiveness of users and share the risk of market volatility. Furthermore, the problem complexity is emphasized by the need of considering the heating system as part of the problem, in order to achieve control on the overall building energy consumption.

Rule-based methods are widely used in practice in current EMSs because of their simplicity and low computation effort [72]. Though easy to implement, these methods may be oversimplified and do not allow to capture the near future behaviour of the process under control. Advanced EMSs typically rely on different forms of optimization, such as linear programming [73], binary linear programming [74], non-linear programming [75], Mixed Integer Linear Programming (MILP) [76], [77], [78], mixed-integer nonlinear programming [79] and multiparametric programming [80]. A detailed description of the above mentioned papers can be found in [81]. In particular MILP formulations are useful not only to manage loads characterized by different levels of controllability (on/off, continuous and semicontinuous controls), but also to handle nonlinearities introduced by the different prices that energy may have depending on its flow direction at the point of connection between the building and the grid [82]. In general, optimization is currently recognized to be effective when integrated in a MPC framework, due to its

intrinsic ability to handle multivariable and non-stationary control problems, also in presence of inaccurate models.

When the optimization problem is too complex to be solved leveraging standard methods, techniques such as genetic algorithms [83], particle swarm optimization [84] and metaheuristic tabu search [85] are used. Other approaches that can be found applied in this research area are the Lagrangian relaxation [86] and Benders decomposition [87]. In-depth reviews about the used optimization techniques can be found in [88] and [89]. Finally, also learning techniques have been applied in the context of residential EMSs, such as artificial neural networks [90] and reinforcement learning applied to Markov decision processes [91]. Interested readers may refer to [61] for an insight on artificial intelligence based EMSs.

Though the building heating system is commonly recognized as a potential source of flexibility, most of the related articles in literature have their special focuses with limited attention on the interactions among thermal equipment/requirements and other controllable electric loads for the purpose of overall nearly zero energy consumption and DR.

Some papers are available on the partial integration of controllable appliances and Heating, Ventilation and Air Conditioning (HVAC) systems, which mainly focus on Combined Heat and Power (CHP) management [92], [93], [94] and [95]. In [96] an optimization based strategy is proposed for integrating variable wind power with the CHP, while still satisfying customers' heating demand changes. In [97] it is shown how aggregates of thermostatically controlled loads (refrigerators, air-conditioners and space heaters) offer significant potential for the provisioning of frequency response services.

In [98], an EMPC strategy is proposed to shift the heating energy consumption according to the time varying energy price. The investigated heating system consists of a heat pump integrated with a hot water tank as active thermal energy storage; two optimization problems are integrated together to optimize both the heat pump electricity consumption and the building heating consumption. In [99], a similar problem is faced, with a focus on the use of price signals to defer the heating loads so that the profit of the retailer is maximized. Finally, in [100] a similar MPC strategy is proposed for the integration of thermal energy storage, HVAC and local RES. The last three papers, though taking into account limited scenarios in terms of managed equipment and resources, incorporate in a basic form some concepts which are at the basis of the present work, like the use of thermal flexibility as a mean for shaping

the net building electricity withdrawal, optimally exploiting local RES and providing power balancing services to market players.

In the present work, the performance of the building is optimized by leveraging synergies of the heat and electric resources. The main contribution of this work and consequent advancement beyond the state of the art is given by the completeness and detail of the scenario investigated (in terms of controlled equipment, control objectives and business cases enabled) and the proposition of a particularly advanced and again complete mathematical problem formulation in addressing combined and synergic management of heat and electric resources. The proposed solution achieves this by combining and extending two lines of research from the authors, one focused mainly on building thermal management [C5], and the second, developed in the series of works [74],[76],[81] dedicated to the control of electric building resources for the purpose of automated participation to DR programs. The analysis, and consequent design, of the MPC controller presented in [C5] was tailored by the authors specifically for the heating system control of a Nearly Zero Energy Building (NZEB), without considerations on potential synergies with power component of the building. This integration required a re-modeling of the thermal dynamics and considerations of the system (as described by (3.21)-(3.28) below), to cope with the increased complexity bought by the MILP formulation of the electrical subsystem. Regarding DR, a first contribution was given by the authors in [101] and [102], where the aggregation of housing units of a NZEB is envisaged for the participation of the building to DR programs. In those papers, the authors dealt with the control issue empirically, with discrete actions on the setpoints of the local controllers. The present work, combining the complex specifics of the proposed load controllers, as [81], to EMSs interfaced with HVAC units, and PEV charging stations, deals with a different approach to the combined control of electric and thermal loads, based on MPC, which enables integrated scenarios characterized by significant control flexibility and exploitation of the integration into the problem formulation of the system dynamics models.

Finally, the present work also includes, in Section 3.3.4, a discussion of the stability properties of the control system, something that is rarely found in literature for such rich problem formulations deriving from real application requirements.

3.3 Mathematical formulation

3.3.1 Objective function

As customary in EMPC, in this work a multi-objective function that captures the physical behaviour of the system and also its economical performance was considered:

$$V = \sum_{i=k}^{k+N-1} \Big\{ a_1 c_i + a_2 \sum_{u \in U} (T_{u,i}^{air} - \tilde{T}_{u,i}^{air})^2 + a_3 (T_i^{boiler} - \tilde{T}_i^{boiler})^2 + \\ + a_4 (SOC_i^{ess} - \tilde{SOC}_i^{ess})^2 + a_5 (P_i^{poc})^2 \Big\}, \tag{3.1}$$

in which k is the current time and $\{a_i\}_{i=1,\dots,5}$ are the weights of the different terms, dictating their relative importance in the multi-objective problem. The summation over N steps into the future represents the so-called "prediction horizon" of the EMPC, since it allows the controller to take actions accounting also for the predicted behaviour of the system. The predictions needed for the evaluation of a cost function with the structure of (3.1) are obtained thanks to the model of the system that is embedded in the controller itself and, for exogenous signals, from short-term predictions. Parameter N, the length of the prediction horizon, is tunable. The longer the prediction horizon, the higher is the complexity of the problem (the higher the number of variables of the problem). In a nominal setting (without any uncertainty), a longer prediction horizon brings the performance of the MPC algorithm closer to the optimum achievable value (i.e. the solution of an infinite-horizon open loop optimization problem). The adoption of a large N is however not advisable because of the uncertainty affecting the forecasts. Given the dynamics of the systems at study, a reasonable value for N is from some minutes to less than 24 hours (we chose $N = 3$ hours, which results in fast solving time and good performance).

EMPC follows the receding horizon paradigm introduced for MPC, as the open-loop problem of the minimization of (3.1) is repeated at every time step k, consequently applying to the system only the first element of the control sequence that optimized the objective function. At each iteration the optimization is done after having observed the system state, hence compensating any discrepancies between the predicted evolution of the system and its real behaviour. This combination of optimization and the iterative state feedback is what gives MPC/EMPC high performance and robustness.

We now briefly discuss (3.1). The first term accounts for the minimization of the overall electricity bill of the building, and is defined further below. The second term is related

to users' comfort and penalizes the deviations of the air temperature in each unit from a given set-point. Air temperature set-points are typically preset by the building manager; they are usually time-varying and they can be changed by the users via the thermostats in the units. The third and the fourth terms penalize, respectively, the deviations of the boiler water temperature and of the ESS SOC from given set-points. They are included to keep the boiler and the ESS close to a state in which they can exchange significant amounts of heat and electric energy (i.e. so to have significant upward and downward control margins). A reasonable choice for $\tilde{T}_i^{boiler}$ and $\tilde{SOC}_i^{ess}$ can be therefore 50% of the allowed temperature and SOC range. The last term penalizes high electric power flows at the point of connection with the grid. This term discourages the presence of excessive peaks in power absorption that may be induced by the minimization of the electricity bill sought by the first term in (3.1), when the energy price drops below a certain threshold, and accounts for equipment depreciation while also incentivising renewable power consumption.

3.3.2 Constraints

One of the main advantages of EMPC is its ability to handle constraints with ease, thanks to the receding horizon paradigm that leads to subsequent optimizations over a limited prediction horizon. Constraints below hold for all $i \in [k, k+N-1]$, $u \in U$, $e \in E$ (the sets of building units and PEVs controlled).

Definition of c_i

The term c_i in (3.1) is the cost/profit deriving from the energy absorbed or injected into the grid at time i. It is a nonlinear term because, to make the formulation of the problem more general and aligned with the reality, it is assumed here that the energy tariff depends on the sign of P_i^{poc}. That is, the cost for buying energy (i.e. when $P_i^{poc} \geq 0$) is assumed different in general from the remuneration received when power is injected into the grid (i.e. when $P_i^{poc} \leq 0$). Let us then denote the tariff at i with $C_i(P_i^{poc})$, to make explicit its dependence on P_i^{poc}. Given this additional notation, it is $c_i = \mathcal{T} P_i^{poc} C_i(P_i^{poc})$. The term can be replaced with an equivalent *linear* one adapting the approach explained in [81]. Boolean variables δ_i^1 and δ_i^2 are added,

with the following constraints:

$$\begin{aligned} \delta_i^1 + \delta_i^2 &= 1 \\ P^{poc,min}\delta_i^1 \leq P_i^{poc} &\leq P^{poc,max}\delta_i^2 \end{aligned} \tag{3.2}$$

It can be verified that, with the above positions, it is $\delta_i^1 = 1$ if and only if $P_i^{poc} \leq 0$ and $\delta_i^2 = 1$ if and only if $P_i^{poc} \geq 0$. Next, let us further denote with c_i^1 the remuneration price obtained at i when power is injected into the grid (i.e. when $\delta_i^1 = 1$, $P_i^{poc} \leq 0$) and with c_i^2 the energy cost when power is consumed from the grid (i.e. when $\delta_i^2 = 1$, $P_i^{poc} \geq 0$). With the above definitions and constraints, the cost at i can be written as $c_i = \mathcal{T} P_i^{poc}(\delta_i^1 c_i^1 + \delta_i^2 c_i^2)$. It is only left to transform the products $P_i^{poc}\delta_i^1$ and $P_i^{poc}\delta_i^2$ into a linear expression, which can be done by adding two additional real valued variables, z_i^1 and z_i^2, together with the following constraints:

$$\begin{aligned} P^{poc,min}\delta_i^1 \leq z_i^1 &\leq P^{poc,max}\delta_i^1 \\ P^{poc,min}\delta_i^2 \leq z_i^2 &\leq P^{poc,max}\delta_i^2 \\ P_i^{poc} - (1-\delta_i^1)P^{poc,max} \leq z_i^1 &\leq P_i^{poc} - (1-\delta_i^1)P^{poc,min} \\ P_i^{poc} - (1-\delta_i^2)P^{poc,max} \leq z_i^2 &\leq P_i^{poc} - (1-\delta_i^2)P^{poc,min} \end{aligned} \tag{3.3}$$

It can be verified that, with the above additional constraints, it is $z_i^1 = P_i^{poc}\delta_i^1$ and $z_i^2 = P_i^{poc}\delta_i^2$. Hence, finally, the cost term c_i can be rewritten in linear form as:

$$c_i = (c_i^1 z_i^1 + c_i^2 z_i^2)\mathcal{T} \tag{3.4}$$

Definition of P_i^{poc}

The electric power flow is defined by the following power balance equation.

$$P_i^{poc} = P_i^{hp} + P_i^{ev} + P_i^{ess} + P_i^{pl} + P_i^{npl} + P_i^{pv}, \tag{3.5}$$

where, in particular:

- P_i^{hp} is the power consumption of the heat pump;
- P_i^{ev} (the aggregated power consumption of the PEVs) is:

$$P_i^{ev} = \sum_{e \in E_i} P_{e,i}^{ev}, \tag{3.6}$$

where E_i is the set of PEVs connected at time i ($E_i := \{e \in E : S_e \leq k \leq F_e\}$) and $P^{ev}_{e,i}$ (the power from/to the single PEV) is defined as in (5)-(8) in [81]:

$$P^{ev}_{e,i} = P^{ev,c}_{e,i} + P^{ev,d}_{e,i}, \tag{3.7}$$

subject to

$$0 \leq P^{ev,c}_{e,i} \leq P^{ev,max}_{e} c^{ev}_{e,i} \tag{3.8}$$
$$0 \leq -P^{ev,d}_{e,i} \leq -P^{ev,min}_{e} d^{ev}_{i,e} \tag{3.9}$$
$$c^{ev}_{e,i} + d^{ev}_{i,e} \leq 1 \tag{3.10}$$

where $P^{ev,c}_{e,i}$ and $P^{ev,d}_{e,i}$ are, respectively, the charging and discharging power, $P^{ev,max}$ the maximum charging/discharging power, $c^{ev}_{e,i}$ a charging indicator variable (equal to 1 if PEV e is charging at time i) and $d^{ev}_{i,e}$ the Boolean discharging indicator variable;

- P^{ess}_i is similarly defined as

$$P^{ess}_i = P^{ess,c}_i + P^{ess,d}_i \tag{3.11}$$

subject to

$$0 \leq P^{ess,c}_i \leq P^{ess,max} c^{ess}_i \tag{3.12}$$
$$0 \leq -P^{ess,d}_i \leq -P^{ess,min} d^{ess}_i \tag{3.13}$$
$$c^{ess}_i + d^{ess}_i \leq 1 \tag{3.14}$$

with similar variables and parameters defined;

- P^{pl}_i (the aggregated consumption of plannable loads) is defined as in (3) in [81]:

$$P^{pl}_i = \sum_{l \in L_i} \sum_{j=j^1_l}^{j^2_l} P_{l,i-j+1} s_{l,j}, \tag{3.15}$$

where P^{pl}_i denotes the sum of the power consumed by the plannable loads at time i. Variable $s_{l,j}$ is a Boolean decision variable and it is $s_{l,j} = 1$ if the plannable load l is started at time j. P^{pl}_i is hence derived by considering the set of loads

L_i potentially active at i:

$$L_i := \{l \in L_k : S_l \leq i \leq min(F_l, k+N-1)\} \tag{3.16}$$

L_k in turn denotes the set of loads to be managed at time k, i.e. the set of loads that have been requested by the users before k and are not started yet:

$$L_k := \{l \in L : (R_l \leq k) \& (state_{l,k} = 0)\} \tag{3.17}$$

$state_{l,k}$ is the state of the load at k: equal to 0 if the load has not started yet, equal to 1 otherwise if the load is already in execution at k.

The update equation for the generic load is:

$$state_{l,i+1} = \begin{cases} 1, & if \quad state_{l,i} = 1 \\ 1, & if \quad s^*_{l,k} = 1 \\ 0, & if \quad s^*_{l,k} = 0 \end{cases} \tag{3.18}$$

where $s^*_{l,k}$ denotes the optimal value of $s_{l,k}$.

Coming back to (3.15), for each load i, the exact power consumption of the load at time i depends on the user preferences: j^1_l denotes the earliest possible starting time such that the load will have power consumption at i, while j^2_l is the last start time such that the load will contribute to power consumption at i. They are given by:

$$\begin{aligned} j^1_l &= max(max(k, S_l), i - N_l + 1) \\ j^2_l &= min(i, min(F_l, k+N-1) - N_l + 1). \end{aligned} \tag{3.19}$$

Exactly one starting time is decided for each load:

$$\sum_{i=S_l}^{F_l - N_l + 1} s_{l,i} = 1 \tag{3.20}$$

Dynamics of the boiler's water temperature (i.e. definition of T^{boiler}_i)

$$\begin{aligned} T^{boiler}_{i+1} =& T^{boiler}_i + \frac{\mathcal{T}}{M c_w} \left[\gamma P^{hp}_i - \sum_{u \in U} G_{u,i} c_w (T^{boiler}_i - T^{pipes}_{u,i}) - \alpha T^{boiler}_i \right], \\ T^{boiler}_k =& T^{boiler,k}, \end{aligned} \tag{3.21}$$

where γ is the Coefficient of Performance (COP) of the heat pump, a positive value (larger than one) that captures the power required to move heat from an energy source (e.g., water, air, ground) to the boiler. The rest of the equation is derived from a simple energy balance, as the control variable $G_{u,i}$, the heated water mass flow governed by the valve that regulates the heating of the housing unit u, governs the flow that transfers heat from the boiler to the housing unit u. The sum of all of these heat flows represents the total heat demand that the boiler should satisfy. The last term in (3.21) represents the heat loss of the boiler, governed by the factor $\alpha \geq 0$.

Due to the presence of the product between a control variable, $G_{u,i}$, and state variables, considering equation (3.21) as a constraint for the problem under study would cause a significant increase in computational complexity. For this reason, the constraint (3.21) was transformed into a liner equivalent with the following substitution:

$$\sum_{u \in U} G_{u,i} c_w (T_i^{boiler} - T_{u,i}^{pipes}) = \sum_{u \in U} \frac{(T_{u,i}^{pipes} - T_{u,i}^{floor})}{R_{floor}^{pipes}}. \tag{3.22}$$

The right hand side of (3.22) represents the heat exchanged between the heating pipes and the floors of the various housing units, utilizing the concept of thermal resistance. Under the assumption that no heat is lost in the distribution system, the two sides of (3.22) represent the same quantity, i.e., the heat flow that the boiler provides, overall, to the housing units. Equation (3.21) then becomes

$$\begin{aligned} T_{i+1}^{boiler} =& T_i^{boiler} + \frac{\mathcal{T}}{M c_w} \left[\gamma P_i^{hp} - \sum_{u \in U} \frac{(T_{u,i}^{pipes} - T_{u,i}^{floor})}{R_{floor}^{pipes}} - \alpha T_i^{boiler} \right], \\ T_k^{boiler} =& T^{boiler,k}. \end{aligned} \tag{3.23}$$

Due to substitution (3.22), the control variable in the equation is no longer $G_{u,i}$, but $T_{u,i}^{pipes}$ instead. This change of variable is legitimate, as it is possible to show that, under reasonable assumptions, there exists an invertible relation between the two.

Assuming a linear relation between the opening of the control valve and the mass flow $G_{u,i}$ through it, as well as ideal mixing condition in the pipes, one can write

$$T_{u,i}^{pipes} = T_{u,i}^{floor} + \frac{G_{u,i}}{G_u^{max}} (T_i^{boiler} - T_{u,i}^{floor}), \tag{3.24}$$

with G_u^{max} the maximum mass flow that the valves allow, making the substitution possible from a mathematical point of view. Moreover, to reflect the physical limitation

of the mass flow (i.e., $0 \leq G_{u,i} \leq G_u^{max}$) on the new control variable, two constraint are added to specify that the temperature of water in the pipes: i) cannot exceed the temperature of the boiler (that is reached when the control valve is completely open) and ii) is at least at temperature equilibrium with the floor (the case when the control valve is completely closed):

$$T_{u,i}^{floor} \leq T_{u,i}^{pipes} \leq T_i^{boiler}. \tag{3.25}$$

We detail in the following the dynamics of the various temperatures of interest characterizing each building unit.

Dynamics of the units' floor temperature (i.e. definition of $T_{u,i}^{floor}$)

$$\begin{aligned} T_{u,i+1}^{floor} &= T_{u,i}^{floor} + \frac{\mathcal{T}}{C^{floor}} \left[\frac{T_{u,i}^{air} - T_{u,i}^{floor}}{R_{floor}^{air}} + \frac{T_{u,i}^{pipes} - T_{u,i}^{floor}}{R_{floor}^{pipes}} \right], \\ T_{u,k}^{floor} &= T_u^{floor,k}, \end{aligned} \tag{3.26}$$

Equation (3.26) describes the effects of the control variable T_i^{pipes} on $T_{u,i+1}^{floor}$. The floor exchanges heat with both the pipes it contains and with the air of the unit. These exchanges are driven, respectively, by the temperature differences $T_{u,i}^{air} - T_{u,i}^{floor}$ and $T_{u,i}^{pipes} - T_{u,i}^{floor}$. The thermal resistances R_{floor}^{air} and R_{floor}^{pipes} determine the heat transfer velocity and depend on the materials (as all the other thermal resistances considered).

Dynamics of the units' air temperature (definition of $T_{u,i}^{air}$)

$$\begin{aligned} T_{u,i+1}^{air} &= T_{u,i}^{air} + \frac{\mathcal{T}}{c_{air}\rho_{air}V_u} \left[\frac{T_{u,i}^{floor} - T_{u,i}^{air}}{R_{floor}^{air}} + \frac{T_{u,i}^{walls} - T_{u,i}^{air}}{R_{air}^{walls}} \right], \\ T_{u,k}^{air} &= T_u^{air,k}, \end{aligned} \tag{3.27}$$

where c_{air} is the specific heat of the air and ρ_{air} the density, while V_u is the air volume in unit u. Equation (3.27) describes the heat exchanged between the air in the unit and the architectural elements. We did not include the effect of air ventilation and heat flows from powered appliances, due to their negligible effects on the heating system in winter days.

Dynamics of the units' walls temperature (definition of $T^{walls}_{u,i}$)

$$\begin{aligned} T^{walls}_{u,i+1} &= T^{walls}_{u,i} + \frac{\mathcal{T}}{C^{wall}}\left[\frac{T^{air}_{u,i} - T^{walls}_{u,i}}{R^{walls}_{air}} + \frac{T^{ext}_{i} - T^{walls}_{u,i}}{R^{ext}_{walls}}\right], \\ T^{walls}_{u,k} &= T^{walls,k}_{u} \end{aligned} \tag{3.28}$$

where T^{ext}_i is the external air temperature at time i, causing a heat loss for the building and a decrease in the ambient air temperatures, to be compensated by the heating controller.

Finally, operational constraints can be added, typically on the maximum or minimum allowed temperatures of operations, such as, in the considered case, $T^{boiler}_i > 38$ °C (to make sure there is always enough domestic hot water) and $T^{floor}_{u,i} < 35$ °C (as maximum floor temperatures is limited by comfort issues).

Dynamics of the ESS (i.e. definition of SOC^{ess}_i)

$$\begin{aligned} SOC^{ess}_{i+1} &= SOC^{ess}_{i} + \frac{\mathcal{T}\cdot(P^{ess}_i - \xi^{ess}|P^{ess}_i|)}{E^{ess}} 100, \\ SOC^{ess}_{k} &= SOC^{ess,k} \end{aligned} \tag{3.29}$$

The SOC is expressed in % of the full charge. The term $\xi^{ess}|P^{ess}_i|$ models the power losses associated with charging and discharging operation, and can be easily linearised considering that $|P^{ess}_i| = P^{ess,c}_i + P^{ess,d}_i$.

Dynamics of the PEVs (i.e. definition of $SOC^{ev}_{e,i}$)

$$\begin{aligned} SOC^{ev}_{e,i+1} &= SOC^{ev}_{e,i} + \frac{\mathcal{T}\cdot(P^{ev}_{e,i} - \xi^{ev}_e|P^{ev}_{e,i}|)}{E^{ev}_e} 100, \\ SOC^{ev}_{e,k} &= SOC^{ev,e,k} \\ SOC^{ev}_{e,F_e} &= SOC^{ev,e,F_e} \end{aligned} \tag{3.30}$$

where SOC^{ev,e,F_e} is the desired final SOC.

Variables range

The controlled variables must lie in a range between a minimum and a maximum allowed value.

$$\begin{aligned} T_{u,i}^{air,min} \leq T_{u,i}^{air} \leq T_{u,i}^{air,max} \\ T_i^{boiler,min} \leq T_i^{boiler} \leq T_i^{bolier,max} \\ SOC^{ess,min} \leq SOC_i^{ess} \leq SOC^{ess,max} \\ SOC_e^{ev,min} \leq SOC_{e,i}^{ev} \leq SOC_e^{ev,max} \end{aligned} \tag{3.31}$$

Notice that the constraints on power and SOC cannot be physically violated if min and max are 0% and 100% of the allowed range. Instead the constraints on temperature can be physically violated (they are soft constraints).

Variables nature

$$\begin{aligned} SOC^{ess}, SOC^{pev}, P, P^{ess} \in \mathbb{R} \\ P^{pl}, P^{pev}, P^{ess,d}, P^{ess,c}, P^{pev,d}, P^{pev,c} \in \mathbb{R} \\ T^{boiler}, T^{pipes}, T^{floor}, T^{air}, T^{walls} \in \mathbb{R} \\ s_l, c^{ess}, d^{ess}, c^{pev} \in \{0,1\} \\ d^{pev}, \delta P_j, z_j \in \{0,1\} \end{aligned} \tag{3.32}$$

3.3.3 Summary of the inputs and outputs of the control system, and of the overall MPC iteration

The MPC control signals are summarized in the nomenclature section, under the label "control variables" and mainly consist in power profiles for the active elements of the system (ESS, PEVs, heat pump, plannable loads) and the actuation profile of the heating system valves. The inputs needed from the controller are also reported in the nomenclature, under the "variables" label. Inputs are mainly given by the feedback on the current state of the system and the reference signals (reference temperatures, reference ESS SOC). All the other symbols introduced in the previous sections are parameters and auxiliary variables needed to build the MPC model.

The MPC control algorithm can be summarized as follows. At each time $k, k+1, ...$ do:

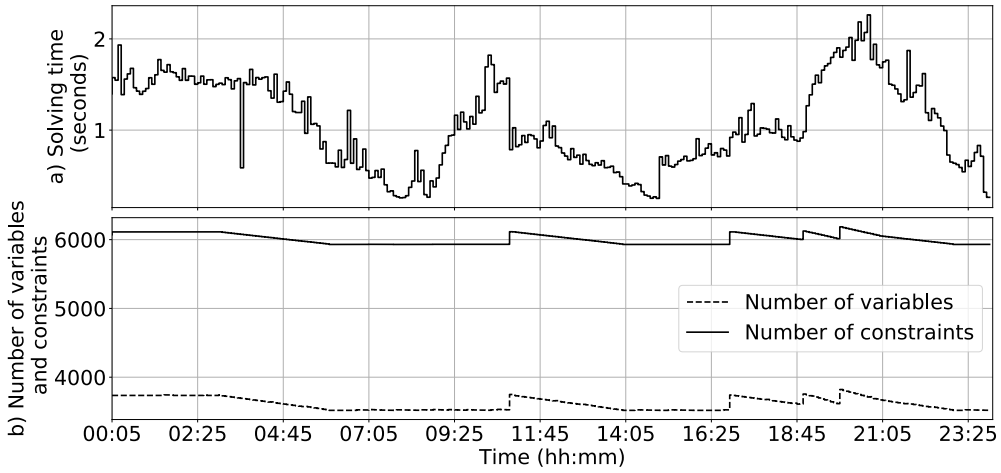

Fig. 3.2 Solving time (a) and number of variables and constraints for the optimization problem to be solved at each time (b) in Simulation 3.

1. Solve:

$$\begin{aligned} &\min (3.1) \\ &\text{subject to} \\ &(3.2) - (3.20),\ (3.23),\ (3.25) - (3.32) \end{aligned} \tag{3.33}$$

2. Apply to the system the first sample of the found optimal control variables.

3.3.4 Problem Complexity, Feasibility and Stability

Problem Complexity

Figure 3.2 reports, in the first subplot, the solving time of each of the MPC iterations done in Simulation 3 (the most complex one). The second subplot reports the total number of constraints and variables in each iteration. This gives an idea of the dimension of the MPC iterations and the time complexity. Time complexity is compatible with the real implementation of the controller (the solving time is well below the sampling time, 5 minutes).

Problem Feasibility

The constraints that can generate infeasibility are the ones reflecting real physical constraints or limitations existing in the controlled system, that is, (3.2) and (3.3) (limits of the power at the point of connection, P^{poc}); (3.8) and (3.9) (PEV power charging limits); (3.12) and (3.13) (ESS power charging limits); the thermal constraints (3.23), (3.26), (3.27), (3.28), which all have a similar mathematical structure, (3.25) on the valve opening limits; (3.29) and (3.30) (on the SOC of the ESS and the PEV), and finally the variables' box constraints (3.31). The remaining constraints do not reflect actual limitations, but are instead needed to define auxiliary variables (see e.g. (3.4)) or to enforce logical constraints (see e.g. (3.14) and (3.20)).

In general, the MPC iteration (3.33) will be infeasible whenever there is an issue of scarcity of resources within the building. For example, (3.2) and (3.3) are violated in case of overload, (3.8) and (3.9) in case there is not sufficient time to recharge the vehicle or the ESS, (3.27) in case there is not enough time and/or energy available to heat the building satisfying the minimum required temperature, etc. In this respect, some considerations have to be made: first of all, proper dimensioning of the thermal and electrical systems should make the occurrence of overloads very rare. Secondly, notice that, event assuming the building to be in a potential overloading condition (e.g. cold winter day with numerous demanding load request, such as many concurrent EV recharging requests), the proposed method makes sure that a feasible solution is returned, provided that it exists (this is because it is based on constrained optimization, i.e., it directly embeds the constraints which may lead to infeasibility).

When instead constraints cannot be satisfied, different strategies can be adopted, such as: selective shedding of loads, possibly based on a shedding priority list (see e.g. [103]), relaxation of (soft) constraints (such as the ones on temperature bounds), as discussed, e.g., in [104], Section 1.2.5. By adopting the latter strategy for example, the soft constraints will be violated every time there are no sufficient resources to satisfy them, and the violation will be the least necessary to keep the problem feasible.

A second question concerns *recursive feasibility*, i.e., the assurance that, if the MPC problem is feasible at a given time, then it will remain feasible for all the successive iterations. Also in this case, from a theoretical point of view, the presented problem cannot be guaranteed to be recursive feasible. To see this, consider the generic MPC iteration at a given time k and assume it is feasible (feasibility depending on the value of all the problem parameters and inputs in the prediction window $[k, k+N-1]$). The

feasibility or infeasibility of the following MPC iteration at $k+1$ will depend on the value of the problem inputs at time $k+N$ (i.e., the new time interval entering the prediction window), which could be such that the iteration is infeasible. As explained e.g. in [104], recursive feasibility could be ensured by proper design of additional terminal constraints and terminal cost terms (denoted in the following as "terminal ingredients"), and with the inclusion of assumptions on the exogenous signals (i.e., the external temperature T^{ext}, the renewable power profile P^{pv}, the power profiles P^{pl}, P^{ev} associated to the user requests, etc.). However, on one hand, this could be a very complex task and, on the other hand, ensuring recursive feasibility would be obtained at the expense of a decrease of the feasibility region of the problem (due to the inclusion of the terminal ingredients, which could over constraint the problem). For this reason, the implementation of dedicated infeasibility management strategies (as the two ones outlined in the above), appears a practical and convenient solution.

MPC Stability

A full and comprehensive analysis of the stability properties of the presented control system is beyond the scope of this work and constitutes future reserach possibilities. The analysis is made complex in particular by the presence of Boolean variables and of the exogenous signals. In the following, the theoretical properties that differentiate the present problem from standard MPC (for which many stability results are known, see e.g. [104]) are highlighted , and a sketch of a stability proof in a simplified yet meaningful scenario is provided, with punctual references to the specialised literature of interest. To start, lets denote with $l(x_i, u_i)$ the stage cost in (3.1) (i.e., $V = \sum_{i=k}^{k+N-1} l(x_i, u_i)$). In this section, x_i denotes the vector grouping all the state variables of the system at i (the state of charge variables SOC^{ess} and all the controlled temperature variables, T^{air}, T^{floor}, T^{wall}, T^{boiler}, in the building units), while u_i denotes the control variables, which ultimately reduces to P_i^{poc}, as explained in the following. We consider a setting in which all the exogenous signals are constant, because, in the opposite case, the state trajectories would depend on the characteristics of those signals, and the stability problem would be properly framed as a problem of stability of trajectories, rather than stability of states (an even more complex stability question, that could be tackled in future works based on the research on periodic MPC, see e.g. [105]). Notice further that no Boolean variables appear in the objective function (3.1), which explicitly depends on the control variable P^{poc} only (which in turn depends only on P_i^{hp}, being all the remaining variables in (3.5) assumed constant). Therefore, we reduce to the analysis

of a simplified problem which includes the objective function (3.1), and the dynamics equations (3.23), (3.26), (3.27), (3.28), (3.29), which are collectively denoted generically as $x_{i+1} = f(x_i, u_i)$, plus all the remaining constraints rewritten in general form as $x_i \in \mathrm{X}$ and $u_i \in \mathrm{U}$, with X and U compact sets. A first aspect which differentiates the formulation in this work from standard MPC is as follows. Denoting with (x^s, u^s) the *best feasible steady-state control-input pair* (i.e. the state-control pair that minimizes l, such that $x^s = f(x^s, u^s)$, $x^s \in \mathrm{X}$ and $u^s \in \mathrm{U}$), one has that $l(x, u) \leq l(x^s, u^s)$ for some feasible (x, u) not corresponding to any equilibrium pair (i.e. the best feasible steady-state control-input pair is not in general the minimizer of the stage cost function, and there are other feasible, non-equilibrium input-state couples with smaller associated stage cost). This fact, which is the characterizing aspect of economic MPC [106], complicates the stability study, since the objective function cannot be directly used as Lyapunov function for the stability proof [106]. In addition, no specific terminal ingredients are introduced in the formulation, in order not to reduce the feasibility region of the algorithm, as discussed in the previous subsection, and this further complicates the stability analysis (a typical terminal constraint considered which ensures stability under mild conditions is $x_N - x^s = 0$, i.e., to require the state at the end of the control window to coincide with the least-cost equilibrium state, x^s). A theoretical result present in literature and of interest for the present case is illustrated in [107], Theorem 4.1, on the practical stability of EMPC without terminal ingredients. The theorem states that, under certain assumptions, outlined below, the EMPC scheme is such that the equilibrium x^s is *practically asymptotically stable* (see [107], Definition 4.1), that is, the state trajectories converge to a neighbourhood of x^s. The same theorem proves that the neighbourhood shrinks to x^s as $N \to \infty$ (incidentally, the same theory also proves recursive feasibility of the EMPC control - here addressed, in a simplified setting). The key assumptions needed to establish the above result are: i) a *strict dissipativity* of the MPC iteration, ii) *exponential reachibility* of x^s, and iii) an additional n_x*-step reachibility* condition of the Jacobian linearization of system $f(x, u)$ (with n_x the dimension of x). These three assumptions are defined in details in [107], Definition 3.2, Assumption 4.2 and Assumption 4.3, respectively. Given the system at study, assumptions ii) and iii) are satisfied provided that the system is correctly dimensioned (e.g., so that it is physically possible to steer the state to x^s, as requested by ii)), while Proposition 4.3 in [108] presents mild conditions (the presence of a *Slater condition*) under which assumption i) is satisfied, in a problem setting to which the case discussed in this work can be reduced (control of linear systems and a linear-quadratic stage cost).

As explained above, in the full, complex scenario, the controller will have to find an optimal trade-off between its objectives, and the resulting feasible operating point (i.e., the state trajectories) will be in general time-varying, according to the characteristics of the exogenous signals.

3.4 Validation

In this section, the building EMS is validated via simulation. The section discusses the simulation cases study, the implementation of the algorithm and a set of validation simulations.

3.4.1 Implementation of the algorithm

The overall MPC problem presented in this work has been coded using the Julia programming language (https://julialang.org/) [109], version 0.7. The quadratic optimization problem constituting the MPC iteration has been modeled using the Julia library JuMP [110] and solved with Gurobi (http://www.gurobi.com/). The simulations have been performed on a Window 10 machine, 64 bit, equipped with an Intel I7-5500U CPU 2.40 GHz and 8 GB RAM.

3.4.2 Case study and simulation setup

A real case study of a smart building under construction in Italy, is considered. The architecture of the micro grid is an innovative fully electric system. The building is completely gas free as all systems are electrically supplied. The suggested micro grid consists of an innovative electric-power system characterized by the following: 1) a single point of connection to the grid; 2) a low-voltage main switch board (MSB) to supply both the common services (heating, elevators, etc.) and the units; 3) a common PV installed on the roof of the building and connected to the MSB; 4) a distribution power system from the MSB for all common technical building systems (TBS); 5) a feeder distribution from the MSB supplying each unit by an independent feeder in a radial scheme; 6) a common ESS with a capacity of 100 kWh and a maximum power of 10 kW is connected to the micro grid. The building is composed of 20 units, with a peak demand of 50 kW. The micro grid supplies: the units of the building (lighting and

sockets), the smart loads of the units (one dishwasher and one washing machine for each unit), the central heating system consisting in a heat pump, a charging station for 5 PEVs. The main simulation parameters are as follows: 5 PEV recharging requests and 31 load requests are considered during the day in order to create a realistic power demand profile and to demonstrate the ability of the controller to manage loads while satisfying user preferences. Heating (HVAC) and domestic hot water (DHW) systems are composed of: 1) a central heating and cooling station with electricity-driven heat pumps; 2) heating, cooling, and DHW distribution system for each unit; 3) a central thermal storage; 4) a metering satellite (SC) for each unit with meters. Heating energy demand of the building is limited by the thick insulation of the envelope. The sampling time $\mathcal{T}$ is equal to 5 minutes. The micro grid requires a building automation control system to improve its effectiveness, and the electricity prices used to calculate the cost c_i in (3.4) were taken from the intra-day market repository of "Gestore dei Mercati Energetici" (GME) and were relative to an average day of January 2019 in Italy. The technical building systems are flanked by a building automation control system with a main server able to host a supervisory system.

In the following, to simulate realistic operation conditions and to account for disturbances and modeling uncertainties, a zero-mean Gaussian noise is added to the state feedback taken by the controller at each time, i.e., in particular to the various temperature measurements taken (i.e., to the feedback of the units' temperature and boiler temperature). The variance of the added Gaussian noise is $0,19$ °C, meaning that in the 99% of the cases, the added noise will be less than $0,5$ °C.

3.4.3 Simulation 1: Baseline scenario with standard control

The first simulation considers standard control of the building, in order to provide a baseline and a benchmark case for evaluating, in the following simulations, the increase in performance assured by the proposed control scheme. The control assumed here is: i) constant charging of the vehicles, at the maximum power allowed at the time of charging; ii) plannable loads are started at the first feasible time; iii) on/off control of the temperature (i.e., heating at maximum level when the temperature is outside of a band of 1 degree around the reference temperature); iv) the storage is always off.

Figure 3.3 reports the resulting power flow at the point of connection with the grid. As it could be expected, the power flow is not smooth and exhibits significant variations when plannable loads or PEV charging start (in particular, the 20 kW spikes in the

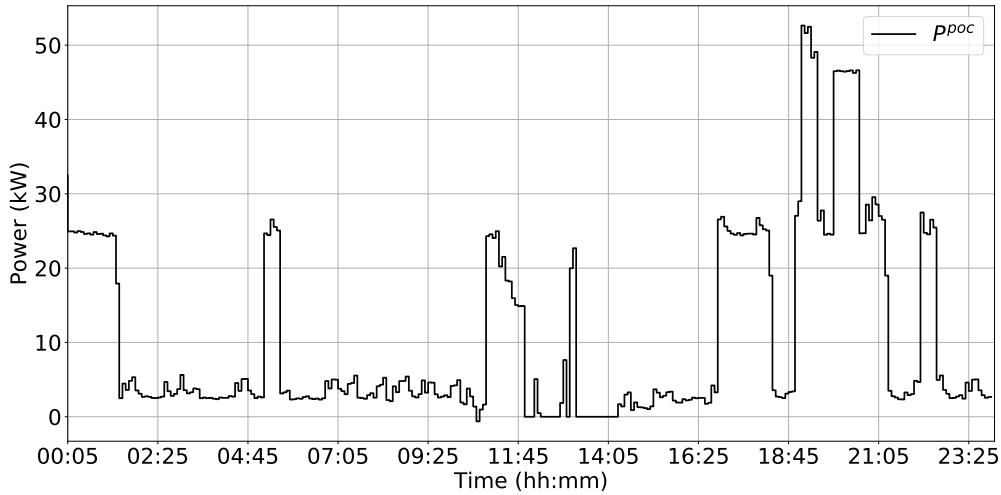

Fig. 3.3 Simulation 1 - power flow at point of connection with the grid.

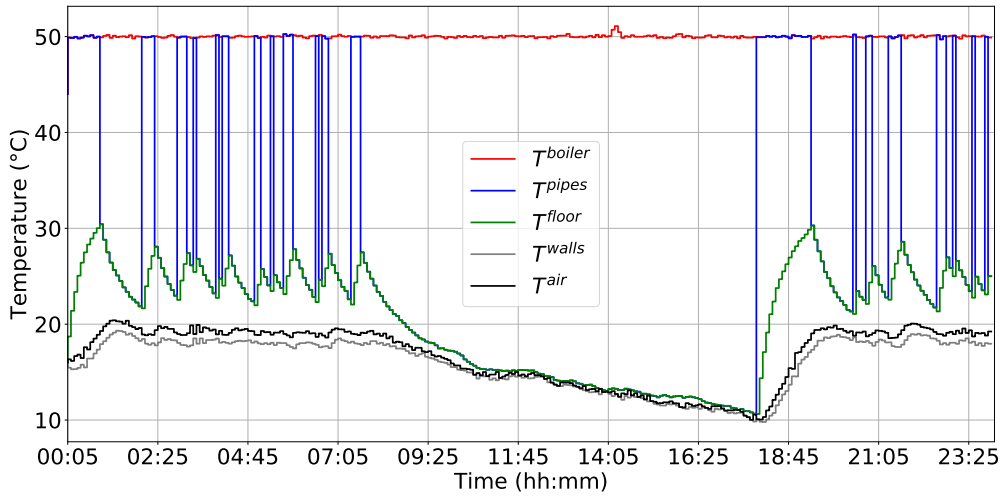

Fig. 3.4 Simulation 1 - temperatures in building unit 1.

figure correspond to the uncontrolled PEV charging processes). Figure 3.4 reports the temperature profile in the first building unit (temperature shows a similar pattern in the other units). The pattern of on-off control is recognised. Table 3.2 reports a more quantitative evaluation of the simulation for one sample unit (unit 1), in terms of: i) the average temperature error in the unit ($avg(err_{T^{air}})$) and ii) the standard deviation of the temperature error ($std(err_{T^{air}})$), both as a proxy of the achieved user comfort; iii) the standard deviation of the power flow at the point of connection ($std(P^{poc})$, as a measure of the smoothness of the flow); iv) the total energy flowing at the point of connection with the grid ($\int P^{poc}$, the lower, the better); and v) the electrical power peak ($max(P^{poc})$, the lower, the better). After a baseline scenario has been established,

Table 3.2 KPI of simulation 1 (baseline scenario).

$avg(err_{T^{air}})$	$std(err_{T^{air}})$	$std(P^{poc})$	$\int P^{poc}$	$max(P^{poc})$
1.4 °C	1.9 °C	12.34 kW	248.17 kWh	52.64 kW

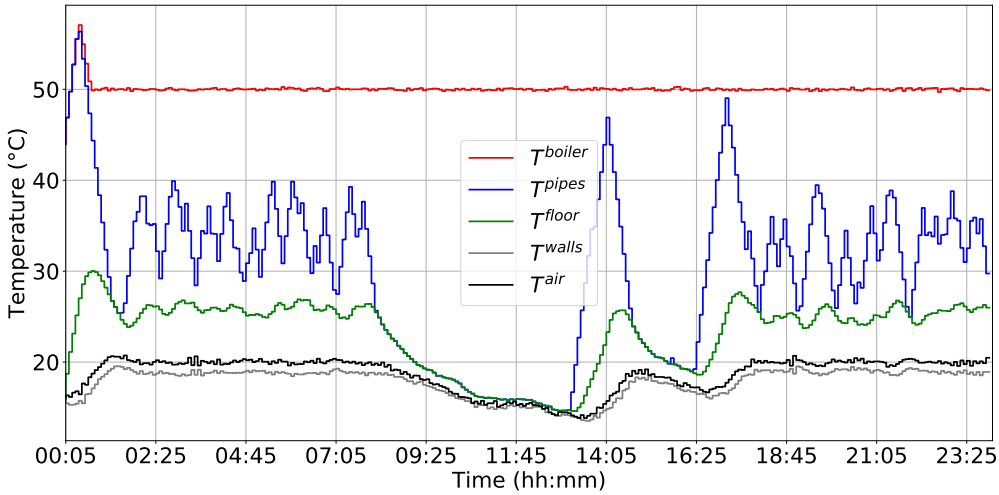

Fig. 3.5 Simulation 2 - temperatures in building unit 1.

in the following sections the performance of the proposed controller is showcased under different scenarios of growing complexity and completeness.

3.4.4 Simulation 2: Pure thermal management

This simulation reports the performance of the controller when its only goal is to best manage thermal loads in the building and satisfy the associated user preferences. To this end, $a_1 = a_4 = a_5 = 0$ is selected in (3.1) (the other weights are set to 1). PEVs and plannable loads are still started manually, as in the previous simulation. Similarly, the ESS is not activated. This is done in order to show how the controller performs when the only load to manage is the thermal one.

Figure 3.5 shows the evolution of the temperature in unit 1. It shows that accurate tracking of the reference temperature is achieved. The power profile at the point of connection is not shown here as it is almost the same as the one in Simulation 1. Table 3.3 reports the key performance indicatorss (KPIs) for this simulation (the peak power reduction and the cost saving compared to Simulation 1 are also reported in this case). Temperature tracking performance is excellent, while it is not surprising that the two other KPIs have values comparable with those in Simulation 1.

Table 3.3 KPI of simulation 2 (pure temperature control).

$avg(err_{T^{air}})$	$std(err_{T^{air}})$	$std(P^{poc})$	$\int P^{poc}$	$max(P^{poc})$	Peak Reduction	Saving
0.36 °C	0.7 °C	12.39 kW	249.20 kWh	52.57 kW	0,13%	0,31%

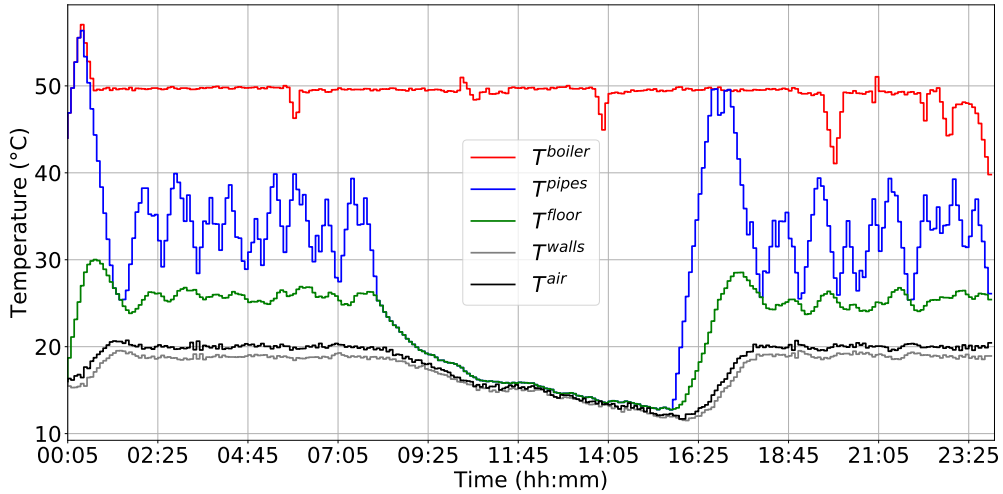

Fig. 3.6 Simulation 3 - temperatures in building unit 1.

3.4.5 Simulation 3: Joint thermal/electrical load management

In this section all the terms in the objective function are enabled (all weights in (3.1) are set to one).

Figure 3.7 reports the profile of the power flow between the building and the grid. By comparing it with Fig. 3.3 it is seen that a much smoother flow is achieved, even if in (3.1) there was no objective that directly incentivised its smoothness. The sudden drop and consequent spike that appears in the figure is mainly related to the ESS state of charge depletion and subsequent recovery, in combination with a particularly favorable power pricing point and low demand related to EVs. These results are mainly due to the power-peak reduction objective (the fifth term in (3.1)) and the predictive nature of the controller. Figure 3.6 and 3.8 report the temperature profiles in unit 1 and in unit 11 (two representative units in the building). The two units have different occupancy times, and the controller ensures excellent performances in both cases. Notice how the controller manages the thermal storage property of the building by "pre-heating" the structures in advance of the hours when temperature tracking has to be ensured. The above qualitative behaviour of the controller is confirmed by the quantitative KPIs resulting from the simulation, reported in table 3.4.

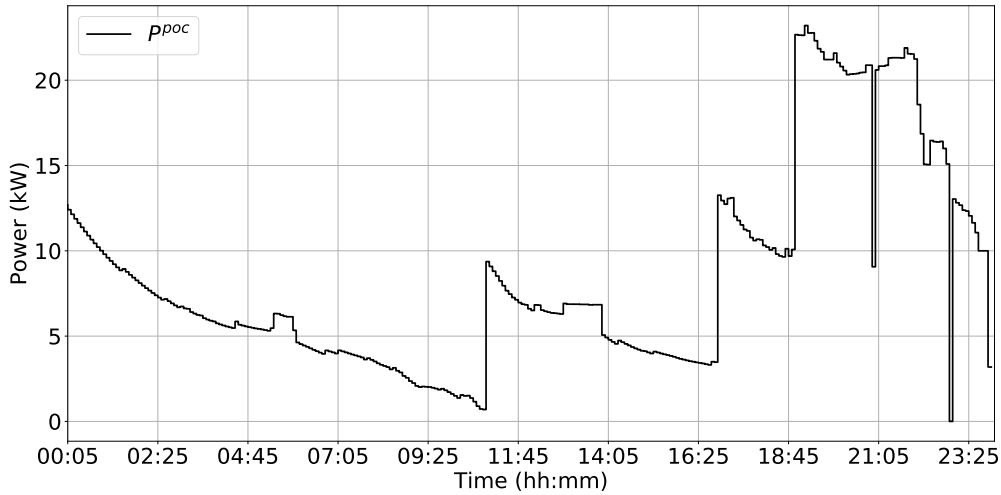

Fig. 3.7 Simulation 3 - power flow at point of connection with the grid.

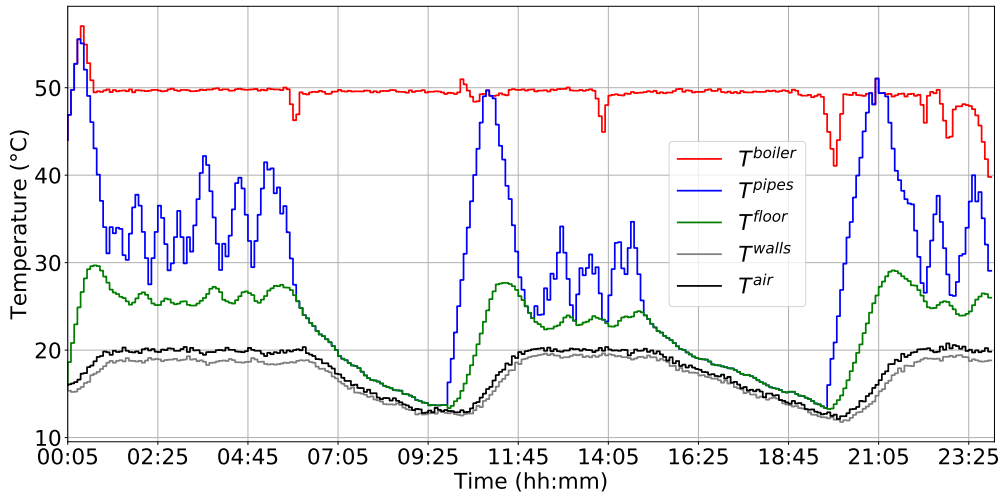

Fig. 3.8 Simulation 3 - temperatures in building unit 11.

It is seen that the controller significantly smooths the power flow at the point of connection with the grid and reduces its peaks, while it also ensures the same temperature control performance as in the previous case and achieves a significant reduction of the energy cost. Moreover, a halving of the peak power withdrawn from the grid is achieved. This is done by intelligent management of the ESS, of the recharging process of the PEVs, of the thermal storage of the building and of the start time of the plannable appliances. Also, the amount of energy flowing at the point of connection is significantly reduced as well, thanks to the self consumption of locally produced PV power.

Table 3.4 KPI of simulation 3 (full control).

$avg(err_{T^{air}})$	$std(err_{T^{air}})$	$std(P^{poc})$	$\int P^{poc}$	$max(P^{poc})$	Peak Reduction	Saving
0.36 °C	0.7 °C	6.25 kW	205.9 kWh	23.2 kW	-55,93%	-19,35%

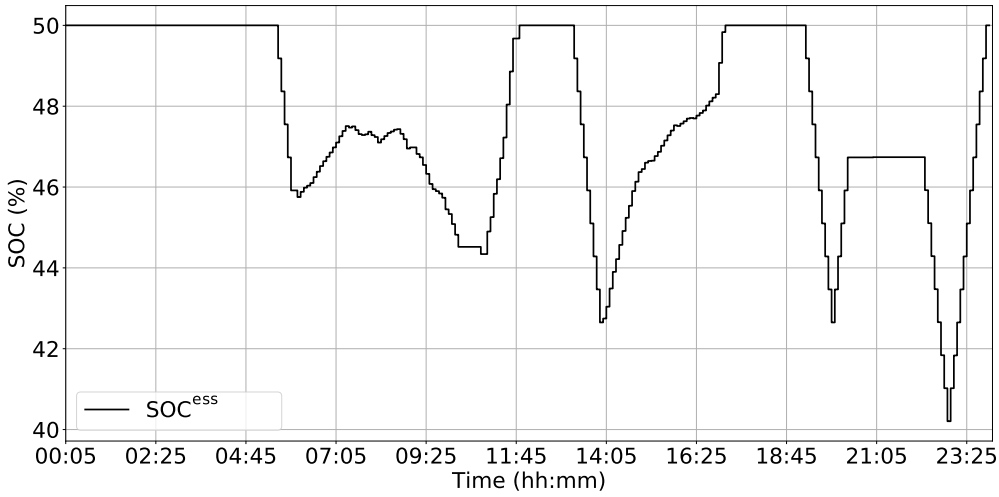

Fig. 3.9 Simulation 3 - evolution of the ESS state of charge.

To showcase how the controller manages loads' flexibility, Fig. 3.9 reports the evolution of the SOC of the ESS. It is seen how the ESS is controlled to contribute to optimizing the building's energy management, while keeping the evolution of the SOC close to the reference value (50%), so to ensure adequate control margins.

Finally, Fig. 3.10 reports the hot water flow valve opening position for unit 1, to show that the proposed control does not introduce undesired chattering behaviour on the actuators. Rate of change constraints and or specific terms in the objective function (to penalise excessive variations in the actuators' inputs) can be added in general to avoid that the resulting control cause high fatigue on the actuators.

3.4.6 Reaction to demand side management signals

Buildings will be in the near future one of the main source of flexibility in the local flexibility electricity markets. Aggregators will pool coalitions of buildings to create a critical mass sufficient to participate in local markets. Price and volume signals will be exchanged between the aggregator and the buildings as a tool to explore the flexibility available at the building side to modify the demand profile.

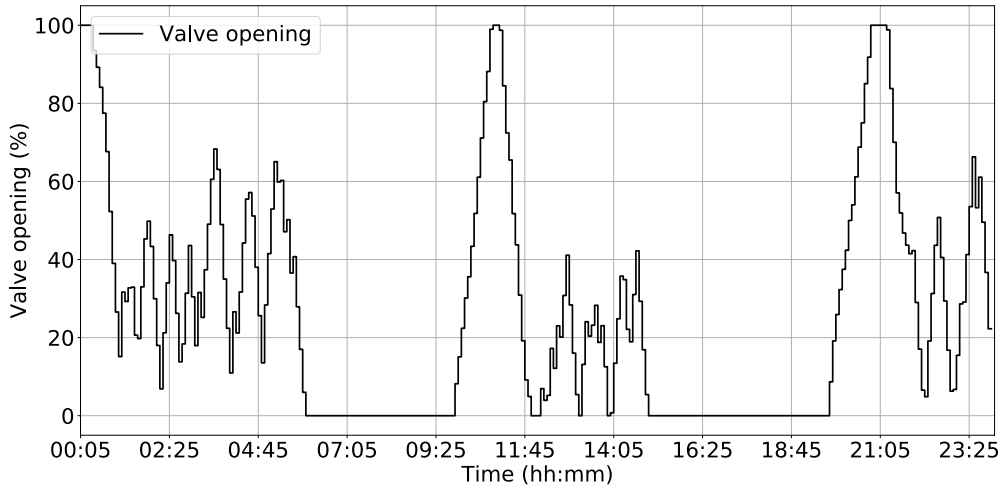

Fig. 3.10 Simulation 3 - Opening position of the hot water valve in unit 1.

The proposed algorithm is naturally capable to re-program the management of the building's load in order to react to a *price signal* from the aggregator, that is, a variation of the price of the energy in a given time interval. Volume signals can be considered as well, that is, requests of reduction/increase of the power flow in a given temporal interval.

3.4.7 "Gentle service degradation"

The proposed controller can cover emergency scenarios and for example ensure quality of experience preservation or gentle service degradation in presence of disruption events, like the temporal loss of the main supply from the grid. The proposed controller is capable to react to notification of the interruption of the power supply from the grid. The controller is capable of reacting as well to abrupt interruption of main power supply, however it would have naturally reduced control margin.

3.4.8 Tuning of the controller parameters

The quantitative performance and the behaviour of the building will vary depending on the selected parameters of the controller, principally the 5 weights in the objective function. The above simulations were meant to show the performance of the controller in different scenarios and were carried out with an empirical selection of the weights of the objective function. One way to tune the proposer controller is to test the

performance in typical operating conditions of the building and varying the weights of the objective function. The KPIs examined in the above sections will form a Pareto frontier. By having these charts the building manager would be able to select the weights depending on his/her optimization goals and priorities (e.g. cost optimization or power peak reduction).

3.5 Conclusion

This work has presented a model predictive control based energy management algorithm for managing heating and electricity loads in a smart building. The managed loads include a heat pump, an electricity storage, electric vehicles and flexible loads. The control objective has been to minimize costs of energy consumption while ensure that the technical constraints of the system are met and the user preference are satisfied, in terms of thermal comfort and execution of loads according to the schedule set by the user (notably including control of electric vehicles). Explicative simulations and KPIs have been presented to show the effectiveness of the controller in optimising resources in a complex and realistic scenario.

Future works will regard the integration of the proposed control scheme with additional control devices, such as air conditioners, and with the description of other relevant physical phenomena, such as radiant and convective loads. More extensive simulations will also be conducted, spacing over different seasonal conditions, in order to fully validate the approach and obtain a complete performance assessment before being validated on real equipment.

Chapter 4

Feedback Linearization-based Satellite Attitude Control with a Life-Support Device without Communications

This chapter reports the results of a research collaboration with the Department of Guidance Navigation & Control Engineering of Thales Alenia Space Italia regarding attitude control and the design of a control for the operation of a life-support device for orbiting satellites. The activities related to the collaboration led to the following publication:

[J2] *Giuseppi, A. Pietrabissa, S. Cilione, and L. Galvagni, "Feedback linearization-based satellite attitude control with a life-support device without communications,"Control Engineering Practice, vol. 90, pp. 221–230, 2019.*

This work develops a control strategy for the life-support device so that it can be attached to an orbiting satellite to extend its operational life. The objective is met in such a way that the original satellite keeps operating without communications between the two systems (also valuable for energy efficiency). The case in which the original satellite is equipped with a feedback-linearization based controller is considered and the control law for the life-support is developed with the same methodology, obtaining a compensating control which recovers the performance of the original control strategy. Simulations validate the approach considering a real case study in various scenarios.

Nomenclature of the chapter

Main Symbols	
$\times, \cdot, \otimes$	Vector and scalar products, quaternion cross product
C	Control horizons of Model Predictive Control
I_n	$(n \times n)$ identity matrix
J_B	Moment of Inertia (MOI) tensor
I_x, I_y, I_z	Principal MOIs
K	Gain for momentum unloading
L_w,L_{wn}	Angular momentum of the reaction wheels for the satellite and the life-support system
$L_f h(x)$	Lie derivative of $h(x)$ along f
m_1, l_1, J^1	Mass, edge length and MOI tensor for the satellite
m_2, l_2, J^2	Mass, edge length and MOI tensor for the life-support system
P	Prediction horizon of Model Predictive Control
q, q_{13}, q_4	Quaternion representation of the attitude, vector and scalar components of the quaternion
q^{ref}	Reference quaternion
Q	Error weight matrix of the controller
R	Control weight matrix of the controller
T	Time constant of the reference
$x = [\text{q } \omega]^T$	State vector
δ	Error quaternion representation of the attitude
τ	External torques
τ_w,τ_{wn}	Torques applied by the reaction wheels of the satellite and of the life-support system
ω	Angular velocity of the inertial reference frame relative to the satellite measured in its coordinates

4.1 Introduction

Prolonging the satellite operation life is becoming a crucial topic in spacecraft research, as it is related to the reduction of space debris, which is one of the main issues that modern space systems is facing [111]. In fact, modern satellite mission planning should take into account not only orbital and attitude control, but also the disposal of the

device once its operation life is elapsed. For this reason, this work envisages the development of a control strategy for the operation of a "life-support" system that can be attached to an orbiting satellite to either extend its operational life once its propellant, or in general the lifetime of some of its components, has been depleted or to provide the satellite with new, updated, equipment, with immediate economic benefits for the spacecraft operator.

The considered life-support system is equipped with a set of reaction wheels, the typical actuator in attitude control problems, and a set of thrusters that may replace the depleted ones of the satellite for the required procedure of angular momentum unloading [112]. The work develops an attitude control law for the life-support satellite, based on feedback linearization, and tests it by implementing mission controllers based on both Linear Quadratic Regulator (LQR) and Model Predictive Control (MPC), controlling the coupled system composed by the original and the life-support satellites.

It will be shown that the proposed control strategy does not require communication between the life-support system and the satellite, with clear advantages in terms of dedicated interfaces and energy efficiency.

The work is organized as follows: Section 4.2 contains a brief review of the state of the art on attitude control related problems and highlights the main contributions; Section 4.3 discusses the preliminary notions necessary to introduce the problem of attitude control; Section 4.4 introduces the problem of feedback linearization, as it is the theoretical backbone of the work; Section 4.5 formulates the attitude control problem for the joint satellite and life-support system, highlighting the control scheme for a typical satellite mission and proposing a nested control strategy that utilizes feedback linearization and LQR or MPC; Section 4.6 shows the results of numerical simulations, based on a real case study, to validate the proposed approach in various operative scenarios; finally, Section 4.7 draws the conclusions and outlines some future researches.

4.2 State of the Art and Contribution of the Work

The problem of attitude control has always been considered one of the most crucial fields of research in space engineering for its relation to satellite operations [113]. Several types of attitude controllers have been proposed, ranging from sliding-mode ones [114] to robust PID [115] and passivity-based ones [116]. In most of the works reported

in this review, the satellite has been modeled as a rigid body and, consequently, the differential equations describing the attitude evolution have been derived from basic kinematics and dynamics rules. Starting from a rigid-body model, one of the most used control techniques in satellite attitude control is feedback linearization, as, e.g., in [117] and [118]. In both papers, the authors consider the satellite system model described in the Byrnes-Isidori *normal form* [119], derived by the measurement of the so-called "vector components" of the quaternion representation of the satellite attitude (see Section 4.3).

Several other papers, as [120] and [121], utilize the quaternion representation to develop their control strategy discussing, respectively, stability related results for large angle maneuvers, derived from Lyapunov's theory, and optimal LQR-based control results. Regarding stability, a significant contribution was given by [122], discussing the global properties of several control laws for quaternion represented attitude problems.

The advantages and shortcomings of the quaternion representation have been discussed extensively in [123], [113] and [124], and such representation is commonly found also in attitude control problem even outside the field of space systems, as in [125] and [126]. In this work, the so-called *error quaternions* (see Section 4.3) are used, which, for example, were also considered in [127] to tackle the earth observation problem by means of a PID control.

Few papers in the literature deal with the operational life extension of a satellite by means of an external support system, and instead typically focus on fault-tolerant control solutions, as [128]–[130]. In [128], a smooth state-feedback control is developed to asymptotically stabilize a satellite, whose operation was compromised by a faulty thruster, around the desired attitude. In [129], a sliding mode control is proposed, taking into account the limitation on the maximum torque and momentum of the reaction wheels available on the satellite. In [130], the authors presented an adaptive controller based on fuzzy logic and backstepping to obtain robust performances with respect to uncertainties in inertia estimation, actuator faults and external disturbances.

Finally, several moment unloading techniques have been studied in order to desaturate the reaction wheels – that are the main control actuators in most of the works presented so far – using either magnetorquers or thrusters to get the external torque required to perform the task while maintaining the desired attitude, as in [131] and [132].

With respect to the mentioned literature, the main contributions of this work are the following ones:

- the modelling and control of a two-body satellite system, formed by the composition of the original satellite and a life-support device able to extend its operational life, and the definition of a control scheme able to assure the feedback linearization of the whole system, not relying on information exchanges between the original satellite and the support system;
- the development of a control law, not reliant on information exchanges between the original satellite and the support system, based on feedback linearization, able to assure asymptotic convergence to the desired attitude, even if the actuators of the original satellite are out-of-order;
- the formulation of the attitude tracking problem for the two-body system in terms of LQR and MPC control, by means of error quaternion modelling;
- the integration of a reaction wheel moment unloading control to assure the stability of the system and the feasibility of the control.

4.3 Preliminaries on Satellite Attitude Control

Quaternions are a convenient way to model the attitude of a rigid body, as they are not affected by singularities such as Euler angles. A unitary quaternion is defined as a 4×1 unitary vector q:

$$q = \begin{bmatrix} q_{13} \\ q_4 \end{bmatrix} \in \mathbb{R}^4$$

where $q_{13} \in \mathbb{R}^3$ takes the name of "vector component" of the quaternion q and $q_4 \in \mathbb{R}$ is its "scalar component".

Some useful operators are defined as follows:

- the cross product between two quaternions q^1, q^2, defined as

$$q^1 \otimes q^2 = \begin{bmatrix} q_4^2 q_{13}^1 + q_4^1 q_{13}^2 - q_{13}^1 \times q_{13}^2 \\ q_4^1 q_4^2 - q_{13}^1 \cdot q_{13}^2 \end{bmatrix}; \tag{4.1}$$

- the cross product between a (3×1)-vector x and a quaternion q

$$x \otimes q = \begin{bmatrix} x \\ 0 \end{bmatrix} \otimes q = [x\otimes]\, q;$$

- the operator

$$[q\otimes] = \begin{bmatrix} q_4 I_3 - [q_{13}\times] & q_{13} \\ -q_{13}^T & q_4 \end{bmatrix},$$

where I_n denotes the $(n \times n)$ identity matrix and

$$[q\times] = \begin{bmatrix} 0 & -q_3 & q_2 \\ q_3 & 0 & -q_1 \\ -q_2 & q_1 & 0 \end{bmatrix}; \tag{4.2}$$

- the operator

$$\Xi(q) = \begin{bmatrix} q_4 I_3 + [q_{13}\times] \\ -q_{13}^T \end{bmatrix} = \begin{bmatrix} q_4 & -q_3 & q_2 \\ q_3 & q_4 & -q_1 \\ -q_2 & q_1 & q_4 \\ -q_1 & -q_2 & -q_3 \end{bmatrix}.$$

Finally, the model of the rigid spacecraft with state vector $x = [\mathrm{q}\ \omega]^T$ is derived, as customary in the literature [123], as

$$\begin{cases} \dot{q} = \frac{1}{2}\ [\omega\otimes]\, q \\ \dot{\omega} = J_B^{-1}\left[\tau - \tau_w - \omega \times (J_B\omega + L_w)\right] \\ \dot{L}_w = \tau_w \end{cases}. \tag{4.3}$$

in which: ω is the angular velocity vector, that represents the rotational velocity of the inertial reference frame with respect to the body frame in the latter coordinates; q is the satellite attitude expressed in quaternions; τ_w and L_w are the torques applied by the reaction wheels and by their angular momentum, respectively; the disturbance τ models external forces, including the ones provided by the thrusters of the satellite; J_B is the Moment of Inertia (MOI) tensor, expressed in the rigid body reference frame.

Note that, other than the kinematic equation of q, the model (4.3) includes the dynamical description of ω, which is governed by τ_w and L_w.

4.4 Preliminaries on Feedback Linearization

In the Multi Input Multi Output (MIMO) case, the problem of feedback linearization consists in finding a control law u such that the nonlinear system

$$\begin{cases} \dot{x} = f(x) + \sum_{i=1}^{m} g_i(x)\, u_i \\ y = h(x) \end{cases}, \tag{4.4}$$

with m inputs and c outputs and where

$x(t) = \in \mathbb{R}^n$,

$u(t) = \in \mathbb{R}^m$,

$y(t) = \in \mathbb{R}^c$,

$f(x) = [f_1(x), \ldots, f_n(x)]$,

$h(x) = [h_1(x), \ldots, h_c(x)]$,

is reduced, around the origin x_0, to a system with a linear input-output map.

For square MIMO systems, the problem of feedback linearization around x_0 has a solution if and only if the system has a vector of relative degree $[r_1 \ldots r_m]$ in x_0, with $\sum_{i=1,\ldots,m} r_i \leq n$ [119] and the decoupling matrix

$$\Delta(x) = \begin{bmatrix} L_{g_1} L_f^{r_1 - 1} h_1(x) & \ldots & L_{g_m} L_f^{r_1 - 1} h_1(x) \\ \vdots & \ddots & \vdots \\ L_{g_1} L_f^{r_m - 1} h_m(x) & \ldots & L_{g_m} L_f^{r_m - 1} h_m(x) \end{bmatrix} \tag{4.5}$$

is nonsingular in x_0.

The control input that realizes the feedback linearization assumes the form

$$u = \Delta(x)^{-1} (\nu - a(x)), \tag{4.6}$$

with

$$a(x) = \begin{bmatrix} L_f^{r_1} h_1(x) \\ \vdots \\ L_f^{r_m} h_m(x) \end{bmatrix} \tag{4.7}$$

and ν being the control signal that governs the linearized system.

The resulting feedback-linearized system (4.4) in normal form is then

$$\begin{cases} \dot{\xi} = \mathrm{A}\xi + \mathrm{B}v \\ \dot{\eta} = z(\xi,\eta) \\ y = \mathrm{C}\xi \end{cases}, \tag{4.8}$$

where $z(\xi,\eta)$ is a smooth function, $A = diag(A_1, A_2, A_3)$, $B = diag(B_1,B_2,B_3)$, and $C = diag(C_1,C_2,C_3)$, are block-diagonal matrices with

$$A_i = \begin{bmatrix} 0 & 1 \\ 0 & 0 \end{bmatrix}, B_i = \begin{bmatrix} 0 \\ 1 \end{bmatrix}, C_i = \begin{bmatrix} 0 & 1 \end{bmatrix}, \quad i = 1,2,3.$$

4.5 Problem Formulation and Control Design

This section presents the feedback-linearized satellite model (section 4.1), the model of the overall satellite and life-support system (section 4.2) and the proposed controller (section 4.3).

4.5.1 Feedback-Linearized Satellite Model

Following [117], this work considers $x = [q,\omega,L_w]^T$, $y = q_{13}$ and $u = \tau_w$ as state, output and input vectors of the system (4.3), respectively, and relies on the following assumption for the model:

Assumption 4.1. In the derivation of the normal form, this work will consider the model (4.3), neglecting the dynamics of L_w (i.e., the third equation of (4.3)), and will assume L_w to be a measured disturbance.

Note that the measure of L_w will be directly utilized (see Section 4.3) to compute dedicated control actions to assure the stability of the dynamics of L_w – separating

the problems of moment unloading and attitude control is a standard practice. In alternative to Assumption 4.1, the dynamics of L_w could be considered as included in the zero dynamics and, as long as its stability is guaranteed by the mentioned dedicated controller, the results of the following sections would still hold. In this work, it was chosen to neglect the dynamics of L_w for the sake of simplicity of the presentation.

With the selected inputs and outputs, the vector of relative degree is $r = [2 \;\; 2 \;\; 2]^T$ and, assuming, as customary, that the diagonal inertia tensor is $J_B = \mathrm{diag}\,(I_x, I_y, \; I_z)$, the decoupling matrix (4.5) is written as

$$\Delta\,(x) = -\begin{bmatrix} \frac{q_4}{2I_x} & -\frac{q_3}{2I_y} & \frac{q_2}{2I_z} \\ \frac{q_3}{2I_x} & \frac{q_4}{2I_y} & -\frac{q_1}{2I_z} \\ -\frac{q_2}{2I_x} & \frac{q_1}{2I_y} & \frac{q_4}{2I_z} \end{bmatrix}, \tag{4.9}$$

whose determinant is

$$\det\left(\Delta\,(x)\right) = -q_4 \frac{\left(q_1^2 + q_2^2 + q_3^2 + q_4^2\right)}{8 I_x I_y I_z}, \tag{4.10}$$

which annihilates for $q_4 = 0$. It is then possible to feedback-linearize the system via the control (4.6) for $q_4 \neq 0$, under the following transformation:

$$\begin{bmatrix} \xi \\ \eta \end{bmatrix} \tag{4.11}$$

yielding to the normal form (4.8), from which it follows $\ddot{q}_{13} = v$.

Noting that the unitary properties of the quaternions is preserved over the attitude dynamics, if q_1, q_2 and q_3 converge to appropriate values, q_4, and hence the zero-dynamics, does not diverge.

4.5.2 Satellite with Support System Model

To control the system formed by the composition of the original satellite with the life-support system, it is needed to model the rigid body representing the overall system and to develop a suitable control scheme that should be deployed into the life-support device.

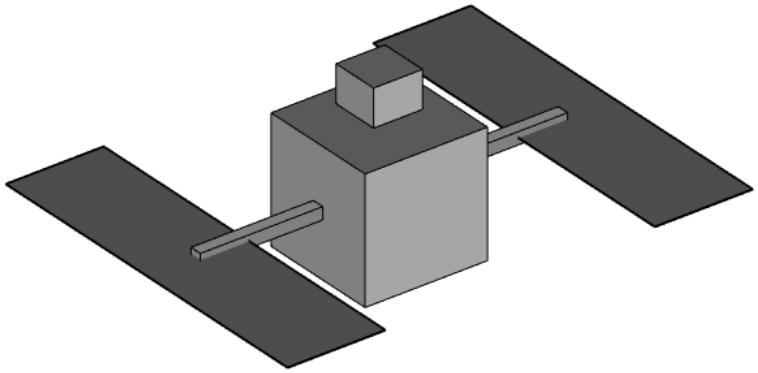

Fig. 4.1 Satellite and Life-Support device connected

The system depicted in Figure 4.1 is considered, in which:

- the coupling between the life-support device and the satellite is rigid and no joint motion is involved;
- the support system is equipped with reaction wheels for the proper attitude control and with thrusters to perform moment unloading, whereas the satellite may have depleted the propellant and/or have out-of-order actuators;
- the Center Of Mass (COM) of the satellite is aligned with respect to the z-axis of the rigid body reference frame of the support device; the x and y axes of the two reference frames are assumed to be parallel.

The original satellite and the support system are modelled as two cubes with mass m_1 and m_2 and edges of length l_1 and l_2, respectively. Let $m = m_1 + m_2$ and let J^1 and J^2 be the MOI tensors of the two bodies, expressed in their rigid body reference frames. To characterize the dynamics of the composite system, it is needed to derive its inertia tensor utilizing the Huygens-Steiner – or parallel axis – theorem [133]:

$$J_n = J_c + m[\left(r^T r\right) I_3 - r r^T], \tag{4.12}$$

where r is the displacement vector between the COM and the new point where the momentum J_n is calculated, while J_c is the momentum with respect to the COM.

Let z_2 be the z-coordinate of the COM of the support system in the reference frame of the satellite. In the composite body reference frame, the coordinates of the COMs of the two original systems are

$$\mathrm{CO}M_1 = \begin{bmatrix} 0 \\ 0 \\ -\frac{m_2 z_2}{m} \end{bmatrix}, \ \mathrm{CO}M_2 = \begin{bmatrix} 0 \\ 0 \\ \frac{m_1 z_2}{m} \end{bmatrix},$$

respectively. Thanks to (4.12), the inertia $J^2_{\mathrm{CO}M_1}$ of the support system evaluated in $\mathrm{CO}M_1$ is derived as:

$$J^2_{\mathrm{CO}M_1} = J^2 + m_2 \begin{bmatrix} {z_2}^2 & 0 & 0 \\ 0 & {z_2}^2 & 0 \\ 0 & 0 & 0 \end{bmatrix}.$$

It is now possible to evaluate the inertia tensor $J^{\mathrm{Tot}}_{\mathrm{CO}M_1}$ of the composite body about $\mathrm{CO}M_1$ as follows:

$$J^{\mathrm{Tot}}_{\mathrm{CO}M_1} = J^1 + J^2_{\mathrm{CO}M_1}.$$

Finally, the MOI of the composite body in its reference frame is

$$J^{\mathrm{Tot}} = J^{\mathrm{Tot}}_{\mathrm{CO}M_1} - m \begin{bmatrix} \left(\frac{m_2 z_2}{m}\right)^2 & 0 & 0 \\ 0 & \left(\frac{m_2 z_2}{m}\right)^2 & 0 \\ 0 & 0 & 0 \end{bmatrix}.$$

Recalling that $z_2 = \frac{l_1}{2} + \frac{l_2}{2}$, it follows:

$$J^{\mathrm{Tot}} = J^1 + J^2 + \begin{bmatrix} m_2 \left(\frac{l_1+l_2}{2}\right)^2 & 0 & 0 \\ 0 & m_2 \left(\frac{l_1+l_2}{2}\right)^2 & 0 \\ 0 & 0 & 0 \end{bmatrix} - \begin{bmatrix} \frac{{m_2}^2 (l_1+l_2)^2}{4m} & 0 & 0 \\ 0 & \frac{{m_2}^2 (l_1+l_2)^2}{4m} & 0 \\ 0 & 0 & 0 \end{bmatrix}. \tag{4.13}$$

The system dynamics is then unchanged, save for the new value of the MOI and the presence of new reaction wheels, whose angular momentum, L_{wn}, follows $\dot{L}_{wn} = \tau_{\mathrm{wn}}$.

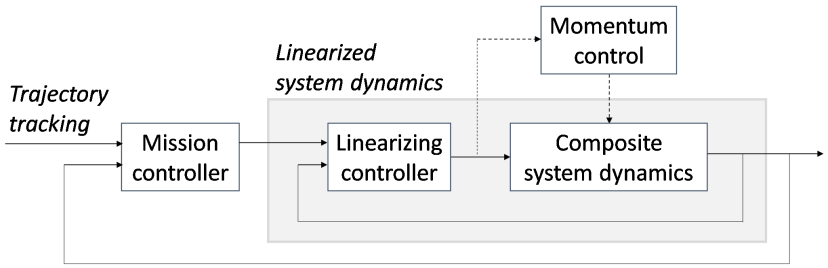

Fig. 4.2 Satellite attitude control via feedback linearization

4.5.3 Proposed Controllers

Overall Control System

Figure 4.2 reports a typical scheme for the satellite attitude control problem, applied to the composite system. An outer control loop, governed by a mission controller, is responsible for the tracking of the reference attitude trajectory, while an internal control loop is responsible for the feedback linearization – which simplifies the task of the mission controller. An additional controller is in charge of managing the momentum built up into the reaction wheels, typically by unloading it according to heuristic laws to avoid their saturation.

The following subsections are going to detail each one of the proposed controllers.

Feedback Linearization of the composite system

It is assumed that the original satellite is controlled by a scheme analogous to the one reported in Figure 4.2, i.e., the satellite is already equipped with a feedback-linearizing controller, which, at the time of the connection, is still active. After the attachment, it follows that

$$\ddot{q}_{13} = a\left(q, L_w + L_{\text{wn}}, \omega, J^{\text{Tot}}\right) + \Delta(J^{\text{tot}}, q)u,$$

where $a(\cdot)$ and $\Delta(\cdot)$ are, with a slight abuse of notation, as in (4.7), (4.9).

To apply feedback linearization, the required input of the overall system, u_{req} , would have to be set to

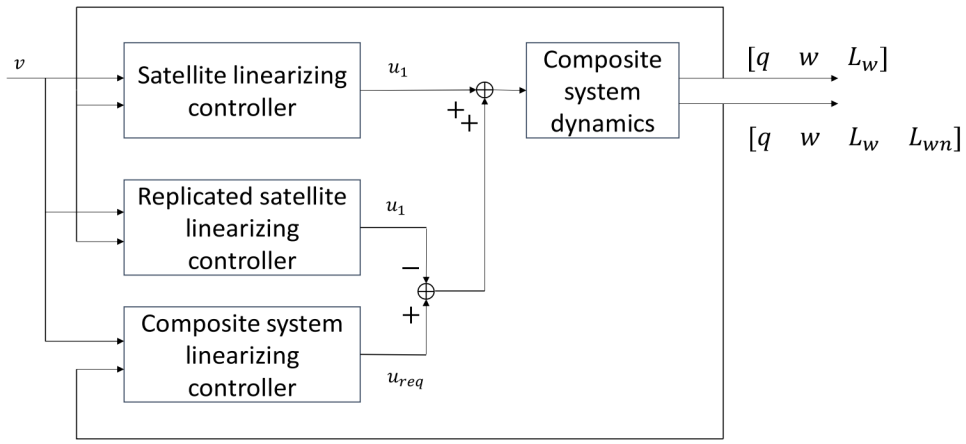

Fig. 4.3 Feedback-linearizing controller

$$u_{\text{req}} = \Delta\left(J^{\text{Tot}}, q\right)^{-1}\left[v - a\left(q, L_w + L_{\text{wn}}, \omega, J^{\text{Tot}}\right)\right], \tag{4.14}$$

but this control law does not consider that the original satellite is already applying, unaware of the presence of the life-support device, its feedback linearization law:

$$u_1 = \Delta\left(J^1, q\right)^{-1}\left[v - a(q, L_w, \omega, J^1)\right]. \tag{4.15}$$

In order to provide a solution for the support of an operative satellite (e.g., in a mission that desires to update the scientific instruments of the satellite), one may think of cancelling the original linearizing controller, actuated by the sole satellite, and of substituting it with a new linearizing controller for the overall system, as depicted in Figure 4.3.

This approach trivially requires the support device to compute a replica of $u_1$and subtract it from u_{req} before applying it to the system. With this solution, besides the mission control command v, the support system needs the sensor readings regarding q, ω and L_w. Even if the former two signals, q and ω, are the same for the satellite and the support system, there is still the signal L_w that must be communicated by the satellite to the support system. This need of communication affects the feasibility of the proposed scheme for all the satellites which are not already provided with an appropriate communication channel.

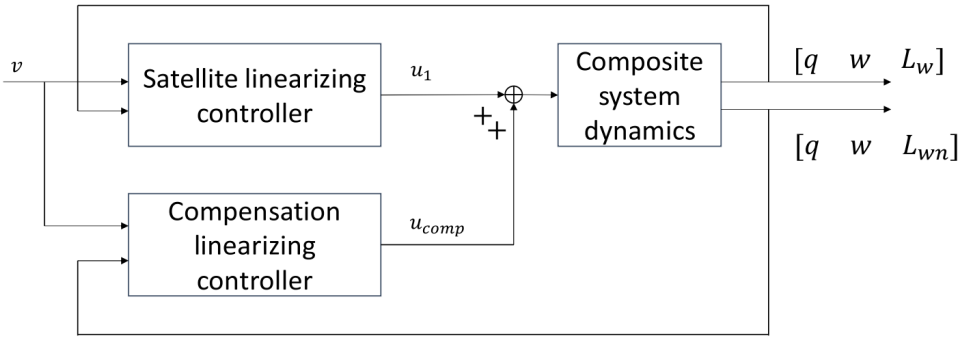

Fig. 4.4 Feedback-linearizing compensation controller

To overcome this problem, it will be shown in the following that it is possible to design a *compensation* controller which directly computes an additive control action that compensates the presence of u_1 without having to explicitly compute u_1 on-line. In other words, to obtain the objective of not interfering with the control logic of the original satellite, the controller compensates the linearizing control u_1 with an additional action u_{comp} in such a way that u_{req} is recovered as $u_{\text{req}} = u_1 + u_{\text{comp}}$ (see Figure 4.4). It will also be shown that the compensation control action will not require the measures of L_w.

Let us consider the control scheme of Figure 4.4 and let the feedback-linearizing compensation torque be

$$u_{\text{comp}} = u_{\text{req}} - u_1, \tag{4.16}$$

which, substituting (4.14) and (4.15), becomes:

$$u_{\text{comp}} = \Delta\left(J^{\text{Tot}}, q\right)^{-1}\left[-a(q, L_w + L_{\text{wn}}, \omega, J^{\text{Tot}}\right] + \; - \Delta\left(J^1, q\right)^{-1}\left[v - a\left(q, L_w, \omega, J^1\right)\right]. \tag{4.17}$$

Considering the model (4.3), with reaction wheels and without external forces applied, setting

$$\tau_w = -J^1\widetilde{u} - \omega \times (J^1\omega + L_w),$$

in which $\widetilde{u}$ is a *proxy control* introduced in the following analysis, it follows $\dot{\omega} = \widetilde{u}$.

By defining $Q(q)$ as the vector including the first three rows of the matrix $\frac{1}{2}\Xi(q)$, one has that

$$\ddot{q}_{13} = Q(q)\ \dot{\omega} + Q(\dot{q})\ \omega,$$

Therefore, by setting

$$\widetilde{u} = \dot{\omega} = \ Q(q)^{-1}(v - Q(\dot{q})\omega),$$

the feedback linearized system $\ddot{q}_{13} = v$ is recovered.

The feedback linearization torque is then

$$u_1 = t_w = -J^1 Q(q)^{-1}(v - Q(\dot{q})\omega) - \omega \times \left(J^1\omega + L_w\right). \tag{4.18}$$

Substituting (4.18) and (4.14) into (4.16) gives us the final expression for the feedback-linearizing compensation torque:

$$u_{\text{comp}} = -\left(J^{\text{tot}} - J^1\right) Q(q)^{-1}[\nu - Q(\dot{q})\omega] - \omega \times \left[\left(J^{\text{tot}} - J^1\right)\omega + L_{\text{wn}}\right], \tag{4.19}$$

which has the same expression of u_1 in equation (4.18), with $\left(J^{\text{tot}} - J^1\right)$ as inertia term and L_{wn} as the momentum of the wheels.

Remark 4.1. The control law (4.19) does not depend on L_w: the support system does not require information regarding the momentum of the reaction wheels of the original satellite, and the only exogeneous signal it receives is ν, which could even be obtained directly by the measurements of q if the support is equipped with a replica of the outer loop controller. This independence is one of the most significant advantages of the proposed control scheme of Figure 4.4, as it does not require any communication interfaces between the two systems and can hence be deployed to satellites already in orbit. As a by-product, the communication-less control scheme is valuable also from the energy-saving viewpoint.

Remark 4.2. The control law (4.19) considers that the satellite is still operating its reaction wheels, and, thus, its dynamics is already feedback-linearized. In this scenario,

the support is needed, e.g., to provide new thrusters or scientific equipment. In case the life-support system has been attached to a satellite that can no longer operate its reaction wheels, the support system oversees the whole control actuation, including the feedback linearization of the complete system. To this end, if the reaction wheels of the satellite are no longer operative, the support system has to directly apply the control law (4.14) with null L_w.

Mission Controller

This section analyses the design of the outer loop controller, which operates on the linearized composite satellite system and whose task is to let the system track a reference trajectory. It is worth remarking that the proposed control scheme is, in general, independent of the implemented mission controller. In fact, any control law designed for a feedback linearized satellite is compatible with the proposed scheme, as the life-support compensates its effect on the system dynamics by providing an additional control action.

To apply standard tracking control algorithms for linear systems, a change of the coordinates of the system (4.8) is needed, as the typical satellite mission does not require to drive the system to its origin but, instead, requires the tracking of a reference trajectory $q^{\text{ref}}(t)$. A trivial solution for the tracking problem would then be the annihilation of the error $e(t) = q_{13}^{\text{ref}}(t) - q_{13}(t)$, which, under feedback linearization (4.14), would lead to

$$\ddot{e}(t) = \ddot{q}_{13}^{\text{ref}}(t) - \nu(t) = \widetilde{\nu}(t),$$

where $\widetilde{\nu}(t)$ is a *proxy control* that governs the error dynamics. The limit of this approach is that the system has no control over the convergence value of q_4, meaning that, without proper considerations, the satellite may attain an attitude that is different from the desired one.

It is then convenient to write the system in the so-called error quaternions coordinates [123], defined as

$$\delta = \begin{bmatrix} \delta_{13} \\ \delta_4 \end{bmatrix} = q \otimes \ q^{0^{-1}},$$

where ${q^0}^{-1}$ is the inverse o the quaternion q^0, yielding

$$\delta_{13} = \Xi(q^0)q,$$
$$\delta_4 = {q^0}^T q.$$

The error quaternion represents the rotational error between the quaternion q and an arbitrary quaternion q^0. By choosing a reference trajectory in the error quaternion coordinates $\delta_{13}^{\text{ref}}(t)$ that converges to $[0\ 0\ 0]^T$ (i.e., $q^{\text{ref}}(t) \to q^0$), the tracking error is defined as

$$\delta_e(t) = \delta_{13}(t) - \delta_{13}^{\text{ref}}(t). \tag{4.20}$$

Due to the particular choice of q^0, annihilating this error asymptotically drives the system to either the identity quaternion $I = [0,0,0,1]^T$ or to $-I$, which represent the same attitude, avoiding then the ambiguity of a formulation based on the error e. For a fixed q^0, the dynamics of the system becomes

$$\dot{\delta} = \dot{q} \otimes {q^0}^{-1} = \frac{1}{2}\left[\omega(t)\otimes\right] q(t) \otimes {q^0}^{-1} = \frac{1}{2}\left[\omega(t)\otimes\right]\delta, \tag{4.21}$$

i.e., the dynamics (4.21) of the system in the error quaternion coordinates is the same as in the original coordinates.

Remark 4.3. Considering that the dynamics of δ and q are the same, all the results of Section 4.1 and Section 4.3 still hold with a trivial coordinate substitution. In particular, the feedback linearization feasibility condition, derived from the nonsingularity of (4.9), translates to $\delta_4(t) \neq 0$. The boundness of $\delta_4(t)$, yields that any controller that annihilates δ_e stabilizes the two-body systems and achieves tracking.

Mission Controller based on Linear Quadratic Regulator (LQR) The LQR is one of the most used controllers for linear systems and relies on the definition of a quadratic cost function that summarizes the control objectives and that usually takes the form:

$$J = \frac{1}{2}\int_{t_0}^{\infty} \left[{\delta_e}^T Q(t)\,\delta_e + \widetilde{\nu}^T R(t)\,\widetilde{\nu}\right] \mathrm{dt}, \tag{4.22}$$

where $Q(t)$ and $R(t)$ are positively definite matrices, representing, respectively, the weights assigned to the error values and to the control effort.

In the standard LQR [134], the control action minimizing (4.22) is available in closed-form:

$$\widetilde{\nu} = -R^{-1}B^T K\delta_e, \tag{4.23}$$

where K is the solution of the Riccati equation associated with the LQR problem.

The control action to implement in (4.15) is then:

$$\nu = \ddot{\delta}_{13}^{\text{ref}} + R^{-1}B^T K\delta_e. \tag{4.24}$$

The main limitation of LQR is that the optimization does not take into account the physical limitations of the system or any form of additional constraint. In particular, the LQR formulation cannot guarantee the feedback linearizing condition $\delta_4 \neq 0$ at all times, nor the actuation of the control. A good candidate to address this limitation is then MPC, as described below.

Mission Controller based on Model Predictive Control The underlying idea of classical MPC is to use a discretized dynamic model of the system, obtained by an exact state-space discretization of the linearized system (4.8), to predict the state trajectory under a given control action and optimize the system evolution over the so-called *prediction horizon* of length P. The optimization is performed every s seconds and computes the control actions over the period P; subsequently, only the first control action is applied to the system, while the other computed ones are discarded.

With a little abuse of notation, let $v[k|h]$ denote the predicted control action value at time $(h+k)\,s$ computed at time hs (note that the same notation will be used hereinafter for other signals), and let the optimal control sequence be denoted by v^*. The proposed MPC formulation, which is explained in the remainder of the section, is the following:

$$\min_{v\in\mathbb{R}^C} J(v) \tag{4.25}$$
s.t.
$$\frac{T}{2}\left(\omega[k|h]^T\delta_{13}[k|h]\right)-\delta_4[k|h]\leq 0,\ \text{if}\ \delta_4[k|h]>0,\quad k=1,\ldots,P, \tag{4.26}$$
$$\frac{T}{2}\left(\omega[k|h]^T\delta_{13}[k|h]\right)-\delta_4[k|h]\geq 0,\ \text{if}\ \delta_4[k|h]<0,\quad k=1,\ldots,P, \tag{4.27}$$
$$a(x[k|h])+\Delta(x[k|h])\,u_{\min}<v[k|h]<a(x[k|h])+\Delta(x[k|h])\,u_{\max},$$
$$k=0,\ldots,P-1. \tag{4.28}$$

The cost function (4.25) has the same rationale of the cost function (4.22) and is of the form

$$J(v)=\frac{1}{2}\sum_{k=1,\ldots,P}\left(\delta_e[k|h]^T Q[k]\,\delta_e[k|h]+v[k-1|h]^T R[k-1]\,v[k-1|h]\right). \tag{4.29}$$

MPC provides a framework in which one can directly impose the constraint $\delta_4\neq 0$ over the prediction window, driving the system to the desired attitude while avoiding the singularity points. In other words, MPC forces the system to follow safer, even if potentially sub-optimal, trajectories.

Note that the feasible solutions are the ones which keep the feedback linearization always active, that is the constraint $\delta_4(t)\neq 0$ must be met for all times $t\in[hT,(h+P)\,s)$ and not only for the instants $(h+k)s$, $k=1,\ldots,P$. A simple solution is to limit the evolution of δ_4 by constraining its discretized dynamics in a conservative way. From (4.3), it follows that

$$\delta_4[k+1|h]-\delta_4[k|h]-\frac{T}{2}\left(\omega[k|h]^T\delta_{13}[k|h]\right),\quad k=1,\ldots,P,$$

meaning that the constraints (4.26), (4.27) guarantee that, in the interval $[ks,(k+1)\,s)$, δ_4 does not reach the value 0, independently from its sign at time k. In other words, constraints (4.26), (4.27) constitute the conditions for the feasibility of the feedback linearization.

Finally, the controller needs to guarantee also that the actuation is feasible, i.e., that the control action computed by the MPC does not saturate the reaction wheels, which, with little abuse of notation, translates into the set of component-wise constraints:

$$u_{\min} < u(t) < u_{\max}.$$

A possible solution is to properly constrain the available control dedicated to the MPC, depending on the current effort demanded by the feedback linearizing control. From equation (4.6), it follows that the portion of the control available to the mission control v is then

$$a(x) + \Delta(x)u_{\min} < v < a(x) + \Delta(x)u_{\max},$$

which translates into the set (4.28) of constraints for the MPC controller. In constraints (4.28), the predicted state $x[k|h]$ is firstly computed in the coordinates (ξ, η) by using the candidate control sequence v as input to the discretized version of system (4.8); then, the predicted state $x[k|h]$ in the original coordinates of (4.3) (i.e., (q, w, L_w)) is retrieved using the inverse of the coordinate transformation (4.11) (which always exists since (4.11) is a diffeomorphism [119].

For the sake of computational complexity reduction, the concept of control horizon is used: starting from time $C \leq P$, the controller holds the value $v(C)$ for all the remaining controls $v[C+1|h], \ldots, v[P-1|h]$ in the prediction window. Note that this simplification provides a sub-optimal solution, whose quality depends on the length of C.

Momentum Unloading

The problem of momentum unloading is commonly considered as disjoint from the attitude control. To add a momentum control, the dynamical equation of the angular momentum is modified to

$$\dot{L_w} = \tau_w + \tau^u,$$

which is stabilized by the simple control law of the form

$$\tau_w + \tau^u = -KL^w, \; K > 0 \tag{4.30}$$

One could choose to apply this type of control either during the periods in which no changes in attitude are envisaged and when momentum wheels are close to their saturation, or continuously during the system operation. Following the latter approach, it is possible to set

$$K = \frac{\tau_{\max}}{L_w^{\text{sat}}}$$

in which $\tau_{\max}$ represents the maximum torque that the wheels are able to provide and L_w^{sat} is the saturation value of the angular momentum of the wheels. This choice of K entails that the discharge increases when the momentum is close to its saturation and does not significantly affect the system otherwise.

The control law (4.30) implies that u (recall that $u = t_w$) is conservatively bounded with respect to its nominal values, as the unloading torque absorbs a portion of the available effort. This physical limitation can be implemented as an additional constraint for the MPC controller, with some awareness, by adapting the values of $u_{\min}$ and $u_{\max}$ in (4.28) depending on the measured L_w. It is worth noting that the receding horizon procedure allows the controller to activate the unloading procedure arbitrarily (e.g., when L_w exceeds a safety threshold) by adding the relative constraints in the optimization. Furthermore, note that to have the unloading torque decoupled from the attitude dynamics, the available thrusters must provide an external torque τ opposite to τ^u, so that when (4.30) is applied into the second equation of (4.3) the original torque τ_w is recovered.

4.6 Simulations

Satellite Setup

A medium size GEO telecommunication (TLC) satellite, 16 kW–2500 kg class, has been selected as a reference case to perform the simulation analyses. The life-support vehicle design has been based on a study case of Thales Alenia Space Italia and it has been modelled connected to the customer TLC satellite on its $-z$ "separation" plane. Table 4.1 reports the main inertia for both the stand-alone satellite and the composed stack configurations. In the first two simulations, the satellite is still operative, and the life-support system is needed to provide new equipment, whereas in the third simulation

Table 4.1 Parameters for the satellite model

Parameter	Value
I_x^1	20000 $Kg \cdot m^2$
I_y^1	3000 $Kg \cdot m^2$
I_z^1	17000 $Kg \cdot m^2$
I_x^{tot}	34595 $Kg \cdot m^2$
I_y^{tot}	5695 $Kg \cdot m^2$
I_z^{tot}	28900 $Kg \cdot m^2$

Table 4.2 Parameters for LQR simulations

Parameter	Value
$\delta_1(0)$	0.5109
$\delta_2(0)$	0.32
$\delta_3(0)$	0.1411
T	1500s
Q	I_6
R	$10^9 \cdot I_3$
K	0.03

the satellite has deactivated its actuators and the life-support system is needed to prolong its operation. A fourth simulation assesses the performances of the proposed controller in scenarios characterized by external disturbances, parametric uncertainties and measurement noise. The fifth and final simulation reports a comparative simulation that shows how the proposed scheme can be adapted to scenarios in which the two spacecraft communicate and implements a fault-tolerant control law to renders a satellite with severe faults operative again.

All the following simulations have been implemented in MATLAB® and Simulink®, using their MPC toolbox when relevant.

LQR-based Mission Controller

In the following, an attitude tracking mission is proposed, within the scenario characterized by the quantities reported in Table 4.2.

The reference trajectory for the mission was chosen as follows

$$\delta_{13}^{\text{ref}} = \delta(0)\, e^{-\frac{t}{T}}, \tag{4.31}$$

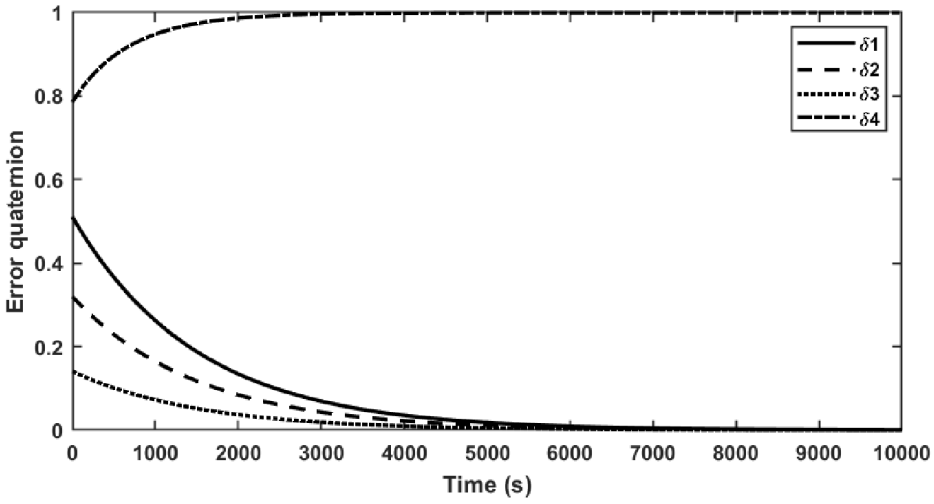

Fig. 4.5 Attitude evolution of satellite's attitude, LQR case

i.e., the control should not only let the satellite converge to the reference attitude (that is, in the error quaternion representation, to $\delta_{13} = [0\ 0\ 0]^T$) but, for the success of the mission, it should approach that attitude with an exponential behavior. The time constant T of (4.31) was set to a value which is realistic for the mission considered in the case study, which requires the control of a TLC satellite that points at a limited area of the earth while orbiting. The complete mission is planned over 10^4 seconds.

Figure 4.5 shows that the implemented control successfully drives the error quaternion to the identity, i.e., the desired final attitude is reached. Figure 4.6 reports how the satellite tracks the desired attitude trajectory, highlighting that, after about 1300s, the error annihilates. Figure 4.7 and Figure 4.8 report the profiles of the attitude control torques for the original satellite and the support system, respectively, highlighting their shared mathematical structure, in line with the compensator nature of (4.19). Finally, Figure 4.9 reports that the moment unloading law proposed achieves its objective.

Due to the fact that LQR does not guarantee the control feasibility, the weighting matrix R in (4.22) was set to a high value ($10^9 \cdot I_3$) to reduce the peak values of the control torques to approximately the typical physical limitations of reaction wheels (~ 0.1Nm).

Even with the selected value, Figure 4.6 shows that the requested control torques are not always within their feasibility margins. To successfully apply the LQR control scheme, during the mission design the control center should consider the expected peak values of the control torques, hence requiring an off-line tuning that may be

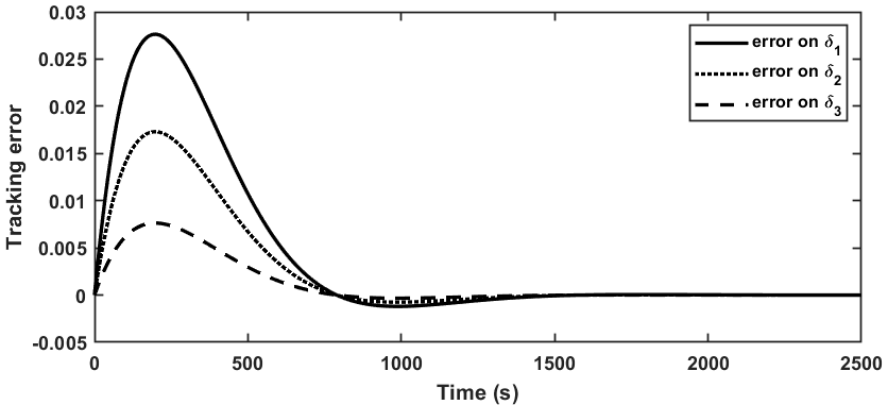

Fig. 4.6 Tracking error evolution, LQR case

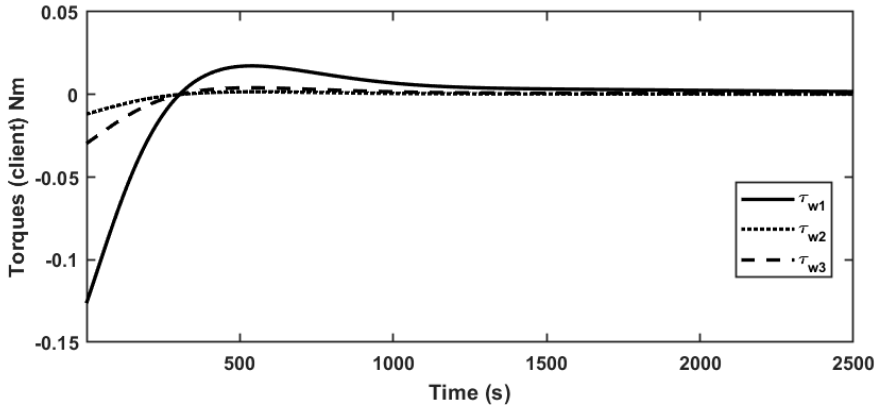

Fig. 4.7 Satellite torque profiles, LQR case

computationally demanding for missions in which the reference trajectory evolves rapidly.

MPC-based mission controller

The simulation setup is similar to the one of the previous case, with the differences reported in Table 4.3. The sampling time s for the controller was set to 60s.

By taking into account the input saturation directly into the problem formulation (4.25)-(4.28), the MPC controller is able to drive the attitude tracking error to zero significantly faster, as reported in Figure 4.10, since and the saturations do not cause the system to evolve in an unexpected way. Thanks to the assured feasibility of the control torques, the weighting matrix R in (4.29) can be set to an arbitrarily

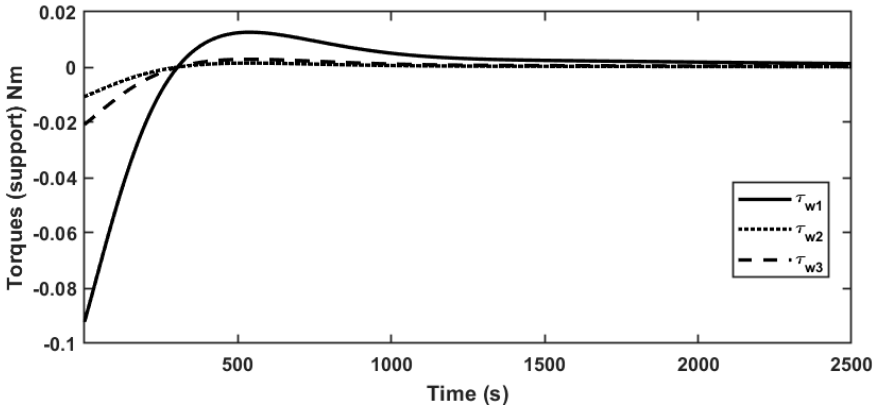

Fig. 4.8 Support torque profiles, LQR case

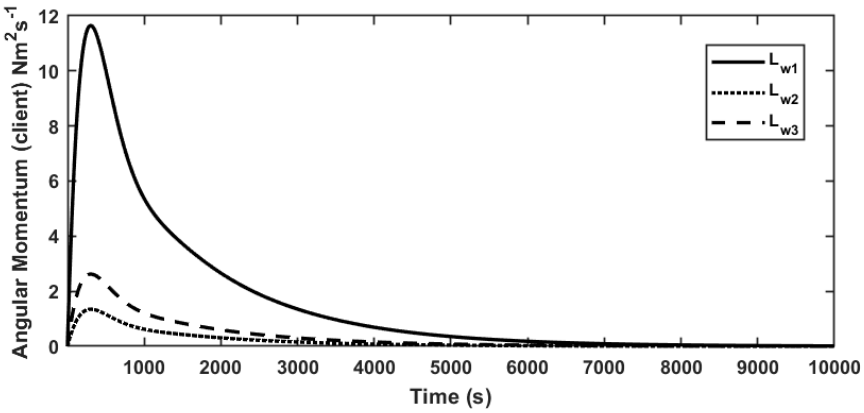

Fig. 4.9 Momentum of the wheels of the Satellite, LQR case

small diagonal positive definite matrix, allowing the controller to focus on the error annihilation and obtain lower convergence times.

A similar torque behavior is obtained, as before, for both the original satellite and the support system, so is reported only the one of the satellite in Figure 4.11.

Since the MPC assures the feasibility of the control by means of singularity avoidance, as explained in Section 4.3, the MPC controller is preferable overall not only in terms of performances and also flexibility.

MPC mission controller in absence of original satellite control

This simulation considers a scenario in which the original satellite cannot operate its reaction wheels any longer, and hence all the control torques are applied by the

Table 4.3 Parameters for MPC simulations

Parameter	Value
P	100
C	80
Q	$I_{6\times P}$
R	$10^{-3} \cdot I_{3\times P}$

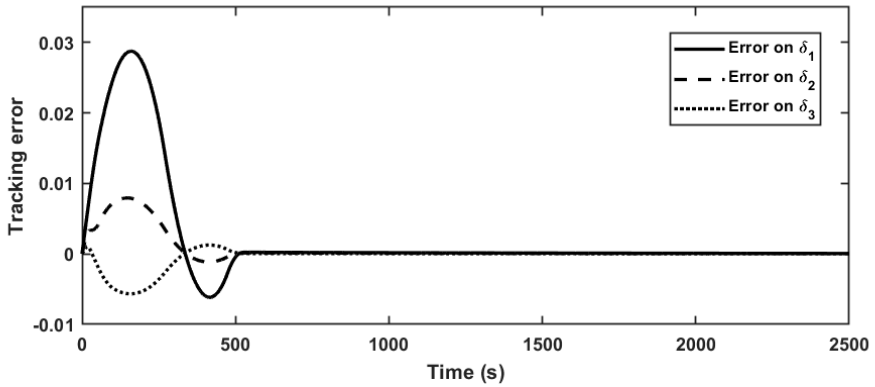

Fig. 4.10 Tracking error evolution, MPC case

life-support device. In this case, the support device enforces the feedback linearizing action of equation (4.14) instead of the compensating control of equation (4.19) (see Remark 4.2).

Figure 4.12 reports the simulation results considering the same scenario of the second simulation and shows that, even if tracking performances have worsened with respect to the previous case, the system is still able to converge to the desired attitude trajectory, successfully making an out-of-order satellite operational again, and still achieving superior performances with respect to the LQR applied to an operative satellite (see the first simulation results).

MPC mission controller in presence of external disturbances, parametric uncertainties and Gaussian white noises

So far, it was assumed that the controller was provided with exact state feedback, but in order to validate the proposed control scheme in a more representative scenario, this assumption may not be reasonable. In fact, even if both the satellite and the life-support are equipped with high-grade star trackers and gyroscopes, respectively for

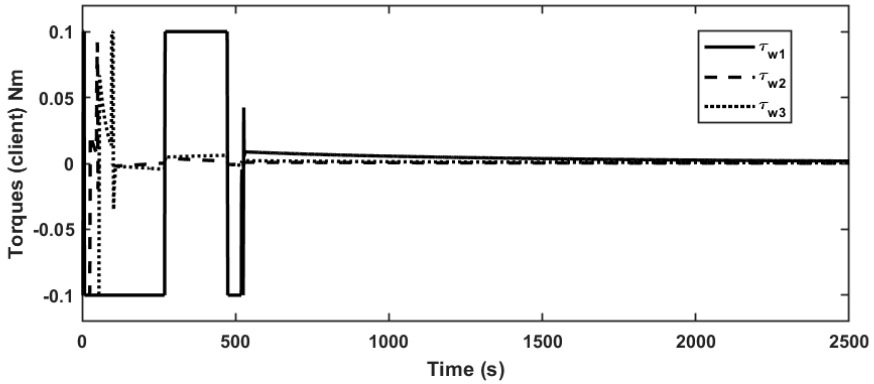

Fig. 4.11 Torque profile for the satellite, MPC case

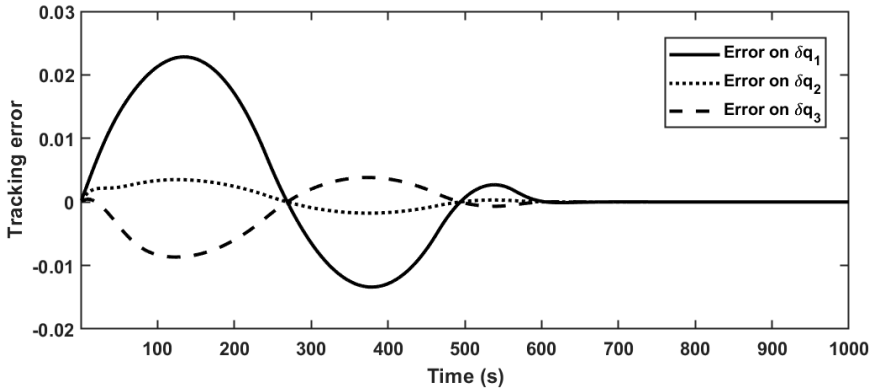

Fig. 4.12 Tracking error evolution, MPC case with non-operative reaction wheels on the satellite

attitude and angular velocity measurements, the measurement noise that affects such sensors cannot be, in principle, neglected. Furthermore, in the previous simulations the MPC controller was provided with an exact evaluation of the MOIs, and no external disturbance was considered.

In this simulation, those simplifications are removed, and, for the sake of comparison, it is assumed that the mission controller is still based on MPC, with the difference that its state feedback is provided by the state estimation obtained from an extended Kalman Filter. It is assumed that the sensors are subject to measurement white Gaussian noises, on attitude and velocity measurements, of zero mean and variances of 10^{-8} and 10^{-6} rad/sec respectively, in line with [135]. For the sake of simplicity, the process noise is also assumed to be characterized by the same variances.

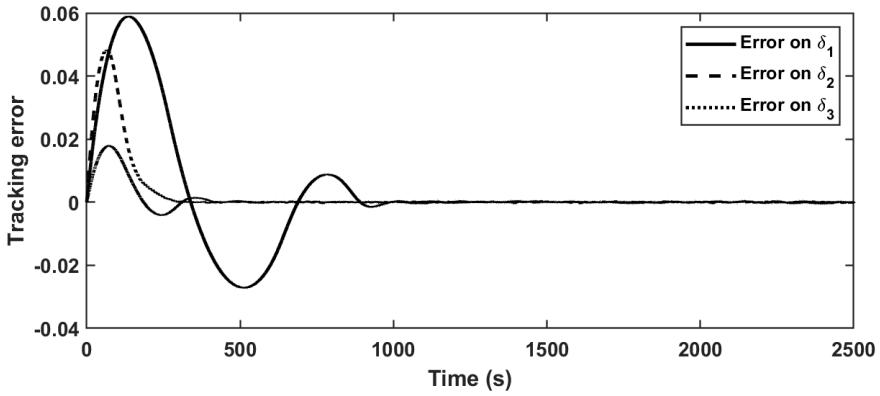

Fig. 4.13 Tracking error evolution, MPC in a realistic scenario

The unmeasured and time-varying external disturbances are described by the torque vector

$$\tau = \begin{bmatrix} 0.03\sin(0.01t) \\ 0.02\sin(0.03t) \\ 0.025\ sin(0.001t) \end{bmatrix}.$$

Finally, the real MOI components of the two-body system are assumed to be 10% higher than the one provided to the controller and reported in Table 4.1.

From the analysis of Figure 4.13, it is evident that the control performances degrade significantly, in both error amplitude and convergence time, but, considering that the controller was mainly designed for a nominal situation, its performances remain reasonable and the attitude tracking mission is still successfully completed.

Using the life-support system to control the satellite in presence of communication

For comparison purposes, this simulation discusses an alternative usage of the life-support system. In this mission, the life-support is used to take over the original satellite control logic and can directly operate the actuators of the satellite. This scenario requires real-time communication between the two systems to exchange measures and control commands, but enables the life-support to implement, in principle, any control logic developed for the problem of attitude tracking. For the sake of comparison, it is

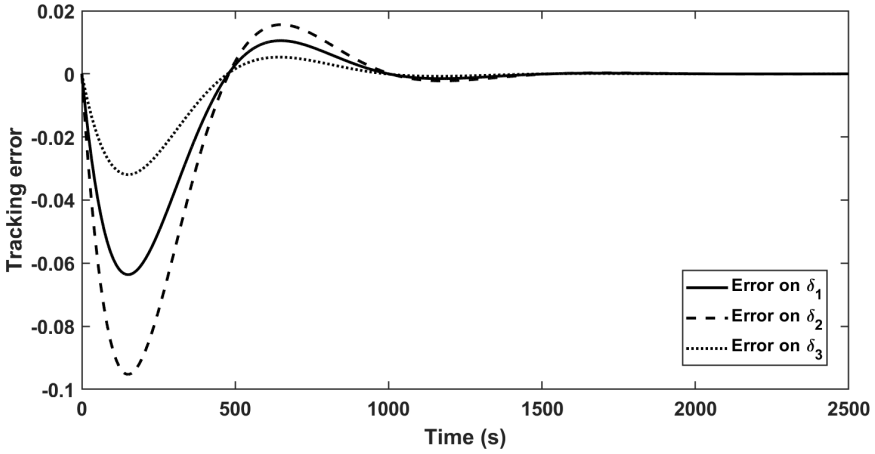

Fig. 4.14 Tracking error evolution, fault-tolerant law

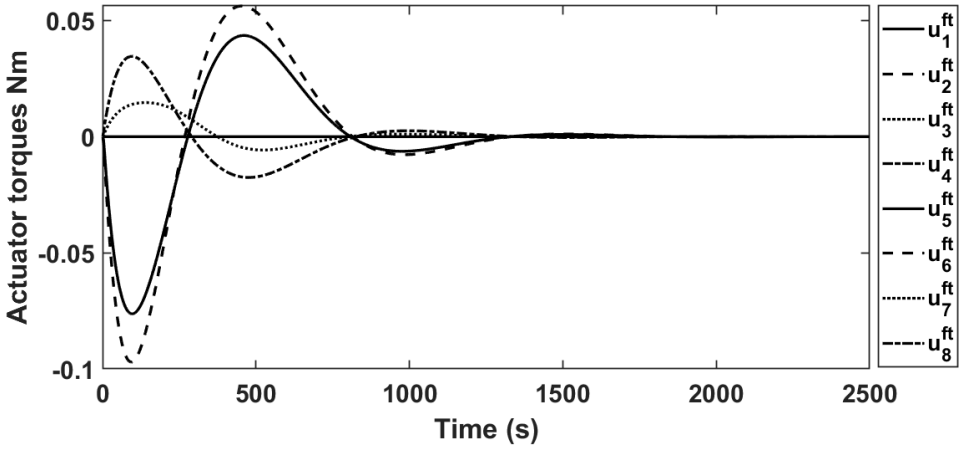

Fig. 4.15 Control torques, fault-tolerant law

further assumed that faults of the actuators are unknown to both controllers, as with the proposed control scheme, and, therefore, a fault-tolerant scheme is considered.

The domain of fault-tolerant control is a natural application of the life-support system: it is an industry standard to provide any satellite with at least four actuators, in order to preserve its operability even in presence of failures, and the life-support, in fact, delivers additional actuators to the orbiting satellite. To this end, the tested control law was derived from the one presented in [136], based on Dynamic Inversion and Time-Delay Control.

For this simulation it is assumed that both the satellite and the life-support system are equipped with four reaction wheels. The nominal distribution matrix, that projects the

torques provided by the reaction wheels over the principal axes of inertia, is assumed to be, for the two body-system, as follows:

$$L_\tau = \begin{bmatrix} 1 & 1 & -1 & -1 & 1 & 1 & -1 & -1 \\ -1 & 1 & 1 & -1 & -1 & 1 & 1 & -1 \\ \sqrt{2} & \sqrt{2} & \sqrt{2} & \sqrt{2} & \sqrt{2} & \sqrt{2} & \sqrt{2} & \sqrt{2} \end{bmatrix},$$

in which the first four columns are relative to the original satellite actuators, as in [136], while the other ones are relative to the life-support system. The distribution of the actuation torques follows $\tau_w = L_\tau \, u^{\text{ft}}$, where the fault-tolerant control law u^{ft} is the vector containing the torques commanded to the actuators.

Furthermore, the original satellite presents total faults on the first two of its actuators, so that the satellite system alone would fail to actuate the commanded torques: in fact, such faults translate into having the first two columns of the original 4×4 distribution matrix substituted by zeros, causing its rank to be less than three and, consequently, the satellite is no longer able to attain arbitrary attitudes, even if controlled by fault-tolerant laws. Conversely, in the considered simulation set up, the distribution matrix of the two-body system remains of full rank and the law designed in [136] is able to complete the attitude tracking mission.

The two-body spacecraft parameters were the ones reported in Table 4.1, as in the previous simulations. The reader is referred to [136] for details on the control law, which is characterized by the control gains τ_1 and τ_1, set to $\tau_1 = 150$, $\tau_2 = 135$ to account for the considered spacecraft model.

Figure 4.14 shows the attitude tracking error evolution[1] and Figure 4.15 presents the actuated control torques. Note that, due to their alignment, the actuation profiles of the remaining reaction wheels of the original satellite coincide with the corresponding ones of the life-support system and are not visible in the figure. It is clear from the figures that the performances have significantly worsened, in particular in terms of error magnitude, but this was expected as the controller calculated the commanded actuation torques having knowledge only on the nominal distribution matrix.

[1]Note that the control law in [136] is designed to track a trajectory defined in terms of Modified Rodriguez Parameters (MRP), but, with trivial transformations it is possible to report the simulation results in the error quaternion attitude representation.

4.7 Conclusions

This work presented a control strategy to govern a life-support system that may be attached to a satellite to increase its operational lifespan. The proposed control scheme for the attitude control problem in the presence of such support system consists of two controllers: the inner one is devoted to feedback linearizing the system, whereas the outer controller, which consequently operates on a linear system, oversees the attitude tracking. Two outer controllers were proposed, based on LQR and on MPC. Thanks to the developed control strategy, the life-support device is capable of performing the attitude control task for the two-body system also in case of non-operational actuators of the original satellites, without requiring communication exchange with the original satellite.

Numerical simulations based on a real case study were reported to validate the results presented, in scenarios spacing from ideal to adverse situations.

Future work is aimed at explicitly providing robustness to the overall scheme, to tackle model inaccuracies, model parameter variations (e.g., due to fuel consumption) and unknown or unmodeled disturbances (e.g., solar and magnetic torque effects), as well as considering flexible spacecrafts [137].

The candidate started the investigation of robust attitude control laws that take into account the uncertainties affecting the so-called high frequency gain B that appears in the normal form of the feedback-linearized system (4.8). By inspection, this class of uncertainties captures the most common problems that affect actuators (i.e. payload deformation, partial operativeness) as well as parameter estimation (i.e. MOI estimation). A first study in which an extended observed based on the work from Wang, Isidori and Su assures asymptotic attitude stabilisation was recently submitted by the candidate as

[SJ3] A. Giuseppi and A. Pietrabissa, "Robust and fault-tolerant spacecraft attitudecontrol with performance recovery based on an extended-observer design," in International Journal of Control, under review.

The integration of such control logic with the life-support and its compliance with a real case study are still in progress activities.

Chapter 5

Capacity-constrained Wardrop equilibria for 5G Multi-Connectivity

This chapter discusses a distributed control law for adversarial routing and load balancing in capacitated networks. The scenario of application are heterogeneous networks capable of offering Multi-Connectivity to their users.
Multi-Connectivity is one of the key features of 5G networks and consists in the possibility for the user equipment to use different access networks simultaneously, to increase the transmission capacity and/or to improve the transmission reliability. Traffic steering is one of the functionalities enabling the Multi-Connectivity, and consists in distributing the traffic load over the access networks available to the user equipment. In this work, the traffic steering problem is modelled as a distributed, non-cooperative and dynamic load-balancing problem and an algorithm is proposed in the context of adversarial network equilibria. By properly defining latency functions representing the load of the access networks, and considering constraints on the access network capacities, the proposed solution is proved, by Lyapunov arguments, to converge to an approximate Wardrop user equilibrium, referred as the Beckmann equilibrium in the literature, in which the latencies of the access networks are equalized. Simulation results validate the approach. The work was done in the scope of the H2020 EU-Korea Project 5G-ALLSTAR and led to the recent submission of the paper:

[SJ2] *F. Delli Priscoli, A. Giuseppi, and A. Pietrabissa, "Capacity-constrained Wardrop equilibria and application to multi-connectivity in 5G networks,"in the Journal of The Franklin Institute, under review*

Nomenclature of the chapter

Main Symbols	
c_p	Maximum load – capacity – of provider $p \in \mathcal{P}$
$\mathcal{I}$	Set of commodities (QoS-Flows)
$l_p^i(\mathbf{x})$	Latency of provider $p \in \mathcal{P}$ and commodity $i \in \mathcal{I}$ under flow $\mathbf{x}$
$\mathcal{L}(\mathbf{x})$	Candidate Lyapunov function
$r_{\text{pq}}^i[k]$	Migration rate of commodity $i \in \mathcal{I}$ from provider p to provider q at time k, with $p, q \in \mathcal{P}$
$\mathcal{P}$, $\mathcal{P}^i$	Set of providers (Access Points), set of providers available to commodity $i \in \mathcal{I}$
$x_p^i[k]$	Load of commodity $i \in \mathcal{I}$ over provider $p \in \mathcal{P}$ at time k
$x_p[k] = = \sum_{i \in \mathcal{I}} x_p^i[k]$	Total load over provider $p \in \mathcal{P}$ at time k
$\mathbf{x} = (x_p)_{p \in \mathcal{P}}$	Flow vector at time k
$\mathcal{X}$	Feasible state space
$\mathcal{X}_{\text{eq}}$, $\mathcal{X}_{\text{eq}}^{\varepsilon}$	Set of Beckmann and ε-Beckmann equilibria
λ^i	Flow demand of commodity $i \in \mathcal{I}$
$\Phi(\mathbf{x})$	Beckmann, McGuire and Winsten potential
$\mu_{\text{pq}}^i(l_p^i,\ l_q^i)$	Migration policy of commodity $i \in \mathcal{I}$ from provider p to provider q, with $p, q \in \mathcal{P}$
σ^i	Migration gain of commodity $i \in \mathcal{I}$

5.1 Introduction

Load Balancing is a classic problem of network control and can be seen as particular case of traffic routing with providers representing unitary paths and latency functions describing the performance of each provider. In adversarial (or selfish) routing, the control algorithms are aimed at leading the network into convenient equilibrium states without the cooperation of its agents. One of such states is known in mean-field game

theory as Wardrop equilibrium (which can be regarded as a Nash equilibrium for infinite players [138]): in such state, the latencies experienced by the agents that constitute the traffic flows are equalised over all their available routes, and, as a consequence, no agent may improve its routing unilaterally. In this paper, we study a particular case of selfish capacitated load balancing, in which the capacities of the service providers are limited. Therefore, as it will be discussed, the proposed control law objective will be to equalize the latencies of all the providers which are not saturated. This network state is a generalization of the Wardrop equilibrium in capacitated networks, and is known in the literature as the Beckmann user equilibrium [139]. Multi-connectivity is an emerging challenge in the heterogeneous network scenario envisaged by 5G, where multiple Radio Access Technologies (RATs), such as LTE, 5G and Satellite networks, are available to connect the network users to the core network [140]. According to the multi-connectivity paradigm, each User Equipment (UE) may be able to be served by several of the various Access Points (AP) of the available RATs, potentially at the same time. The problem, referred to in the 5G literature as *multi-connectivity*, consists in dynamically choosing which APs shall serve each UE and deciding how much traffic relevant to each UE shall be routed through each of the serving APs. This paper focuses on the downlink direction, i.e., it refers to the traffic transmitted from the core network to the UEs via the APs; nevertheless, similar considerations apply when considering the uplink direction.

In this work, the performance of the network APs are measured in terms of *latency functions* that capture the communication power required each AP to serve the various *commodities*. In the considered 5G scenario, such commodities consist in the so-called QoS-Flows, which are streams of data that i) share the same Quality of Service (QoS) requirements, such as capacity demand and tolerated delay, and (ii) are directed to UEs served by the same set of APs. Each latency function accounts for the transmission power required by a given AP to serve a given QoS-Flow, while meeting its QoS requirements, and may include various scaling factors, as operator preferences or different usage tariffs. Consequently, the objective of the load balancing algorithm is to dynamically *steer* the downlink traffic in such a way that the values of the latency functions are equalized.

The described scenario is typical in adversarial routing and load balancing problems, as the various connections are not concerned with the overall network state and aim at optimising their own, individual, performances. The two main problems in the algorithm development are i) the fact that the latency functions are not known a-priori,

but can be only measured, ii) the fact that a distributed approach is needed since a centralized approach would require too much control traffic to exchange information among the potentially thousands of UEs.

In this paper, a distributed, non-cooperative and dynamic load balancing algorithm is consequently developed in the context of adversarial network equilibria; specifically, the algorithm considers each single packet included in a QoS-Flow as an *agent,* able to make a decision regarding the AP it is assigned to. Such decisions are based on the measurements of the latency functions, obtained starting from the observation of the transmission power of the APs over which the commodity is routed, and are made unilaterally in an adversarial framework, with no concern for the overall system performance.

The main motivations behind this work are then (i) to design a dynamic adversarial capacitated load balancing algorithm and to prove, using Lyapunov and Invariance Principle arguments, how the difference equation governing the global state of the system converges to an approximated Beckmann equilibrium, and (ii) to show the effectiveness of such an approach through its application to the multi-connectivity problem in a simulated 5G network scenario.

The work is organized as follows: Section 5.2 presents the state-of-the-art on Multi-Connectivity in 5G-networks and on Wardrop load balancing and the proposed novelties; Section 5.3 presents the algorithm and the convergence proof; Section 5.4 shows the simulation results; Section 5.5 draws the conclusions.

5.2 State of the Art and Proposed Innovations

Section 5.2.1 motivates the choice of a distributed adversarial load-balancing algorithm to address the multi-connectivity problem in 5G networks, whereas Section 5.2.2 summarizes the works in the literature relevant to dynamic selfish routing and load balancing and the proposed innovations.

5.2.1 Multi-Connectivity and Traffic Steering in 5G Networks

This work addresses the problem of traffic steering, i.e., of selecting which APs a QoS-Flow shall utilise to connect the UEs with the core network by modelling it as a load-balancing problem.

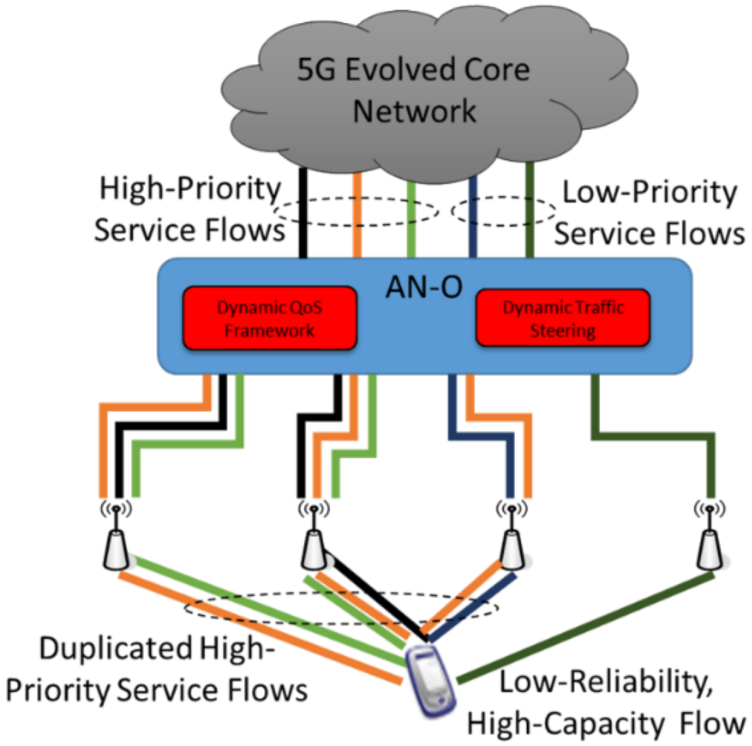

Fig. 5.1 Dynamic Traffic Steering framework from [3]

This vision is compliant with the latest developments of the 5G architecture (see Figure 5.1), as designed by 5GPPP in [3]. Multi-connectivity comprises the concept of dynamic traffic steering, which envisages the ability of dynamically steering the traffic, partitioned into QoS-Flows among the various available APs of the RATs, based on feedbacks on the current AP performances. In this framework, QoS-Flows may be duplicated over different APs to increase their resiliency, while other ones may be split over multiple RATs to increase their throughput or to better meet their QoS requirements.

Within the 5G architecture, the traffic steering problem is solved in three different ways: (i) with a User-Centric approach, where each UE decides its connection preferences according to local measures of some performance indicator; (ii) in a Radio Access Network (RAN)-Assisted fashion, in which the decision is still made by the UEs but the RAN provides them with additional information on the network state; (iii) with a RAN-Controlled approach, where all decisions are made by the RAN, which is a centralised unit by nature, or delegated to the distributed control units that govern the single APs.

Several works study the problem of multi-connectivity in the heterogeneous network framework proposed by 5G, from both architectural [141], [142] and algorithmic [143]–[145] points of view. Multi-connectivity enables the problem of optimally steering the network traffic over the available APs, in such a way that the QoS requirements of the various QoS-Flows are met [146], [147]. The problem of access network selection has been studied utilising several different approaches, spacing from fuzzy-logic control to multiple-attribute decision-making and combinatorial optimisation [145]. Common solutions utilise the concept of utility and latency functions, as in this work, to capture the network performances [41], [145], [148]. Several works in the literature also employ game-theoretic approaches for the AP selection, typically in adversarial frameworks, as [145], [149], [150], leading the networks to Nash equilibrium states.

Regarding game theoretic solutions, one possible modelling choice is to have an adversarial game between the users, as in [150], [151] that envisage a setup similar to the one used in this work. In such scenarios, the users compete to attain the best connection quality while eventually also minimising their costs. An alternative approach is to set up a game between the various network operators, each controlling a set of APs as in [148], [149], and focusing on their economic performances.

The algorithm proposed in this work utilises *differential game theory*, a branch of game theory that studies dynamical systems, and shares some of the characteristics of the previously mentioned works, as the adversarial nature of its equilibrium. The control algorithm designed in this work will be proven to drive the communication network state to a convenient equilibrium state, and this convergence will be attained by following an explicit discrete-time control law, with no need for round-games or price/cost bidding auctions. Contrary to optimisation-based works, the proposed control law is also suitable to steer the traffic flows in real-time, and, being a distributed decision process, it does not require any significant control traffic overhead.

The previous aspects, together with the explicit inclusion of constraints on the available transmission capacity, makes the proposed approach a suitable candidate for the deployment in 5G scenarios, in which the low latency and power consumption aspects are of crucial importance. With reference to the mentioned Dynamic Traffic Steering framework [3], the algorithm can be implemented in RAN-Assisted and in the RAN-Controlled configurations: in the former case, the algorithm would run in the UEs based on the information received by the RAN; in the latter case, the algorithm would run directly in the RAN or in the distributed controllers of the various APs.

5.2.2 Adversarial Load Balancing in 5G Networks and Beckmann Equilibria

The problem of optimally distributing the flow is one of the most fundamental and challenging aspects of any network operation. In the framework of selfish routing, the network flow is formed by a stream of infinitely-many decision-making agent [152] that compete for attaining the best performance, without consideration for the congestion, and consequent performance degradation, that their decisions cause to the other agents.

Wardrop equilibria [153] were then introduced to describe a network state in which no single agent can unilaterally improve its performances (e.g., in terms of travel time, as in the original Wardrop formulation). Being an adversarial kind of equilibria, the overall network performance is not optimised and the performance loss is referred as *price of anarchy* in the literature [23]. The concept of Wardrop equilibrium has been extended to various families of networks, among which the capacitated ones [139], [154]–[156], and problems, as the load balancing one [157]–[159]. Even if Wardrop equilibria can be computed by centralized algorithms in polynomial time [160], for the low connection latency promised by 5G – and the consequent agile and fast traffic steering requirements – distributed approaches are more suitable, motivating development of a dynamic algorithm.

Based on a simple representation of the network dynamics in terms of difference equations derived from the flow conservations laws, this paper proposes a load balancing solution over the nodes of a dynamical network that represents the 5G infrastructure [161], [162], consisting in the connections between several APs and their users with the core network. In doing so, the algorithm takes into account that the amount of traffic each AP can support is limited, or *capacitated*, due to transmission power constraints and, in general, resource scarcity. This limitation implies that the user equilibrium to which the network will converge may not be in principle the Wardrop equilibrium [155], which is defined for unconstrained networks. Several works [139], [154]–[156] extended the original formulation of the Wardrop user equilibrium, which corresponds to a situation in which all the latencies of each commodity are equalised, to deal with capacitated networks. The resulting equilibrium, known as Beckman user equilibrium, is such that the latencies of all the unsaturated APs of each commodity are equalised. Differently from [139], [154]–[156], this work proposes a dynamic algorithm which will be proven to converge to a Beckmann equilibrium.

Regarding dynamic load balancing solutions for Wardrop equilibria in the literature, several works utilise the concepts of *learning and exploration to cope with the limited feedback information that the decision-making agents have access to. To attain a better knowledge of the system state and dynamics, the agents sample different flow distribution strategies and then exploit the learned* system characteristics to converge to optimal states. The authors of [163] present an asynchronous and distributed algorithm that employs reinforcement learning to update transmission probabilities, based on an estimation of the network edges latencies. In [164], an iterative and distributed learning solution is proven to converge to a Wardrop equilibrium state using Lyapunov arguments, as in this work.

An important contribution has been given by Fischer et al. in [165]–[167]. In [165] and [166], a round-based algorithm is developed to solve a game among the various commodities, aimed at redistributing the traffic flow and reaching an approximated Wardrop equilibrium. In [167], a similar set up is analysed assuming that the information available to the agents may be stale. In [J5], a dynamic discrete-time load-balancing algorithm is presented in the context of Virtual Private Networks, which converges to an approximate Wardrop equilibrium.

The present work extends the results of previous works, starting from the algorithm in [J5], mainly in two directions:

i) the convergence properties of the algorithm are studied in the multi-commodity case, a requirement for application in the 5G framework, that was not explicitly discussed in the cited works;

ii) the algorithm analysis and design are extended to the case of capacitated networks, not dealt with by the dynamic algorithms in the literature, enabling the application of the solution to more realistic case studies in several domains.

5.3 Proposed Wardrop Load Balancing Algorithm

Section 5.3.1 describes the basic definitions needed for the algorithm analysis; Section 5.3.2 presents the load balancing algorithm and the convergence proof; Section 5.3.3. models the 5G traffic steering problem as a load balancing one.

5.3.1 Preliminaries on Wardrop and Beckmann Equilibria and on Lyapunov Stability

As anticipated in Section 5.2, this paper further develops a well-known model for selfish routing [165], where an infinite population of agents carries an infinitesimal amount of load each, and builds on the previous work [J5] concerning distributed load balancing algorithms. The proposed control scheme relies on common assumptions on the latency functions. The considered network consists in a set of $\mathcal{P}$ providers, which serve a set $\mathcal{I}$ of commodities. Each commodity $i \in \mathcal{I}$ is characterised by a flow demand λ^i and is served by a subset of providers $\mathcal{P}^i \subset \mathcal{P}$. Each provider p is characterised by a latency function l_p and by a capacity c_p.

Assumption 5.1. The latency functions $l_p(\xi)$ are positive, non-decreasing and Lipschitz continuous with constant β_p, for $\xi \in [0, c_p]$, where c_p is the capacity of provider p, for all $p \in \mathcal{P}$. Furthermore, the maximum Lipchitz constant of all the l_p's is denoted as $\overline{\beta} = \max_{p \in \mathcal{P}} \beta_p$.

The assumption is not restrictive in real use-cases since the provider performances decreases with their load.

In non-capacitated algorithms, if x_p^i indicates the amount of the flow of commodity i allocated on the provider p, the set of feasible states is defined as

$$\mathcal{X} = \left\{ \mathbf{x} = (x_p)_{p \in \mathcal{P}} \,|\, x_p = \sum_{i \in \mathcal{I}} x_p^i, \quad x_p^i \geq 0, \forall p \in \mathcal{P}^i, \quad \sum_{p \in \mathcal{P}^i} x_p^i = \lambda^i, \forall i \in \mathcal{I} \right\}, \tag{5.1}$$

and a flow $\mathbf{x} \in \mathcal{X}$ is at a Wardrop equilibrium if, for each commodity $i \in \mathcal{I}$, the latencies of the loaded providers are equalized, i.e., if $l_p(x_p) \leq l_q(x_q)$ for all $p \in \mathcal{P}^i$ such that $x_p^i > 0$ and for all $q \in \mathcal{P}^i$.

By defining the Beckmann-McGuire-Winsten potential

$$\Phi(\mathbf{x}) = \sum_{p \in \mathcal{P}} \int_0^{x_p} l_p(\xi) \, \mathrm{d}\xi, \tag{5.2}$$

the Wardrop equilibria are the solutions of the optimization problem

$$\min_{\mathbf{x} \in \mathcal{X}} \Phi(\mathbf{x}). \tag{5.3}$$

Capacity-constrained networks are characterized by the additional capacity constraints

$$x_p \leq c_p, \forall p \in \mathcal{P}. \tag{5.4}$$

A flow $\mathbf{x} \in \mathcal{X}$ is feasible if constraints (5.4) hold, and the set of feasible states is defined as

$$\mathcal{X}_{\text{CP}} = \{\mathbf{x} \in \mathcal{X} \ | x_p \leq c_p, \forall p \in \mathcal{P}\}. \tag{5.5}$$

Considering commodity $i \in \mathcal{I}$ under a flow $\mathbf{x} \in \mathcal{X}_{\text{CP}}$, provider $p \in \mathcal{P}^i$ is defined as *capacity-constrained* or *saturated* if $x_p = c_p$.

A flow $\mathbf{x} \in \mathcal{X}_{\text{CP}}$ is at a Beckmann user equilibrium if, for each commodity, the latencies of the loaded and unconstrained providers are equalized, i.e., more precisely:

Definition 5.1 [139]. A flow $\mathbf{x} \in \mathcal{X}_{\text{CP}}$ is at a Beckmann user equilibrium if $l_p(x_p) \leq l_q(x_q)$ for all $p \in \mathcal{P}^i$ such that $x_p^i > 0$, for all $q \in \mathcal{P}^i$ such that $x_q < c_q$ and for all $i \in \mathcal{I}$.

The set of equilibria is then

$$\mathcal{X}_{\text{eq}} = \left\{\mathbf{x} \in \mathcal{X}_{\text{CP}} | l_p(x_p) \leq l_q(x_q), \forall p \in \mathcal{P}^i \text{ s.t. } x_p^i > 0, \ \forall q \in \mathcal{P}^i \text{ s.t. } x_q < c_q, \forall i \in \mathcal{I}\right\}. \tag{5.6}$$

Let us consider the minimization problem (5.3) with constraints (5.4), hereinafter referred to capacity-constrained problem (CP). The Beckman user equilibria [156] are the optimal solutions of the CP.

Property 5.1 [139]. If the set of feasible solutions $\mathcal{X}_{\text{CP}}$ of the CP is nonempty, the optimization problem consists in minimizing a convex function over a nonempty polytope and, thus, the set of optimal flows $\mathcal{X}_{\text{eq}}$ is nonempty and convex.

The algorithm convergence proof of Section 5.3.2 relies on LaSalle invariance principle for discrete-time nonlinear systems [168], [169].

Definition 5.2. $\mathcal{L} : \mathcal{X} \to \mathbb{R}$ is a candidate Lyapunov function for a discrete-time nonlinear system $\mathbf{x}[k+1] = f(\mathbf{x}[k])$ if

i) $\mathcal{L} \in \mathcal{C}^1$ and $\mathcal{L}(\mathbf{x})$ is bounded below and positive definite on $\mathcal{X}$;

iii) If $\mathbf{x}_{\text{eq}} \in \mathcal{X}_{\text{eq}}$, where $\mathcal{X}_{\text{eq}}$ is the set of equilibrium points, $\mathcal{L}(\mathbf{x}_{\text{eq}}) = 0$ and $\mathcal{L}(\mathbf{x}) > 0 \; if \; \mathbf{x} \notin \mathcal{X}_{\text{eq}}$;

iii) Along forward trajectories, $\mathcal{L}$ satisfies

$$\Delta\mathcal{L}(\mathbf{x}[k]) := \mathcal{L}(f(\mathbf{x}[k])) - \mathcal{L}(\mathbf{x}[k]) \leq 0, \; k = 0, 1, 2, \ldots$$

Theorem 5.1 [169]. Let $\mathcal{L}(\mathbf{x})$ be a candidate Lyapunov function for the discrete-time nonlinear system $\mathbf{x}[k+1]=f(\mathbf{x}[k])$. Then, any bounded trajectory tends to the largest invariant subset M contained in the set of points defined by $\Delta\mathcal{L}(\mathbf{x}) = 0$.

5.3.2 Capacitated Load Balancing Algorithm and Convergence Proof

For each commodity i$\in \mathcal{I}$, the control action consists in the decision, at time k, of *migrating* part of the flow mapped onto a given provider p to another provider q, with $p, q \in \mathcal{P}^i$. By denoting the rate of such migration with $r^i_{\text{pq}}[k]$, the system dynamics is written as

$$\mathbf{x}[k+1] = f(\mathbf{x}[k]), k = 0, 1, 2, \ldots \tag{5.7}$$

with

$$x_p[k] = \sum_{i \in \mathcal{I}} x^i_p[k], \tag{5.8}$$

$$x^i_p[k+1] = x^i_p[k] + \tau \sum_{q \in \mathcal{P}^i} \left(r^i_{\text{qp}}[k] - r^i_{\text{pq}}[k] \right), \tag{5.9}$$

and with feasible initial conditions

$$\mathbf{x}[0] \in \mathcal{X}_{\text{CP}}. \tag{5.10}$$

for all $p, q \in \mathcal{P}^i$ and $i \in \mathcal{I}$

The proposed controller builds on the dynamic algorithm in [J5], which expresses the migration rate as

$$r^i_{\mathrm{pq}}[k] = x^i_p[k]\,\sigma^i \mu^i_{\mathrm{pq}}[k], \tag{5.11}$$

where σ^i is a positive migration gain and $\mu^i_{\mathrm{pq}}[k]$ is the migration policy, representing the decision of whether (if it is positive) or not (if it is equal to zero) migrate some flow from provider p to provider q.

As in [J5] for the Wardrop equilibria, approximated Beckmann user equilibria are defined.

Definition 5.3. The set of ε-Beckmann user equilibria is defined as

$$\begin{aligned}\mathcal{X}^{\varepsilon}_{\mathrm{eq}} = \Big\{ \mathbf{x} \in \mathcal{X}_{\mathrm{CP}} | l_p(x_p) \leq l_q(x_q) + \varepsilon, \forall p \in \mathcal{P}^i \text{ s.t. } x^i_p > 0,\ \forall q \in \mathcal{P}^i \text{ s.t.} \\ x_q \leq c_q - \frac{\varepsilon}{2\overline{\beta}}, \forall i \in \mathcal{I} \Big\}.\end{aligned} \tag{5.12}$$

where $\varepsilon \geq 0$ represents a maximum tolerated latency mismatch.

Remark 5.1. The defined sets are such that $\mathcal{X}^{\varepsilon}_{\mathrm{eq}} \overset{\varepsilon \to 0}{\to} \mathcal{X}_{\mathrm{eq}}$ and $\mathcal{X}_{\mathrm{eq}} \subseteq \mathcal{X}^{\varepsilon}_{\mathrm{eq}} \subseteq \mathcal{X}_{\mathrm{CP}}$: the objective of the controller is then, starting from a physically admissible state in $\mathcal{X}_{\mathrm{CP}}$, to reach an approximated equilibrium state in $\mathcal{X}^{\varepsilon}_{\mathrm{eq}}$, whose degree of approximation with respect to the equilibrium state in $\mathcal{X}_{\mathrm{eq}}$ reduces with ε.

The tolerance ε is introduced since the kind of migration rates of equation (5.11) cannot guarantee convergence in the discrete-time case, however small the sampling period [167]. A flow $\mathbf{x} \in \mathcal{X}_{\mathrm{CP}}$ is then at ε-Beckman equilibrium if, for each commodity, the latencies of the loaded and ε-unconstrained providers are equalized, where we define a provider $p \in \mathcal{P}^i$ to be ε-unconstrained if $x_p < c_p - \frac{\varepsilon}{2\overline{\beta}}$.

In the proposed algorithm, the migration decision is defined as

$$\mu^i_{\mathrm{pq}}[k] = \begin{cases} 0, & if\ l_p(x_p[k]) - l_q(x_q[k]) \geq \varepsilon \text{ or if } x_q[k] \geq c_q - \frac{\varepsilon}{2\overline{\beta}} \\ 1, & \text{otherwise} \end{cases} \tag{5.13}$$

The controlled system dynamics, hereafter denoted as load-balancing (5.20) dynamics, is then expressed by equations (5.9), (5.11), (5.13), with control gains set as

$$\sigma^i = \frac{\varepsilon}{2\tau\overline{\beta}\lambda^i\left(|\mathcal{P}^i|-1\right)|\mathcal{I}|}, \tag{5.14}$$

and with the tolerance set as

$$0 < \varepsilon \leq \min_{i\in\mathcal{I}} \overline{\beta}\lambda^i\,|\mathcal{I}|. \tag{5.15}$$

Remark 5.2. The approximated capacity-constrained user equilibria are such that, for each commodity, the latencies of the loaded and ε-unconstrained providers are equalized within the tolerance ε. Then, for a given equilibrium flow $\mathbf{x} \in \mathcal{X}^{\varepsilon}_{\text{eq}}$ and for each commodity $i\in\mathcal{I}$, three classes of providers exist: the unloaded providers $p \in \mathcal{P}^i$ such that $x^i_p = 0$; the ε-constrained providers $p \in \mathcal{P}^i$ such that $x_p > c_p - \frac{\varepsilon}{2\overline{\beta}}$; the ε-unconstrained providers, whose latencies are equalized.

The convergence property of the algorithm relies on the following 3 lemmata.

Lemma 5.1. Under Assumption 5.1, considering the LB dynamics, the latency variation of a provider $p \in \mathcal{P}^i$ in one time-step is bounded by

$$|l_p\left(x_p\left[k+1\right]\right) - l_p\left(x_p\left[k\right]\right)| \leq \frac{\varepsilon}{2}. \tag{5.16}$$

Proof. Considering the generic commodity $i\in\mathcal{I}$, provider $p \in \mathcal{P}^i$ and time k, the maximum latency decrease occurs when no commodities migrate their populations from the other providers to provider p:

$$l_p\left(x_p\left[k+1\right]\right) = l_p\left(x_p\left[k\right] + \tau\sum_{q\in\mathcal{P}}\left(r_{\text{qp}}\left[k\right] - r_{\text{pq}}\left[k\right]\right)\right) \geq l_p\left(x_p\left[k\right] - \tau\sum_{p\in\mathcal{P}} r_{\text{pq}}\left[k\right]\right) \tag{5.17}$$

Since β_p is the Lipschitz constant of the function $l_p\left(\cdot\right)$ between 0 and c_p, it follows that

$$l_p\left(x_p\left[k+1\right]\right) \geq l_p\left(x_p\left[k\right]\right) - \tau\beta_p\sum_{q\in\mathcal{P}} r_{\text{pq}}\left[k\right]. \tag{5.18}$$

Considering equations (5.11) and (5.14), the last term of equation (5.18) is written as

$$
\begin{aligned}
&\tau\beta_p \sum_{q\in\mathcal{P}} r_{\mathrm{pq}}[k] = \tau\beta_p \sum_{j\in\mathcal{I}} \sum_{q\in\mathcal{P}^j} r^j_{\mathrm{pq}}[k] = \\
&= \tau\beta_p \sum_{j\in\mathcal{I}} \sum_{q\in\mathcal{P}^j} x^j_p[k]\,\sigma^j \mu^j_{\mathrm{pq}}[k] = \\
&= \sum_{j\in\mathcal{I}} \tau\beta_p x^j_p[k]\,\sigma^j \sum_{q\in\mathcal{P}^j} \mu^j_{\mathrm{pq}}[k] = \\
&= \sum_{j\in\mathcal{I}} \tau\beta_p x^j_p[k]\,\frac{\varepsilon}{2\tau\overline{\beta}\lambda^j(|\mathcal{P}^j|-1)\,|\mathcal{I}|} \sum_{q\in\mathcal{P}^j} \mu^j_{\mathrm{pq}}[k] = \\
&\leq \sum_{j\in\mathcal{I}} \frac{\varepsilon}{2\,|\mathcal{I}|} = \frac{\varepsilon}{2},
\end{aligned}
\tag{5.19}
$$

where the inequality holds since $x^j_p[k] \leq \lambda^i$, $\beta_p \leq \overline{\beta}$ and since, recalling equation (5.13), there are at most $\left(\left|\mathcal{P}^j\right|-1\right)$ terms equal to 1 in $\sum_{q\in\mathcal{P}} \mu^j_{\mathrm{pq}}[k]$. It follows that

$$
l_p(x_p[k+1]) \geq l_p(x_p[k]) - \frac{\varepsilon}{2}. \tag{5.20}
$$

Similarly, the maximum latency increase occurs when no commodities migrate their populations from provider p to other providers:

$$
l_p(x_p[k+1]) \leq l_p(x_p[k]) + \tau\beta_p \sum_{q\in\mathcal{P}} r_{\mathrm{qp}}[k], \tag{5.21}
$$

which yields

$$
l_p(x_p[k+1]) \leq l_p(x_p[k]) + \frac{\varepsilon}{2}. \tag{5.22}
$$

■

Lemma 5.2. $\mathcal{X}_{\mathrm{CP}}$ is a positively invariant set for the LB dynamics.

Proof. We need to show that, for all $k \geq 0$, for all $p \in \mathcal{P}^i$ and for all $i \in \mathcal{I}$, i) $\sum_{p\in\mathcal{P}^i} x^i_p[k] = \lambda^i$, ii) $x^i_p[k] \geq 0$, iii) $x_p[k] \leq c_p$.

i) Considering that $x[0] \in \mathcal{X}_{\mathrm{CP}}$, equations (5.9), (5.11) and (5.8) yield that the population remains constant, since

$$x_p^i[k+1]-x_p^i[k]=\sum_{p\in\mathcal{P}^i}\sum_{q\in\mathcal{P}^i}\left(r_{\mathrm{qp}}^i[k]-r_{\mathrm{pq}}^i[k]\right)=\sum_{p\in\mathcal{P}^i}\sum_{q\in\mathcal{P}^i}r_{\mathrm{qp}}^i[k]-\sum_{q\in\mathcal{P}^i}\sum_{p\in\mathcal{P}^i}r_{\mathrm{qp}}^i[k]=0 \tag{5.23}$$

and thus that $\sum_{p\in\mathcal{P}^i}x_p^i[k]=\sum_{p\in\mathcal{P}^i}x_p^i[0]=\lambda^i,\forall k\geq 0$.

ii) Given that $x_p^i[0]\geq 0$, it is proven below by induction that $x_p^i[k]\geq 0,\forall k\geq 0$. Assuming that $x_p^i[k]\geq 0$, for a given k, it is sufficient to prove that

$$x_p^i[k+1]=x_p^i[k]+\tau\sum_{q\in\mathcal{P}^i}\left(r_{\mathrm{qp}}^i[k]-r_{\mathrm{pq}}^i[k]\right)\geq 0,\forall p\in\mathcal{P}^i. \tag{5.24}$$

If $x_p^i[k]=0$, it follows that $r_{\mathrm{pq}}^i[k]=0$ and thus equation (5.24) yields $x_p^i[k+1]\geq 0$.

If $x_p^i[k]>0$, from equation (5.11) it follows that $r_{\mathrm{pq}}^i[k]\geq 0$. Thus, the following inequality holds (in the worst case, no providers migrate part of their population to a provider p):

$$x_p^i[k+1]\geq x_p^i[k]-\tau\sum_{q\in\mathcal{P}^i}r_{\mathrm{pq}}^i[k]. \tag{5.25}$$

A sufficient condition for inequality (5.24) to hold is then

$$x_p^i[k]-\tau\sum_{q\in\mathcal{P}^i}r_{\mathrm{pq}}^i[k]\geq 0. \tag{5.26}$$

Recalling equations (5.11) and (5.13), eq. (5.26) is written as

$$\begin{aligned}
&x_p^i[k]-\tau\sum_{q\in\mathcal{P}^i}r_{\mathrm{pq}}^i[k]=x_p^i[k]-\tau\sum_{q\in\mathcal{P}^i}x_p^i[k]\sigma^i\mu_{\mathrm{pq}}^i[k]=\\
&=x_p^i[k]\left(1-\tau\sigma^i\sum_{q\in\mathcal{P}^i}\mu_{\mathrm{pq}}^i[k]\right)=\\
&\geq x_p^i[k]\left(1-\tau\sigma^i(\left|\mathcal{P}^i\right|-1)\right),
\end{aligned} \tag{5.27}$$

where the inequality holds since the summation has at most $\left(\left|\mathcal{P}^i\right|-1\right)$ terms equal to 1. In the case $x_p^i[k]>0$, equations (5.14) and (5.15) are sufficient for equation (5.27) to be non-negative;

iii) Given that $x_p[0] \leq c_p$, it is proven below by induction that $x_p[k] \leq c_p, \forall k \geq 0$. Assuming that $x_p[k] \leq c_p$, for a given k, it is sufficient to prove that

$$x_p[k+1] = x_p[k] + \tau \sum_{i \in \mathcal{I}} \sum_{q \in \mathcal{P}^i} \left(r_{\mathrm{qp}}^i[k] - r_{\mathrm{pq}}^i[k] \right) \leq c_p, \forall p \in \mathcal{P}^i. \tag{5.28}$$

If $x_p[k] \geq c_p - \frac{\varepsilon}{2\overline{\beta}}$ equation (5.13) entails that $r_{\mathrm{qp}}^i[k]=0$ for all $q \in \mathcal{P}^i$ and $i \in \mathcal{I}$ and, thus, from equation (5.9), that $x_p[k+1] \leq x_p[k]$.

Otherwise, if $x_p[k] < c_p - \frac{\varepsilon}{2\overline{\beta}}$, we consider that

$$\begin{aligned} x_p[k+1] &\leq x_p[k] + \tau \sum_{i \in \mathcal{I}} \sum_{q \in \mathcal{P}^i} r_{\mathrm{qp}}^i[k] = x_p[k] + \tau \sum_{i \in \mathcal{I}} x^i[k]\, \sigma^i \sum_{q \in \mathcal{P}^i} \mu_{\mathrm{qp}}^i[k] \\ &\leq x_p[k] + \sum_{i \in \mathcal{I}} \frac{\varepsilon}{2\overline{\beta}\,|\mathcal{I}|} = x_p[k] + \frac{\varepsilon}{2\overline{\beta}} \end{aligned} \tag{5.29}$$

■

Lemma 5.3. The function

$$\mathcal{L}(\mathbf{x}) := \Phi(\mathbf{x}) - \Phi_{\min}. \tag{5.30}$$

is a candidate Lyapunov function for the LB dynamics.

Proof. The function $\mathcal{L}(\mathbf{x})$ is positive definite in $\mathcal{X}_{\mathrm{CP}}$ by definition, since $\Phi_{\min}$ is the minimum value of $\Phi(\mathbf{x})$ for all the minimizers of the CP.

Let $\Delta\mathcal{L}(\mathbf{x}[k])$ denote the difference of the Lyapunov function $\mathcal{L}(\mathbf{x})$ along the solutions of the controlled system:

$$
\begin{aligned}
&\Delta\mathcal{L}(\mathbf{x}[k]) = \mathcal{L}(\mathbf{x}[k+1]) - \mathcal{L}(\mathbf{x}[k]) = \\
&= \sum_{p\in\mathcal{P}} \int_{x_p[k]}^{x_p[k+1]} l_p(\xi)\, d\xi \leq \\
&\leq \sum_{p\in\mathcal{P}} (x_p[k+1] - x_p[k])\, l_p(x_p[k+1]) = \\
&= \sum_{i\in\mathcal{I}} \sum_{p\in\mathcal{P}} \tau \left(\sum_{q\in\mathcal{P}} r^i_{\mathrm{qp}}[k] - \sum_{q\in\mathcal{P}} r^i_{\mathrm{pq}}[k] \right) l_p(x_p[k+1]) = \\
&= \tau \sum_{i\in\mathcal{I}} \sum_{p\in\mathcal{P}} \sum_{q\in\mathcal{P}} r^i_{\mathrm{pq}}[k]\, (l_q(x_q[k+1]) - l_p(x_p[k+1]))
\end{aligned}
\tag{5.31}
$$

where the inequality holds from geometric considerations: If $x_p[k+1] > x_p[k]$, recalling that the l_p's are nondecreasing functions, the definite integral $\int_{x_p[k]}^{x_p[k+1]} l_p(\xi)\, d\xi$ *is smaller than the quantity* $(x_p[k+1] - x_p[k])\, l_p(x_p[k+1])$; conversely, if $x_p[k+1] < x_p[k]$, the integral $\int_{x_p[k+1]}^{x_p[k]} l_p(\xi)\, d\xi$ is larger than the quantity $(x_p[k] - x_p[k+1])\, l_p(x_p[k+1])$.

Analysing each term of the inner summation, two cases hold: if $r^i_{\mathrm{qp}}(t) = 0$ the term is null, otherwise, if $r^i_{\mathrm{qp}}(t) > 0$, the term is negative. In fact, it is shown below that, if $r^i_{\mathrm{pq}}[k] > 0$, it holds that $l_p(x_p[k+1]) - l_q(x_q[k+1]) > 0$.

Lemma 5.1 states that

$$
\begin{aligned}
&l_p(x_p[k+1]) - l_q(x_q[k+1]) \geq \\
&\geq \left(l_p(x_p[k]) - \frac{\varepsilon}{2} \right) - \left(l_q(x_q[k]) + \frac{\varepsilon}{2} \right) \\
&= l_p(x_p[k]) - l_q(x_q[k]) - \varepsilon > 0
\end{aligned}
\tag{5.32}
$$

where the inequality holds since a necessary condition for $r^i_{\mathrm{pq}}[k] > 0$ is that $l_p(x_p[k]) - l_q(x_q[k]) > \varepsilon$ (see equation (5.13)).

■

Finally, the following theorem prove the convergence towards an approximated Beckmann user equilibrium.

Theorem 5.2. The trajectories of the LB dynamics asymptotically tend to the set of equilibria $\mathcal{X}^{\varepsilon}_{\mathrm{eq}}$.

Proof. Given that *Lemma 5.2* states that $\mathcal{L}(\mathbf{x})$ is a candidate Lyapunov function for the LB dynamics, the proof relies on the LaSalle invariance principle of Theorem 5.1, i.e., on showing that $\mathcal{X}_{\text{eq}}^{\varepsilon}$ is the maximum invariant set where $\Delta\mathcal{L} = 0$.

Let $\mathbf{x} \in \mathcal{X}_{\text{eq}}^{\varepsilon}$ and $\mathbf{x}[0] = \mathbf{x}$. By comparing definition (5.6) and equation (5.13), it holds that $r_{\text{pq}}^{i}[k] = 0$ for all $p, q \in \mathcal{P}^{i}$ and $i \in \mathcal{I}$, which entails i) that $\mathbf{x}[k] = \mathbf{x}[0] = \mathbf{x}_{\text{eq}} \in \mathcal{X}_{\text{eq}}^{\varepsilon}$ for all $k > 0$, i.e., that $\mathcal{X}_{\text{eq}}^{\varepsilon}$ is a positively invariant set, and ii) that $\Delta\mathcal{L}(\mathbf{x}[k]) = 0$ in $\mathcal{X}_{\text{eq}}^{\varepsilon}$ (see equation (5.31)).

To show that $\mathcal{X}_{\text{eq}}^{\varepsilon}$ is the maximum set where $\Delta\mathcal{L}(\mathbf{x}[k]) = 0$, it is proven below that $\Delta\mathcal{L}(\mathbf{x}[k]) < 0$ if $\mathbf{x}[k] = \mathbf{x}$, with $\mathbf{x} \notin \mathcal{X}_{\text{eq}}$. In fact, by definition (5.12), in this case there exist at least one pair of providers $p, q \in \mathcal{P}^{i}$ and a commodity $i \in \mathcal{I}$ such that $l_p(x_p[k]) - l_q(x_q[k]) > \varepsilon$, with $x_p^i[k] > 0$ and $x_q[k] < c_q - \frac{\varepsilon}{2\beta}$, which, in turn, yields $r_{\text{pq}}^{i}[k] > 0$ (see equations (5.11), (5.14) and (5.13)). Having established that $r_{\text{pq}}^{i}[k] > 0$ with $l_p(x_p(t)) - l_q(x_q(t)) > \varepsilon$, it follows that the corresponding term of the inner summation of equation (5.31) is negative, which is a sufficient condition for $\Delta\mathcal{L}(\mathbf{x}[k]) < 0$ (recalling that, in the proof of Lemma 5.3, it is shown that the terms of equation (5.31) are non-positive).

■

5.3.3 5G Traffic steering as a dynamic load-balancing problem

In the dynamic multi-connectivity framework of 5G networks [3], each UE selects the serving APs for its QoS-Flows. When the traffic of multiple UEs is characterized by the same QoS requirements and can be served by the same set of APs, such traffic is often considered as a single aggregated QoS-Flow to simplify the network control. In this work, consistently with 5G specifications, we consider these aggregated QoS-Flows to be the commodities that flow over the 5G infrastructure.

The various APs p in the set of APs $\mathcal{P}$ are modelled as resource (capacity) providers, among which the load balancing algorithm will distribute the QoS-Flows, and each AP is associated with a different latency function l_p. In the following, the latency functions are assumed to be representative of the transmission power required for serving the QoS-Flows, but in general they can model several other performance indices under mild hypotheses, as it will be discussed.

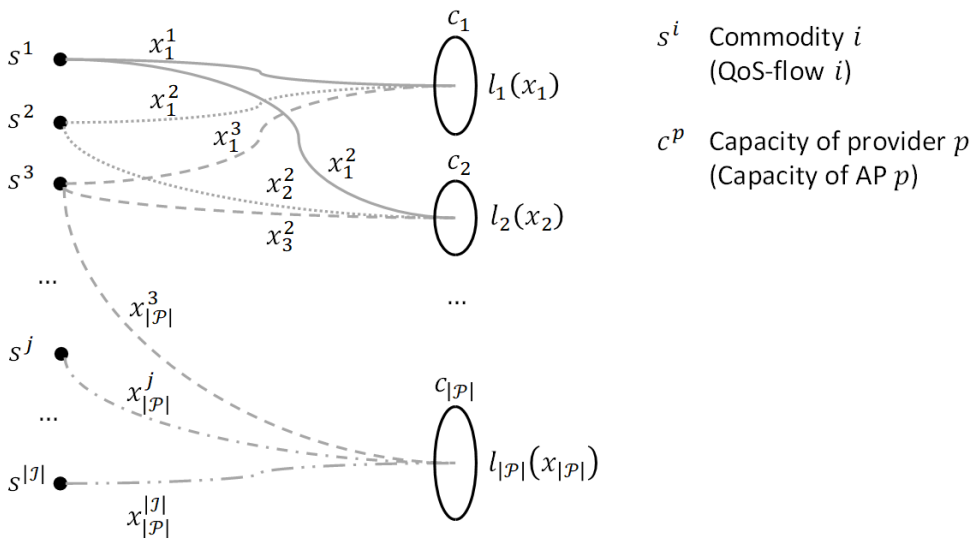

Fig. 5.2 Load balancing graph

Each commodity i in the set of commodities $\mathcal{I}$ is assumed to be characterised by a constant bitrate λ^i, a reasonable assumption for aggregated QoS-Flows over a limited time window, and the state variable of the system at time k, $x_p^i[k]$, represents the bitrate of commodity i assigned to the AP p in the set $\mathcal{P}^i \subset \mathcal{P}$ of the APs available to commodity i. The amount of bitrate that an AP p can sustain is limited by its maximum transmission power c_p, causing the network to be capacity constrained. Additionally, in the framework of *network slicing*, in which third-party tenants manage a set of network resources, such constrains could also be imposed by the network operator as representative of the amount of resources that characterises the network slice.

The modelled problem reported in Figure 5.2 consists then in a load-balancing among the various paths that connect the APs to the UEs belonging to a commodity i. At a Beckmann user equilibrium, each of the commodities will have its traffic distributed in such a way that the experienced latencies over the unconstrained APs it utilises is equalised.

5.4 Numerical Simulation

This section reports the simulation setup and results in sections 5.4.1 and IV.B, respectively.

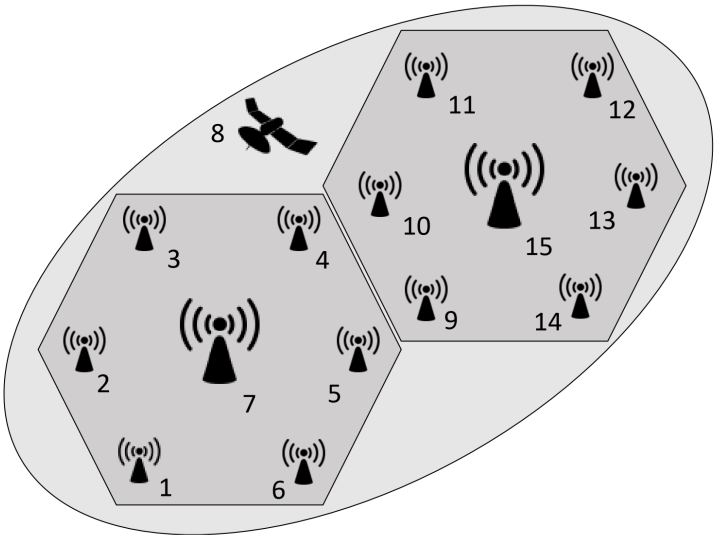

Fig. 5.3 Network representation

5.4.1 Simulation Setup

For the validation of the proposed algorithm, we consider the network depicted in Figure 5.3, consisting in an area covered by two macro-cells (providers 7 and 15). In each of the coverage zones of the two macro-cells there are six micro-cells (providers $1-6$ and $9-14$), while a high-capacity satellite (provider 8) offers connectivity in the whole area.

A total of 20 aggregated QoS-Flows (commodities) are transmitting in the area, each one characterised by a different set of APs available for routing its traffic. As introduced in Section 5.3.3, since the QoS-Flows represent the aggregated traffic received by all the UEs in a given area that share the

same available APs, it is reasonable to assume their cumulative bitrate to be equal to a constant $\lambda^i \in [4,13]$ Gbps, for each commodity i. In the example scenario, all the commodities can be served by the satellite connection, twelve commodities by a pair of adjacent micro-cells (e.g., (1,2), (2,3), ..., in Figure 5.3) and by the macro-cell which covers the micro-cells, eight commodities by a group of three adjacent micro cells (e.g., (1,2,3), (2,3,4), ..., in Figure 5.3) and by their corresponding macro cell.

Following the Shannon–Hartley theorem, the amount of power required for an AP to transmit an information flow has an exponential relation with its throughput, i.e.

$$P_p(x_p[k]) = \left(2^{\frac{x_p[k]}{W_p}} - 1\right)\frac{N_0}{G_p}, \tag{5.33}$$

in which W_p represents the AP bandwidth, N_0 captures the thermal noise and interference and G_p is the inverse of the path loss L_p that depends on the carrier frequency f_p and on the distance of the UE.

Due to the structure of (5.33), a possible representation for the latency functions l_p is

$$l_p(x_p) = \alpha_p 2^{\gamma_p x_p}, \tag{5.34}$$

In which the parameters α_p, γ_p can be used to capture the differ power usage associated to the various APs and the operator preferences. In the depicted scenario, the algorithm objective becomes the one of routing the traffic of each QoS-Flow over the different APs in such a way to minimise, unilaterally, their latency and consequently their power consumption. This scenario is representative of a situation in which the various QoS-Flows, in principle owned by different tenants, are charged by the network operators depending on their energy usage or a situation in which balancing the traffic benefits. Several different choices could be made for the latency function, spacing from quantities that capture connection reliability, to transmission delay and user satisfaction, as the only requirements that such functions must satisfy are represented by Assumption 5.1.

Table 5.1 Characteristics of micro, macro and satellite cells

Param.	*Micro-cell*	*Macro-cell*	*Satellite*
$\overline{P_p}$	1 W	41 W	2 W
d_p	$[0.1, 0.2]$ km	$[0.2, 0.3]$ km	35000 km
f_p	21 GHz	2.1 GHz	20 GHz
W_p	1 GHz	0.2 GHz	0.8 GHz
c_p	17.84 *Gbps*	4.4 *Gbps*	2 *Gbps*

Table 5.2 Average values for the latency parameters

Param.	*Micro-cell*	*Macro-cell*	*Satellite*
α_p	$5 \cdot 10^{-6}$	10^{-5}	$23 \cdot 10^{-2}$
γ_p	1	5	1.25

Regarding the capacitated nature of the considered network, one has to consider that throughput available over an AP is

limited by either a network operator resource allocation policy, (in terms of dedicated network resources in the various APs, as envisaged in network slicing), or the equipment limitation (as maximum transmission power $\overline{P_p}$ or its bandwidth).

Table 5.1 reports the numerical values that characterise the network under study, in which standard micro and macro cells coexist with a satellite characterised by an isotropic gain of 60 dBi. We denote with d_p the average distance of the UEs served by the AP p, and derive c_p from (5.33) in ideal conditions (e.g., no interference) as an upper bound. To stress the capacitated nature of the problem, in addition we imposed that the micro-cell 5 maximum bitrate was capacitated at 14 $Gbps$.

The values of Table 5.1 were used to identify reasonable values for the parameters α_p, γ_p of (34), whose average values are reported in Table 5.2, that will be used in our simulations.

Concerning the parameters of the controller, the choice of latency functions leads to the value $\overline{\beta}$=3.4 W/GHz, the latency tolerance is selected as $\varepsilon = 0.01$ and the sampling time as $\tau = 10^{-3}s$.

5.4.2 Simulation Results

Simulation runs were initialized in an imbalanced way, without any load on the macro-cells, as all the load was randomly distributed over the micro-cells and the satellite.

The reported simulations showed a convergence time to an ε-Beckmann equilibrium in the order of 150s, averaged over 25 runs. It is worth remarking that such convergence time is not related to the 5G QoS requirements, as it is assumed that the various access points are able to provide the proper QoS level (e.g., connection latency, average BER, reliability level,...) if their capacities are not violated.

Figure 5.4 shows, for an example run, how the maximum latency mismatch over all the commodities, defined as

$$e[k] = \max_{i\in\mathcal{I}} \left\{ \max_{p\in\mathcal{P}^i | x_p^i[k]>0} l_p(x_p[k]) - \min_{q\in\mathcal{P}^i | x_q[k]<c_q-\frac{\varepsilon}{2\overline{\beta}}} l_q(x_q[k]) \right\},$$

decreases with time and, even if the initial conditions are quite unbalanced, with $e[k] > 2$, after 100s $e[k]$ is already below 0.03.

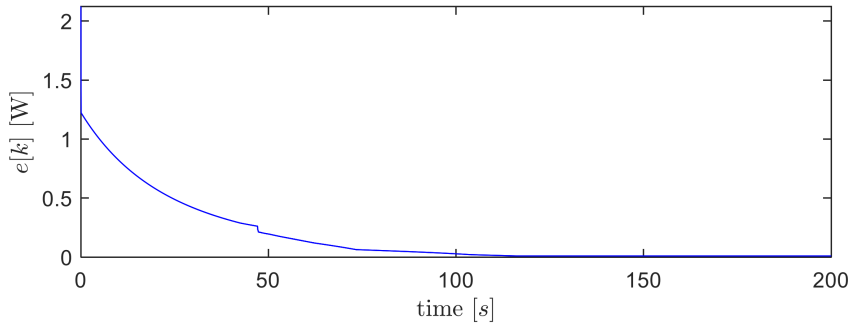

Fig. 5.4 Maximum latency mismatch during the simulation.

As examples of simulation results, Figure 5.5 reports the evolution of the latencies that characterise the commodities 9, 11 and 5, for all of their available APs.

The upper plot shows that the latencies of the APs available to QoS-Flow 9 converge to a common value, as expected, within the threshold ε; in particular, we can notice how the commodity rapidly starts using the (initially unused) available macro-cell.

The middle plot shows that QoS-Flow 11 avoids using the satellite, even if it is available in $\mathcal{P}^i$, in order to achieve a lower convergence latency value.

The lowest plot shows the latencies of the QoS-Flow 5 and highlights that the latency of micro-cell 5 does not converge to the latencies of the other used APs (micro-cell 6, macro-cell 7): the reason is that, in the simulation scenario, the available capacity of micro-cell 5 is lower than the one of the other micro-cells and becomes ε-saturated after about $60s$ – thus, by definition, the population of QoS-Flow 5 still converges to an ε-Beckmann equilibrium.

Finally, Figure 5.6 shows the population dynamics over the APs, highlighting how most of the traffic is routed over the micro cells, while still utilising the macro cells and satellite to balance the overall power consumption in terms of latency experienced.

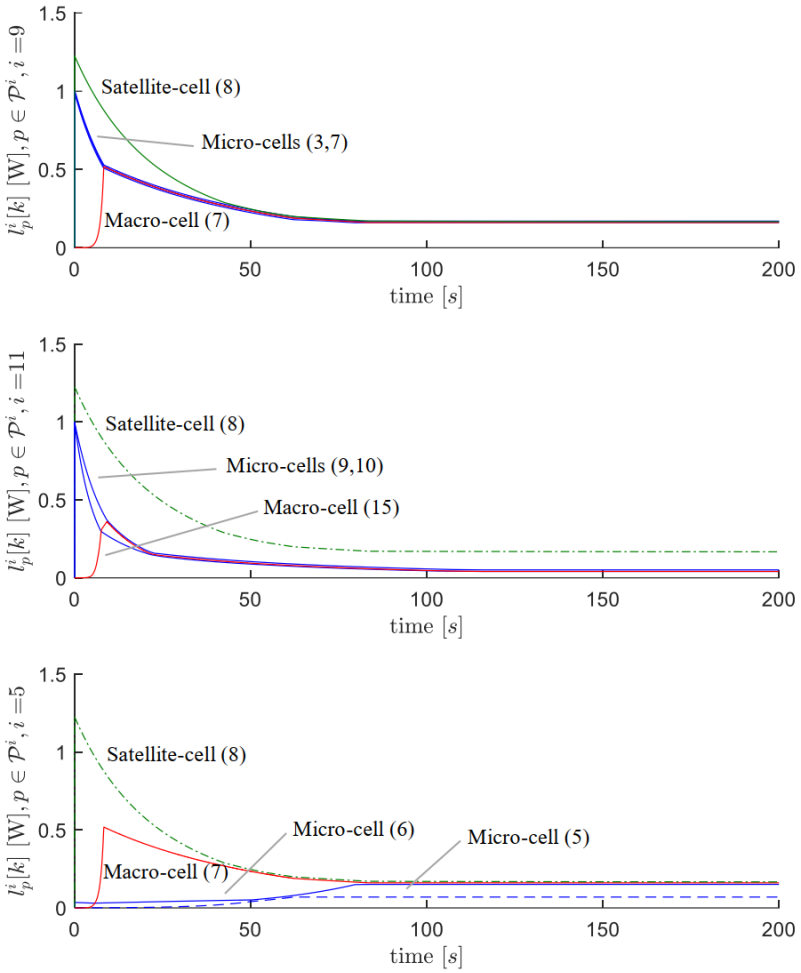

Fig. 5.5 Commodity latency examples during the simulation (solid lines: unconstrained providers used by the commodity; dash-dotted lines: unconstrained providers not used by the commodity; dashed lines: constrained providers).

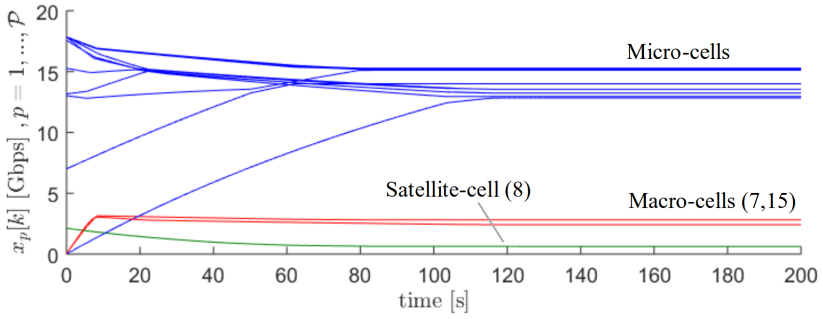

Fig. 5.6 Access points loads

5.5 Conclusions

This work deals with the problem of Multi-Connectivity, one of the key features of 5G networks, which enables the user equipment to simultaneously transmit/receive traffic flows, referred to as QoS-Flows, over different access networks, with the aim of increasing the transmission rate and/or to improve the transmission reliability. In Multi-Connectivity, the *traffic steering* functionality is in charge of distributing the traffic load of each QoS-Flow over the different access network This work proposes to model the traffic steering problem as a distributed, non-cooperative and dynamic load-balancing problem. A latency function is associated to each pair QoS-Flow and access network and is computed as the power required by the QoS-Flow considering the current access network load and the QoS-Flow requirements in terms of bit error rate. The aim is to distribute the overall network load among the access networks in such a way that an equilibrium point is reached. Also, the problem model includes the fact that the access network capacities are limited: the resulting problem is a capacitated load-balancing one.

By using Lyapunov arguments, the proposed algorithm is proved to converge to an approximate Beckmann user equilibrium, in which the latencies of the access networks are equalized up to a tolerated latency mismatch. Simulation results validate the approach, showing how the proposed algorithms deals with capacitated providers.

Beside the modelling of the 5G Traffic Steering problem as a dynamic load-balancing one, this work presents, up to the authors' knowledge, the first multi-commodity, dynamic and adversarial load-balancing algorithm which explicitly considers capacitated providers. Future work is aimed i) at introducing latency constraints in the problem formulation in order to model more Quality-of-Service constraints of the 5G services; ii) at considering time-varying loads and iii) in the extension of the approach to time-delayed case.

Regarding point iii) a contribution was recently submitted for publication as

[SJ1] *A. Giuseppi and A. Pietrabissa, "Wardrop equilibrium in discrete-time selfish routing with time-varying bounded delays," in IEEE Transactions on Automatic Control, under review.*

Chapter 6

General Conclusion and Perspectives

This thesis gathered four of the main research activities completed by the candidate during the three years of his PhD. The researches focus on the field of control of Cyber-Physical Systems (CPS), a topic the candidate had the opportunity to study thanks to his participation in the EU-funded research project H2020 ATENA and in the H2020 EU-Korea project 5G-ALLSTAR.

During his work as researcher in the ATENA project the candidate studied Critical Infrastructures as a large-scale CPS whose security is of the utmost importance, as they provide services fundamental for our society. The topic of security, and the frequent interaction with researchers from the Israel Electric Company, led to the design and development of the first of the four control solutions presented in this work, being the dynamic reconfiguration of the power distribution network.
The proposed controller was based on Economic Model Predictive Control (EMPC) to allow the system to be operated in a preventive way and improve service resiliency by avoiding states associated to high risk levels.

The same methodology was applied to the problem of power and heating management in smart buildings, where user requests and use case requirements were translated into logical constraints for the controller.

The third study reported in this thesis was developed during a research collaboration opportunity with the manufacturer Thales Alenia Space Italia. The company detailed one of its real cases of interest, related to the extension of the operative life of legacy,

already orbiting, satellites. The research activities led to the development of a control scheme for a life-support system that can be attached to an orbiting satellite. Such scheme was based on feedback linearization, under which it was proven that the two interconnected spacecraft may operate in parallel without requiring communication or information exchanges, as the life-support compensates for its effects on the dynamics of the original satellite.

The last problem studied by the candidate dealt with selfish routing and load balancing in dynamical networks, and was carried out in the H2020 EU-Korea project 5G-ALLSTAR. The discrete-time control law designed in the work was proven by Lyapunov arguments to drive the state of the network, assumed to be formed by capacitated providers, to equilibria that represent an approximation of the Wardrop user equilibrium. This theoretical result can easily be applied to 5G heterogeneous networks for the problems of Multi-Connectivity and Traffic Steering, playing a fundamental role in the seamless integration of satellite connection with 5G, and improvement of connection resiliency, that are the aim of the project.

The candidate is currently studying several topics that represent an extension of the works presented in this manuscript. Regarding spacecraft control, the collaboration with Thales Alenia Space Italia allowed the candidate to be introduced to the problem of large-scale flexible satellites and the nonlinear problem that characterise them. The topic of robustness is also being explored, currently focusing on the uncertainties that affect the high-frequency gain matrix that appears in the normal form of the attitude dynamics.
Regarding Power Networks, the candidate is studying a nonlinear robust protection scheme to defend the transmission network against the effects of a malicious control action that took over one compromised generator.
Finally, in the scope of control of 5G networks, the candidate is exploring Reinforcement Learning based approaches to the selfish routing and load balancing problem, while also finalising the extension of the control law presented in this thesis to time-delayed scenarios.

The following and final chapter of the manuscript contains the publication list of the candidate, mostly related to the activities of the three years of his PhD, and the entire thesis bibliography.

Bibliography

Publication List

Journal papers

[J1] F. Liberati, A. Di Giorgio, A. Giuseppi, A. Pietrabissa, and F. Delli Priscoli, "Efficient and risk-aware control of electricity distribution grids," *IEEE System Journal*, 2020.

[J2] A. Giuseppi, A. Pietrabissa, S. Cilione, and L. Galvagni, "Feedback linearization-based satellite attitude control with a life-support device without communications," *Control Engineering Practice*, vol. 90, pp. 221–230, 2019.

[J3] F. Liberati, A. Di Giorgio, A. Giuseppi, A. Pietrabissa, E. Habib, and L. Martirano, "Joint model predictive control of electric and heating resources in a smart building," *IEEE Transactions on Industry Applications*, 2019.

[J4] F. Adamsky, M. Aubigny, F. Battisti, M. Carli, F. Cimorelli, T. Cruz, A. Di Giorgio, C. Foglietta, A. Galli, A. Giuseppi, F. Liberati, A. Neri, S. Panzieri, F. Pascucci, J. Proenca, P. Pucci, L. Rosa, and R. Soua, "Integrated protection of industrial control systems from cyber-attacks: The atena approach," *International Journal of Critical Infrastructure Protection*, vol. 21, pp. 72–82, 2018.

[J5] A. Pietrabissa, L. Ricciardi Celsi, F. Cimorelli, V. Suraci, F. Delli Priscoli, A. Di Giorgio, A. Giuseppi, and S. Monaco, "Lyapunov-based design of a distributed wardrop load-balancing algorithm with application to software-defined networking," *IEEE Transactions on Control Systems Technology*, 2018.

[J6] F. Liberati, A. Giuseppi, A. Pietrabissa, V. Suraci, A. Di Giorgio, M. Trubian, D. Dietrich, P. Papadimitriou, and F. Delli Priscoli, "Stochastic and exact methods for service mapping in virtualized network infrastructures," *International Journal of Network Management*, vol. 27, no. 6, 2017.

[J7] A. Pietrabissa, F. Delli Priscoli, A. Di Giorgio, A. Giuseppi, M. Panfili, and V. Suraci, "An approximate dynamic programming approach to resource management in multi-cloud scenarios," *International Journal of Control*, vol. 90, no. 3, pp. 508–519, 2017.

Conference papers

[C1] A. Giuseppi, A. Tortorelli, R. Germanà, F. Liberati, and A. Fiaschetti, "Securing cyber-physical systems: An optimization framework based on osstmm and genetic algorithms," in *2019 27th Mediterranean Conference on Control and Automation, MED 2019*, 2019.

[C2] A. Giuseppi, E. De Santis, and A. Di Giorgio, "Model predictive control of energy storage systems for power regulation in distribution networks," in *2019 IEEE International Conference on Systems, Man, and Cybernetics*, 2019.

[C3] F. Liberati, A. Giuseppi, and A. Di Giorgio, "Distributed model predictive control of electric vehicles charging," in *2019 IEEE International Conference on Systems, Man, and Cybernetics*, 2019.

[C4] A. Giuseppi, R. Germanà, and A. Di Giorgio, "Risk adverse virtual power plant control in unsecure power systems," in *2018 26th Mediterranean Conference on Control and Automation, MED 2018*, 2018, pp. 210–216.

[C5] L. Martirano, E. Habib, A. Giuseppi, and A. Di Giorgio, "Nearly zero energy building model predictive control for efficient heating," in *2018 IEEE Industry Applications Society Annual Meeting, IAS 2018*, 2018.

[C6] M. Panfili, A. Giuseppi, A. Fiaschetti, H. B. Al-Jibreen, A. Pietrabissa, and F. Delli Priscoli, "A game-theoretical approach to cyber-security of critical infrastructures based on multi-agent reinforcement learning," in *2018 26th Mediterranean Conference on Control and Automation, MED 2018*, 2018, pp. 460–465.

[C7] V. Suraci, L. Ricciardi Celsi, A. Giuseppi, G. Manfredi, and A. Di Giorgio, "Distributed wardrop load balancing in multi-mtu scada systems," in *2018 26th Mediterranean Conference on Control and Automation, MED 2018*, 2018, pp. 466–472.

[C8] A. Di Giorgio, A. Giuseppi, F. Liberati, A. Ornatelli, A. Rabezzano, and L. Ricciardi Celsi, "On the optimization of energy storage system placement for protecting power transmission grids against dynamic load altering attacks," in *2017 25th Mediterranean Conference on Control and Automation, MED 2017*, 2017, pp. 986–992.

[C9] A. Di Giorgio, A. Giuseppi, F. Liberati, and A. Pietrabissa, "Controlled electricity distribution network black start with energy storage system support," in *2017 25th Mediterranean Conference on Control and Automation, MED 2017*, 2017, pp. 781–786.

[C10] V. Suraci, L. Ricciardi Celsi, A. Giuseppi, and A. Di Giorgio, "A distributed wardrop control algorithm for load balancing in smart grids," in *2017 25th Mediterranean Conference on Control and Automation, MED 2017*, 2017, pp. 761–767.

[C11] J. F. Riera, J. Batalle, J. Bonnet, M. Dias, M. McGrath, G. Petralia, F. Liberati, A. Giuseppi, A. Pietrabissa, A. Ceselli, A. Petrini, M. Trubian, P. Papadimitrou, D. Dietrich, A. Ramos, J. Melian, G. Xilouris, A. Kourtis, T. Kourtis, and E. K. Markakis, "Tenor: Steps towards an orchestration platform for multi-pop nfv deployment," in *IEEE NETSOFT 2016 - 2016 IEEE NetSoft Conference and Workshops: Software-Defined Infrastructure for Networks, Clouds, IoT and Services*, 2016, pp. 243–250.

[C12] A. Pietrabissa, S. Battilotti, F. Facchinei, A. Giuseppi, G. Oddi, M. Panfili, and V. Suraci, "Resource management in multi-cloud scenarios via reinforcement learning," in *Chinese Control Conference, CCC*, vol. 2015-September, 2015, pp. 9084–9089.

Submitted Papers

[SJ1] A. Giuseppi and A. Pietrabissa, "Wardrop equilibrium in discrete-time selfish routing with time-varying bounded delays," in *IEEE Transactions on Automatic Control*, under review.

[SJ2] F. Delli Priscoli, A. Giuseppi, and A. Pietrabissa, "Capacity-constrained wardrop equilibria and application to multi-connectivity in 5g networks," in *Journal of the Franklin Institute*, under review.

[SJ3] A. Giuseppi and A. Pietrabissa, "Robust and fault-tolerant spacecraft attitude control with performance recovery based on an extended-observer design," in *International Journal of Control*, under review.

[SJ4] A. Giuseppi, F. Lisi, and A. Pietrabissa, "Automatic transportation mode recognition on smartphone data based on deep neural networks," in *Journal of Intelligent Transportation Systems: Technology, Planning, and Operations*, under review.

[SJ5] A. Tortorelli, A. Fiaschetti, A. Giuseppi, V. Suraci, R. Germanà, and F. Delli Priscoli, "A security metric for assessing the security level of critical infrastructures," in *International Journal of Critical Computer-Based Systems*, under review.

[SC1] A. Giuseppi, A. Pietrabissa, F. Liberati, R. Germanà, and F. Delli Priscoli, "Traffic steering and network selection in 5g networks based on reinforcement learning," in *European Control Conference 2020 (ECC2020)*, under review.

[SC2] R. Germanà, A. Giuseppi, A. Pietrabissa, and A. Di Giorgio, "Ensuring the stability of power systems against dynamic load altering attacks: A robust control scheme using energy storage systems," in *European Control Conference 2020 (ECC2020)*, under review.

Patents

[P1] F. Cincotti, D. G. Ferriero, A. Giuseppi, A. Pietrabissa, C. Poli, L. Ricciardi Celsi, *Patent application it-102018000002114 - APP-CI, "assistente predittivo personalizzato per il controllo di interfacce uomo-computer per pazienti con disabilità motorie basato su metodi di model predictive control e machine learning"*, 2017.

References

[1] C. M. Ramkissoon, B. Aufderheide, B. W. Bequette, and J. Vehí, "A review of safety and hazards associated with the artificial pancreas," *IEEE Reviews in Biomedical Engineering*, vol. 10, pp. 44–62, 2017.

[2] J. Lee, B. Bagheri, and H.-A. Kao, "A cyber-physical systems architecture for industry 4.0-based manufacturing systems," *Manufacturing letters*, vol. 3, pp. 18–23, 2015.

[3] 5GPPP Architecture Working Group, "5gppp architecture working group view on 5g architecture," Tech. Rep., 2017.

[4] B. Krogh, M. Ilic, and S. S. Sastry, "National workshop on beyond scada: Networked embedded control for cyber-physical systems (nec4cps): Research strategies and roadmap," Team for Research in Ubitquitous Secure Technology (TRUST), Tech. Rep., Jul. 2007. [Online]. Available: http://www.truststc.org/pubs/262.html.

[5] E. A. Lee and S. A. Seshia, *Introduction to embedded systems: A cyber-physical systems approach*. Mit Press, 2016.

[6] N. Jazdi, "Cyber physical systems in the context of industry 4.0," in *2014 IEEE International Conference on Automation, Quality and Testing, Robotics*, May 2014, pp. 1–4.

[7] E. Hozdic, "Smart factory for industry 4.0: A review," *International Journal of Modern Manufacturing Technologies*, vol. 7, no. 1, pp. 28–35, 2015.

[8] S. Karnouskos, "Cyber-physical systems in the smartgrid," in *2011 9th IEEE International Conference on Industrial Informatics*, IEEE, 2011, pp. 20–23.

[9] Y. Jie, J. Y. Pei, L. Jun, G. Yun, and X. Wei, "Smart home system based on iot technologies," in *2013 International Conference on Computational and Information Sciences*, IEEE, 2013, pp. 1789–1791.

[10] J. M. Bradley and E. M. Atkins, "Coupled cyber-physical system modeling and coregulation of a cubesat," *IEEE Transactions on Robotics*, vol. 31, no. 2, pp. 443–456, Apr. 2015.

[11] A. T. Klesh, J. W. Cutler, and E. M. Atkins, "Cyber-physical challenges for space systems," in *2012 IEEE/ACM Third International Conference on Cyber-Physical Systems*, Apr. 2012, pp. 45–52.

[12] Y. Zhang, M. Qiu, C. Tsai, M. M. Hassan, and A. Alamri, "Health-cps: Healthcare cyber-physical system assisted by cloud and big data," *IEEE Systems Journal*, vol. 11, no. 1, pp. 88–95, Mar. 2017.

[13] I. Lee and O. Sokolsky, "Medical cyber physical systems," in *Design automation conference*, IEEE, 2010, pp. 743–748.

[14] C.-R. Rad, O. Hancu, I.-A. Takacs, and G. Olteanu, "Smart monitoring of potato crop: A cyber-physical system architecture model in the field of precision agriculture," *Agriculture and Agricultural Science Procedia*, vol. 6, pp. 73–79, 2015.

[15] A. Iyengar, A. Kundu, and G. Pallis, "Healthcare informatics and privacy," *IEEE Internet Computing*, vol. 22, no. 2, pp. 29–31, 2018.

[16] K. Zarkogianni, A. Vazeou, S. G. Mougiakakou, A. Prountzou, and K. S. Nikita, "An insulin infusion advisory system based on autotuning nonlinear model-

predictive control," *IEEE Transactions on Biomedical Engineering*, vol. 58, no. 9, pp. 2467–2477, Sep. 2011.

[17] F. Pasqualetti, F. Dörfler, and F. Bullo, "Attack detection and identification in cyber-physical systems," *IEEE Transactions on Automatic Control*, vol. 58, no. 11, pp. 2715–2729, Nov. 2013.

[18] A. Humayed, J. Lin, F. Li, and B. Luo, "Cyber-physical systems security—a survey," *IEEE Internet of Things Journal*, vol. 4, no. 6, pp. 1802–1831, Dec. 2017.

[19] H. Song, G. A. Fink, and S. Jeschke, *Security and Privacy in Cyber-Physical Systems*. Wiley Online Library, 2017.

[20] L. Pietre-Cambacedes and C. Chaudet, "The sema referential framework: Avoiding ambiguities in the terms security and safety," *International Journal of Critical Infrastructure Protection*, vol. 3, no. 2, pp. 55–66, 2010.

[21] M. B. Line, O. Nordland, L. Røstad, and I. A. Tøndel, "Safety vs security?" In *PSAM conference, New Orleans, USA*, 2006.

[22] D. Mayne, J. Rawlings, C. Rao, and P. Scokaert, "Constrained model predictive control: Stability and optimality," *Automatica*, vol. 36, no. 6, pp. 789–814, 2000.

[23] T. Roughgarden, *Selfish routing and the price of anarchy*. MIT Press, 2005.

[24] A. K. Srivastava, A. A. Kumar, and N. N. Schulz, "Impact of distributed generations with energy storage devices on the electric grid," *IEEE Systems Journal*, vol. 6, no. 1, pp. 110–117, Mar. 2012.

[25] W. Nwesaty, A. I. Bratcu, and O. Sename, "Power sources coordination through multivariable linear parameter-varying/h_∞ control with application to multi-source electric vehicles," *IET Control Theory & Applications*, vol. 10, no. 16, pp. 2049–2059, 2016.

[26] C. Kwon and I. Hwang, "Cyber attack mitigation for cyber–physical systems: Hybrid system approach to controller design," *IET Control Theory & Applications*, vol. 10, no. 7, pp. 731–741, 2016.

[27] R. A. Jabr, R. Singh, and B. C. Pal, "Minimum loss network reconfiguration using mixed-integer convex programming," *IEEE Transactions on Power Systems*, vol. 27, no. 2, pp. 1106–1115, May 2012.

[28] N. C. Koutsoukis, D. O. Siagkas, P. S. Georgilakis, and N. D. Hatziargyriou, "Online reconfiguration of active distribution networks for maximum integration of distributed generation," *IEEE Transactions on Automation Science and Engineering*, vol. 14, no. 2, pp. 437–448, 2017.

[29] R. A. Jabr, "Radial distribution load flow using conic programming," *IEEE Transactions on Power Systems*, vol. 21, no. 3, pp. 1458–1459, Aug. 2006.

[30] Y. Liu, J. Li, and L. Wu, "Coordinated optimal network reconfiguration and voltage regulator/DER control for unbalanced distribution systems," *IEEE Transactions on Smart Grid*, pp. 1–1, 2018.

[31] M. N. B. Muhtazaruddin, N. A. Bani, S. A. M. Aris, H. M. Kaidi, A. Y. A. Fatah, J. J. Jamia, F. Muhammad-Sukki, and S. H. Abu-Bakar, "Distribution power loss minimization via distributed generation, capacitor and network reconfiguration," *Indonesian Journal of Electrical Engineering and Computer Science*, vol. 5, no. 3, pp. 488–495, 2017.

[32] L. Bai, T. Jiang, F. Li, H. Chen, and X. Li, "Distributed energy storage planning in soft open point based active distribution networks incorporating network

reconfiguration and dg reactive power capability," *Applied Energy*, vol. 210, pp. 1082–1091, 2018.

[33] C. Lee, C. Liu, S. Mehrotra, and Z. Bie, "Robust distribution network reconfiguration," *IEEE Transactions on Smart Grid*, vol. 6, no. 2, pp. 836–842, Mar. 2015.

[34] D.-L. Duan, X.-D. Ling, X.-Y. Wu, and B. Zhong, "Reconfiguration of distribution network for loss reduction and reliability improvement based on an enhanced genetic algorithm," *International Journal of Electrical Power & Energy Systems*, vol. 64, pp. 88–95, 2015.

[35] L. Pfitscher, D. Bernardon, L. Canha, V. Montagner, V. Garcia, and A. Abaide, "Intelligent system for automatic reconfiguration of distribution network in real time," *Electric Power Systems Research*, vol. 97, pp. 84–92, 2013.

[36] H. Hijazi, C. Coffrin, and P. V. Hentenryck, "Convex quadratic relaxations for mixed-integer nonlinear programs in power systems," *Mathematical Programming Computation*, vol. 9, no. 3, pp. 321–367, Sep. 2017.

[37] S. F. Santos, D. Z. Fitiwi, M. R. Cruz, C. M. Cabrita, and J. P. Catalão, "Impacts of optimal energy storage deployment and network reconfiguration on renewable integration level in distribution systems," *Applied energy*, vol. 185, pp. 44–55, 2017.

[38] M. Lavorato, J. F. Franco, M. J. Rider, and R. Romero, "Imposing radiality constraints in distribution system optimization problems," *IEEE Transactions on Power Systems*, vol. 27, no. 1, pp. 172–180, Feb. 2012.

[39] H. Ahmadi and J. R. Martí, "Mathematical representation of radiality constraint in distribution system reconfiguration problem," *International Journal of Electrical Power & Energy Systems*, vol. 64, pp. 293–299, 2015.

[40] T. H. Chang, T. E. Lee, and C. H. Lin, "Distribution network reconfiguration for load balancing with a colored Petri net algorithm," in *2017 International Conference on Applied System Innovation (ICASI)*, May 2017, pp. 1040–1043.

[41] T. T. Nguyen, T. T. Nguyen, A. V. Truong, Q. T. Nguyen, and T. A. Phung, "Multi-objective electric distribution network reconfiguration solution using runner-root algorithm," *Applied Soft Computing*, vol. 52, pp. 93–108, 2017.

[42] M. R. M. Cruz, S. F. Santos, D. Z. Fitiwi, and J. P. S. Catalão, "Coordinated distribution network reconfiguration and distributed generation allocation via genetic algorithm," in *2017 IEEE International Conference on Environment and Electrical Engineering and 2017 IEEE Industrial and Commercial Power Systems Europe (EEEIC / I CPS Europe)*, Jun. 2017, pp. 1–6.

[43] IEE, "IEEE guide for electric power distribution reliability indices - redline," *IEEE Std 1366-2012 (Revision of IEEE Std 1366-2003) - Redline*, pp. 1–92, May 2012.

[44] D. Masucci, C. Foglietta, C. Palazzo, and S. Panzieri, "Improved multi-criteria distribution network reconfiguration with information fusion," in *2016 19th International Conference on Information Fusion (FUSION)*, Jul. 2016, pp. 256–263.

[45] X. Lu, N. Chen, Y. Wang, L. Qu, and J. Lai, "Distributed impulsive control for islanded microgrids with variable communication delays," *IET Control Theory & Applications*, vol. 10, no. 14, pp. 1732–1739, 2016.

[46] M. Ellis, H. Durand, and P. D. Christofides, "A tutorial review of economic model predictive control methods," *Journal of Process Control*, vol. 24, no. 8, pp. 1156–1178, 2014.

[47] J. B. Rawlings, D. Angeli, and C. N. Bates, "Fundamentals of economic model predictive control," in *2012 IEEE 51st IEEE Conference on Decision and Control (CDC)*, Dec. 2012, pp. 3851–3861.

[48] P. Kundur, N. J. Balu, and M. G. Lauby, *Power system stability and control*. McGraw-hill New York, 1994, vol. 7.

[49] X. Liu, A. Aichhorn, L. Liu, and H. Li, "Coordinated control of distributed energy storage system with tap changer transformers for voltage rise mitigation under high photovoltaic penetration," *IEEE Transactions on Smart Grid*, vol. 3, no. 2, pp. 897–906, Jun. 2012.

[50] S.-S. Shin, J.-S. Oh, S.-H. Jang, J.-H. Cha, and J.-E. Kim, "Active and reactive power control of ess in distribution system for improvement of power smoothing control," *Journal of Electrical Engineering & Technology*, vol. 12, no. 3, pp. 1007–1015, 2017.

[51] J. Pereira, J. Alves, and M. Matos, "Optimization of electrical distribution network operation based on EPSO," in *2015 18th International Conference on Intelligent System Application to Power Systems (ISAP)*, Sep. 2015, pp. 1–6.

[52] S. Civanlar, J. J. Grainger, H. Yin, and S. S. H. Lee, "Distribution feeder reconfiguration for loss reduction," *IEEE Transactions on Power Delivery*, vol. 3, no. 3, pp. 1217–1223, Jul. 1988.

[53] Terna s.p.a., *Terna s.p.a. web site*, 2017. [Online]. Available: http://www.terna.it.

[54] Gurobi Optimization, *Gurobi milp solver*. [Online]. Available: http://www.gurobi.com/.

[55] Organisation for Economic Co-Operation and Development, *Energy Technology Perspectives 2017: Catalysing Energy Technology Transformations*. OECD, 2017.

[56] European Parliament, Council of the European Union, "Directive 2010/31/EU of the European Parliament and of the Council of 19 May 2010 on the energy performance of buildings," *Official Journal of the European Union*, vol. 153, pp. 13–35, 18.6.2010.

[57] ——, "Directive (EU) 2018/844 of the European Parliament and of the Council of 30 May 2018 amending Directive 2010/31/EU on the energy performance of buildings and Directive 2012/27/EU on energy efficiency (Text with EEA relevance)," *Official Journal of the European Union*, vol. L 156, pp. 75–91, 19.6.2018.

[58] B. Kouvaritakis and M. Cannon, "Model predictive control," *Switzerland: Springer International Publishing*, 2016.

[59] M. Beaudin and H. Zareipour, "Home energy management systems: A review of modelling and complexity," *Renewable and Sustainable Energy Reviews*, vol. 45, pp. 318–335, 2015.

[60] Z. Yang, M. Y. Chow, G. Hu, and Y. Zhang, "Guest editorial new trends of demand response in smart grids," *IEEE Transactions on Industrial Informatics*, vol. 11, no. 6, pp. 1505–1508, Dec. 2015.

[61] H. Shareef, M. S. Ahmed, A. Mohamed, and E. A. Hassan, "Review on home energy management system considering demand responses, smart technologies, and intelligent controllers," *IEEE Access*, vol. 6, pp. 24 498–24 509, 2018.

[62] G. R. Newsham, B. J. Birt, and I. H. Rowlands, "A comparison of four methods to evaluate the effect of a utility residential air-conditioner load control program on peak electricity use," *Energy Policy*, vol. 39, no. 10, pp. 6376–6389, 2011, Sustainability of biofuels.

[63] J. Widen, "Improved photovoltaic self-consumption with appliance scheduling in 200 single-family buildings," *Applied Energy*, vol. 126, no. Supplement C, pp. 199–212, 2014.

[64] G. R. Newsham and B. G. Bowker, "The effect of utility time-varying pricing and load control strategies on residential summer peak electricity use: A review," *Energy Policy*, vol. 38, no. 7, pp. 3289–3296, 2010, Large-scale wind power in electricity markets with Regular Papers.

[65] J. Torriti, "The significance of occupancy steadiness in residential consumer response to time-of-use pricing: Evidence from a stochastic adjustment model," *Utilities Policy*, vol. 27, no. Supplement C, pp. 49–56, 2013.

[66] C. Bartusch and K. Alvehag, "Further exploring the potential of residential demand response programs in electricity distribution," *Applied Energy*, vol. 125, no. Supplement C, pp. 39–59, 2014.

[67] A. Kiessling, "Modellstadt mannheim (moma) - abschlussbericht: Beiträge van moma zur transformation des energiesystems für nachhaltigkeit, beteiligung, regionalität und verbundheid," *Final Report*, 2013.

[68] R. D'hulst, W. Labeeuw, B. Beusen, S. Claessens, G. Deconinck, and K. Vanthournout, "Demand response flexibility and flexibility potential of residential smart appliances: Experiences from large pilot test in belgium," *Applied Energy*, vol. 155, no. Supplement C, pp. 79–90, 2015.

[69] E. Klaassen, C. Kobus, J. Frunt, and J. Slootweg, "Responsiveness of residential electricity demand to dynamic tariffs: Experiences from a large field test in the netherlands," *Applied Energy*, vol. 183, no. Supplement C, pp. 1065–1074, 2016.

[70] COMED, *The COMED residential real time pricing program*, [Online].Available: www.comed.com/Documents/. 2012.

[71] M. Muratori and G. Rizzoni, "Residential demand response: Dynamic energy management and time-varying electricity pricing," *IEEE Transactions on Power Systems*, vol. 31, no. 2, pp. 1108–1117, Mar. 2016.

[72] M. Shakeri, M. Shayestegan, H. Abunima, S. S. Reza, M. Akhtaruzzaman, A. Alamoud, K. Sopian, and N. Amin, "An intelligent system architecture in home energy management systems (hems) for efficient demand response in smart grid," *Energy and Buildings*, vol. 138, no. Supplement C, pp. 154–164, 2017.

[73] A. Hawkes and M. Leach, "Modelling high level system design and unit commitment for a microgrid," *Applied Energy*, vol. 86, no. 7, pp. 1253–1265, 2009.

[74] A. Di Giorgio and L. Pimpinella, "An event driven smart home controller enabling consumer economic saving and automated demand side management," *Applied Energy*, vol. 96, pp. 92–103, 2012.

[75] S. Y. Derakhshandeh, A. S. Masoum, S. Deilami, M. A. S. Masoum, and M. E. H. Golshan, "Coordination of generation scheduling with pevs charging

in industrial microgrids," *IEEE Transactions on Power Systems*, vol. 28, no. 3, pp. 3451–3461, Aug. 2013.

[76] A. D. Giorgio and F. Liberati, "Near real time load shifting control for residential electricity prosumers under designed and market indexed pricing models," *Applied Energy*, vol. 128, pp. 119–132, 2014.

[77] J. Silvente, G. M. Kopanos, E. N. Pistikopoulos, and A. EspuÃ±a, "A rolling horizon optimization framework for the simultaneous energy supply and demand planning in microgrids," *Applied Energy*, vol. 155, no. Supplement C, pp. 485–501, 2015.

[78] J. Silvente and L. G. Papageorgiou, "An MILP formulation for the optimal management of microgrids with task interruptions," *Applied Energy*, vol. 206, no. Supplement C, pp. 1131–1146, 2017.

[79] H. T. Roh and J. W. Lee, "Residential demand response scheduling with multiclass appliances in the smart grid," *IEEE Transactions on Smart Grid*, vol. 7, no. 1, pp. 94–104, Jan. 2016.

[80] G. M. Kopanos and E. N. Pistikopoulos, "Reactive scheduling by a multiparametric programming rolling horizon framework: A case of a network of combined heat and power units," *Industrial & Engineering Chemistry Research*, vol. 53, no. 11, pp. 4366–4386, 2014.

[81] F. Liberati and A. Di Giorgio, "Economic model predictive and feedback control of a smart grid prosumer node," *Energies*, vol. 11, no. 1, 2018.

[82] A. Parisio, E. Rikos, and L. Glielmo, "A model predictive control approach to microgrid operation optimization," *IEEE Transactions on Control Systems Technology*, vol. 22, no. 5, pp. 1813–1827, Sep. 2014.

[83] N. Jayasekara and P. Wolfs, "A hybrid approach based on GA and direct search for periodic optimization of finely distributed storage," in *Innovative Smart Grid Technologies Asia (ISGT)*, Nov. 2011, pp. 1–8.

[84] M. A. A. Pedrasa, T. D. Spooner, and I. F. MacGill, "Coordinated scheduling of residential distributed energy resources to optimize smart home energy services," *IEEE Transactions on Smart Grid*, vol. 1, no. 2, pp. 134–143, Sep. 2010.

[85] L. D. Ha, S. Ploix, E. Zamai, and M. Jacomino, "Tabu search for the optimization of household energy consumption," in *2006 IEEE International Conference on Information Reuse Integration*, Sep. 2006, pp. 86–92.

[86] Y. Han, P. Young, and D. Zimmerle, "Microgrid generation units optimum dispatch for fuel consumption minimization," *Journal of Ambient Intelligence and Humanized Computing*, vol. 4, no. 6, pp. 685–701, 2013.

[87] Z. Yang, R. Wu, J. Yang, K. Long, and P. You, "Economical operation of microgrid with various devices via distributed optimization," *IEEE Transactions on Smart Grid*, vol. 7, no. 2, pp. 857–867, Mar. 2016.

[88] C. Gamarra and J. M. Guerrero, "Computational optimization techniques applied to microgrids planning: A review," *Renewable and Sustainable Energy Reviews*, vol. 48, no. Supplement C, pp. 413–424, 2015.

[89] S. M. Nosratabadi, R.-A. Hooshmand, and E. Gholipour, "A comprehensive review on microgrid and virtual power plant concepts employed for distributed energy resources scheduling in power systems," *Renewable and Sustainable Energy Reviews*, vol. 67, no. Supplement C, pp. 341–363, 2017.

[90] E. Matallanas, M. Castillo-Cagigal, A. Gutierrez, F. Monasterio-Huelin, E. Caamano-Martin, D. Masa, and J. Jimenez-Leube, "Neural network controller for active demand-side management with pv energy in the residential sector," *Applied Energy*, vol. 91, no. 1, pp. 90–97, 2012.

[91] D. O'Neill, M. Levorato, A. Goldsmith, and U. Mitra, "Residential demand response using reinforcement learning," in *Smart Grid Communications (SmartGridComm), First IEEE International Conference on*, Oct. 2010, pp. 409–414.

[92] C. Yan, X. Xue, S. Wang, and B. Cui, "A novel air-conditioning system for proactive power demand response to smart grid," *Energy Conversion and Management*, vol. 102, pp. 239–246, 2015.

[93] G. M. Kopanos, M. C. Georgiadis, and E. N. Pistikopoulos, "Energy production planning of a network of micro combined heat and power generators," *Applied Energy*, vol. 102, no. Supplement C, pp. 1522–1534, 2013, Special Issue on Advances in sustainable biofuel production and use - XIX International Symposium on Alcohol Fuels - ISAF.

[94] P. Ivanova, A. Sauhats, and O. Linkevics, "District heating technologies: Is it chance for chp plants in variable and competitive operation conditions?" *IEEE Transactions on Industry Applications*, vol. 55, no. 1, pp. 35–42, Jan. 2019.

[95] A. Pellegrino, V. R. M. Lo Verso, L. Blaso, A. Acquaviva, E. Patti, and A. Osello, "Lighting control and monitoring for energy efficiency: A case study focused on the interoperability of building management systems," *IEEE Transactions on Industry Applications*, vol. 52, no. 3, pp. 2627–2637, May 2016.

[96] C. Shao, Y. Ding, J. Wang, and Y. Song, "Modeling and integration of flexible demand in heat and electricity integrated energy system," *IEEE Transactions on Sustainable Energy*, vol. 9, no. 1, pp. 361–370, Jan. 2018.

[97] S. H. Tindemans, V. Trovato, and G. Strbac, "Decentralized control of thermostatic loads for flexible demand response," *IEEE Transactions on Control Systems Technology*, vol. 23, no. 5, pp. 1685–1700, Sep. 2015.

[98] A. M. A. Ahmed, L. Mihet-Popa, C. Agert, Y. Zong, J. Bruna, and X. Xiao, "Potential energy flexibility for a hot-water based heating system in smart buildings via economic model predictive control," in *2017 International Symposium on Computer Science and Intelligent Controls (ISCSIC)*, Oct. 2017, pp. 1–5.

[99] O. Kilkki, A. Alahäivälä, and I. Seilonen, "Optimized control of price-based demand response with electric storage space heating," *IEEE Transactions on Industrial Informatics*, vol. 11, no. 1, pp. 281–288, Feb. 2015.

[100] S. Rastegarpour, M. Ghaemi, and L. Ferrarmi, "A predictive control strategy for energy management in buildings with radiant floors and thermal storage," in *2018 SICE International Symposium on Control Systems (SICE ISCS)*, Mar. 2018, pp. 67–73.

[101] L. Martirano, E. Habib, G. Parise, G. Greco, M. Manganelli, F. Massarella, and L. Parise, "Demand side management in microgrids for load control in nearly zero energy buildings," *IEEE Transactions on Industry Applications*, vol. 53, no. 3, pp. 1769–1779, May 2017.

[102] L. Martirano, G. Parise, G. Greco, M. Manganelli, F. Massarella, M. Cianfrini, L. Parise, P. di Laura Frattura, and E. Habib, "Aggregation of users in a residential/commercial building managed by a building energy management system (bems)," *IEEE Transactions on Industry Applications*, vol. 55, no. 1, pp. 26–34, Jan. 2019.

[103] V.-H. Bui, A. Hussain, H.-M. Kim, and Y.-H. Im, "Optimal energy management of building microgrid networks in islanded mode considering adjustable power and component outages," *Energies*, vol. 11, no. 9, p. 2351, 2018.
[104] J. B. Rawlings, D. Q. Mayne, and M. Diehl, *Model Predictive Control: Theory, Computation, and Design*. Nob Hill Publishing, 2017.
[105] J. Köhler, M. A. Müller, and F. Allgöwer, "On periodic dissipativity notions in economic model predictive control," *IEEE Control Systems Letters*, vol. 2, no. 3, pp. 501–506, Jul. 2018.
[106] M. Diehl, R. Amrit, and J. B. Rawlings, "A lyapunov function for economic optimizing model predictive control," *IEEE Transactions on Automatic Control*, vol. 56, no. 3, pp. 703–707, Mar. 2011.
[107] T. Faulwasser, L. Grüne, M. A. Müller, *et al.*, "Economic nonlinear model predictive control," *Foundations and Trends in Systems and Control*, vol. 5, no. 1, pp. 1–98, 2018.
[108] T. Damm, L. Grüne, M. Stieler, and K. Worthmann, "An exponential turnpike theorem for dissipative discrete time optimal control problems," *SIAM Journal on Control and Optimization*, vol. 52, no. 3, pp. 1935–1957, 2014.
[109] J. Bezanson, A. Edelman, S. Karpinski, and V. Shah, "Julia: A fresh approach to numerical computing," *SIAM Review*, vol. 59, no. 1, pp. 65–98, 2017.
[110] I. Dunning, J. Huchette, and M. Lubin, "Jump: A modeling language for mathematical optimization," *SIAM Review*, vol. 59, no. 2, pp. 295–320, 2017.
[111] J.-C. Liou, "Planetary science: Risks in space from orbiting debris," *Science*, vol. 311, no. 5759, pp. 340–341, Jan. 20, 2006.
[112] Z. Ismail and R. Varatharajoo, "A study of reaction wheel configurations for a 3-axis satellite attitude control," *Advances in Space Research*, vol. 45, no. 6, pp. 750–759, 2010.
[113] M. H. Kaplan, *Modern spacecraft dynamics and control*. Wiley, 1976.
[114] S.-C. Lo and Y.-P. Chen, "Smooth sliding-mode control for spacecraft attitude tracking maneuvers," *Journal of Guidance, Control, and Dynamics*, vol. 18, no. 6, pp. 1345–1349, Nov. 23, 1995.
[115] L.-L. Show, J.-C. Juang, C.-T. Lin, and Y.-W. Jan, "Spacecraft robust attitude tracking design: Pid control approach," IEEE, 2002, 1360–1365 vol.2.
[116] F. Lizarralde and J. Wen, "Attitude control without angular velocity measurement: A passivity approach," *IEEE Transactions on Automatic Control*, vol. 41, no. 3, pp. 468–472, Mar. 1996.
[117] H. Bang, J.-S. Lee, and Y.-J. Eun, "Nonlinear attitude control for a rigid spacecraft by feedback linearization," *KSME International Journal*, vol. 18, no. 2, pp. 203–210, Feb. 2004.
[118] M. Navabi and M. R. Hosseini, "Spacecraft quaternion based attitude input-output feedback linearization control using reaction wheels," IEEE, Jun. 2017, pp. 97–103.
[119] A. Isidori, *Nonlinear Control Systems*, ser. Communications and Control Engineering. London: Springer London, 1995.
[120] B. Wie and P. M. Barba, "Quaternion feedback for spacecraft large angle maneuvers," *Journal of Guidance, Control, and Dynamics*, vol. 8, no. 3, pp. 360–365, May 1985.

[121] P. Ghiglino, J. L. Forshaw, and V. J. Lappas, "Oqtal: Optimal quaternion tracking using attitude error linearization," *IEEE Transactions on Aerospace and Electronic Systems*, vol. 51, no. 4, pp. 2715–2731, Oct. 2015.

[122] J.-Y. Wen and K. Kreutz-Delgado, "The attitude control problem," *IEEE Transactions on Automatic Control*, vol. 36, no. 10, pp. 1148–1162, 1991.

[123] F. L. Markley and J. L. Crassidis, *Fundamentals of Spacecraft Attitude Determination and Control*. Springer, New York, NY, 2014.

[124] P. H. Zipfel, *Modeling and Simulation of Aerospace Vehicle Dynamics, Second Edition*. Reston ,VA: American Institute of Aeronautics and Astronautics, Jan. 2007.

[125] E. Fresk and G. Nikolakopoulos, "Full quaternion based attitude control for a quadrotor," Tech. Rep., 2013.

[126] E. Reyes-Valeria, R. Enriquez-Caldera, S. Camacho-Lara, and J. Guichard, "Lqr control for a quadrotor using unit quaternions: Modeling and simulation," IEEE, Mar. 2013, pp. 172–178.

[127] Q. Wang, J. Yuan, and Z. Zhu, "The application of error quaternion and pid control method in earth observation satellite's attitude control system," IEEE, 2005, pp. 128–131.

[128] C. I. Byrnes and A. Isidori, "On the attitude stabilization of rigid spacecraft," *Automatica*, vol. 27, no. 1, pp. 87–95, Jan. 1, 1991.

[129] B. Xiao, Q. Hu, and Y. Zhang, "Adaptive sliding mode fault tolerant attitude tracking control for flexible spacecraft under actuator saturation," *IEEE Transactions on Control Systems Technology*, vol. 20, no. 6, pp. 1605–1612, 2012.

[130] A.-M. Zou and K. D. Kumar, "Adaptive fuzzy fault-tolerant attitude control of spacecraft," *Control Engineering Practice*, vol. 19, no. 1, pp. 10–21, Jan. 1, 2011.

[131] J.-F. Tregouet, D. Arzelier, D. Peaucelle, C. Pittet, and L. Zaccarian, "Reaction wheels desaturation using magnetorquers and static input allocation," *IEEE Transactions on Control Systems Technology*, vol. 23, no. 2, pp. 525–539, Mar. 2015.

[132] Y. Yang, "Spacecraft attitude and reaction wheel desaturation combined control method," *IEEE Transactions on Aerospace and Electronic Systems*, vol. 53, no. 1, pp. 286–295, Feb. 2017.

[133] H. Goldstein, C. Poole, J. Safko, and S. Addison, "Classical mechanics," *American Journal of Physics*, vol. 70, p. 782, 2002.

[134] K. Zhou, J. C. Doyle, and K. Glover, *Robust and optimal control*. Prentice Hall, 1996.

[135] R. Mehra, S. Seereeram, D. Bayard, and F. Hadaegh, "Adaptive kalman filtering, failure detection and identification for spacecraft attitude estimation," IEEE, 2002, pp. 176–181.

[136] J. Jin, S. Ko, and C.-K. Ryoo, "Fault tolerant control for satellites with four reaction wheels," *Control Engineering Practice*, vol. 16, no. 10, pp. 1250–1258, Oct. 1, 2008.

[137] Y. Zhu, L. Guo, J. Qiao, and W. Li, "An enhanced anti-disturbance attitude control law for flexible spacecrafts subject to multiple disturbances," *Control Engineering Practice*, vol. 84, pp. 274–283, Mar. 2019.

[138] H. Kameda, J. Li, C. Kim, and Y. Zhang, *Optimal Load Balancing in Distributed Computer Systems*, ser. Telecommunication Networks and Computer Systems. London: Springer London, 1997.

[139] J. R. Correa, A. S. Schulz, and N. E. Stier-Moses, "Selfish routing in capacitated networks," *Mathematics of Operations Research*, vol. 29, no. 4, pp. 961–976, Nov. 1, 2004.

[140] M. El Helou, M. Ibrahim, S. Lahoud, K. Khawam, D. Mezher, and B. Cousin, "A network-assisted approach for rat selection in heterogeneous cellular networks," *IEEE Journal on Selected Areas in Communications*, vol. 33, no. 6, pp. 1055–1067, Jun. 2015.

[141] I. Da Silva, G. Mildh, J. Rune, P. Wallentin, J. Vikberg, P. Schliwa-Bertling, and R. Fan, "Tight integration of new 5g air interface and lte to fulfill 5g requirements," IEEE, May 2015, pp. 1–5.

[142] A. Morgado, K. M. S. Huq, S. Mumtaz, and J. Rodriguez, "A survey of 5g technologies: Regulatory, standardization and industrial perspectives," *Digital Communications and Networks*, vol. 4, no. 2, pp. 87–97, Apr. 2018.

[143] J.-O. Kim, "Feedback-based traffic splitting for wireless terminals with multi-radio devices," *IEEE Transactions on Consumer Electronics*, vol. 56, no. 2, pp. 476–482, May 2010.

[144] A. A. Sabbagh, R. Braun, and M. Abolhasan, "A comprehensive survey on rat selection algorithms for heterogeneous networks," *World Academy of Science, Engineering and Technology*, 2011.

[145] L. Wang and G.-S. G. Kuo, "Mathematical modeling for network selection in heterogeneous wireless networks — a tutorial," *IEEE Communications Surveys & Tutorials*, vol. 15, no. 1, pp. 271–292, 2013.

[146] M. Dryjanski and M. Szydelko, "A unified traffic steering framework for lte radio access network coordination," *IEEE Communications Magazine*, vol. 54, no. 7, pp. 84–92, Jul. 2016.

[147] D. Zhang, S. Li, M. Sun, and Z. O'Neill, "An optimal and learning-based demand response and home energy management system," *IEEE Transactions on Smart Grid*, vol. 7, no. 4, pp. 1790–1801, Jul. 2016.

[148] H. Chan, P. Fan, and Z. Cao, "A utility-based network selection scheme for multiple services in heterogeneous networks," vol. 2, IEEE, 0, pp. 1175–1180.

[149] J. Antoniou and A. Pitsillides, "4g converged environment: Modeling network selection as a game," IEEE, Jul. 2007, pp. 1–5.

[150] M. Cesana, N. Gatti, and I. Malanchini, "Game theoretic analysis of wireless access network selection: Models, inefficiency bounds, and algorithms," ICST, 2008, p. 6.

[151] D. Niyato and E. Hossain, "Dynamics of network selection in heterogeneous wireless networks: An evolutionary game approach," *IEEE Transactions on Vehicular Technology*, vol. 58, no. 4, pp. 2008–2017, May 2009.

[152] T. Roughgarden and É. Tardos, "How bad is selfish routing?" *Journal of the ACM*, vol. 49, no. 2, pp. 236–259, Mar. 2002.

[153] J. G. Wardrop, "Some theoretical aspects of road traffic research," *Proceedings of the Institution of Civil Engineers*, vol. 1, no. 3, pp. 325–362, May 1952.

[154] H. Z. Aashtiani, H. Poorzahedy, and M. Nourinejad, "Extending wardrop's first principle for capacitated networks," *Transportmetrica A: Transport Science*, pp. 1–30, 2018.

[155] P. Marcotte, S. Nguyen, and A. Schoeb, "A strategic flow model of traffic assignment in static capacitated networks," *Operations Research*, vol. 52, no. 2, pp. 191–212, Apr. 2004.
[156] A. S. Schulz and N. S. Moses, "On the performance of user equilibria in traffic networks," ser. SODA '03, Philadelphia, PA, USA: Society for Industrial and Applied Mathematics, 2003, pp. 86–87.
[157] E. Altman, H. Kameda, and Y. Hosokawa, "Nash equilibria in load balancing in distributed computer systems," *International Game Theory Review*, vol. 04, no. 02, pp. 91–100, Jun. 2002.
[158] D. Grosu and A. T. Chronopoulos, "Noncooperative load balancing in distributed systems," *Journal of Parallel and Distributed Computing*, vol. 65, no. 9, pp. 1022–1034, Sep. 2005.
[159] H. Kameda, J. Li, C. Kim, and Y. Zhang, "Optimal load balancing in distributed computer systems," 2012.
[160] M. Beckmann, C. B. McGuire, and C. B. Winsten, "Studies in the economics of transportation," 1956.
[161] G. Como, K. Savla, D. Acemoglu, M. A. Dahleh, and E. Frazzoli, "Robust distributed routing in dynamical networks–part ii: Strong resilience, equilibrium selection and cascaded failures," *IEEE Transactions on Automatic Control*, vol. 58, no. 2, pp. 333–348, Feb. 2013.
[162] ——, "Robust distributed routing in dynamical networks—part i: Locally responsive policies and weak resilience," *IEEE Transactions on Automatic Control*, vol. 58, no. 2, pp. 317–332, Feb. 2013.
[163] V. Borkar and P. Kumar, "Dynamic cesaro-wardrop equilibration in networks," *IEEE Transactions on Automatic Control*, vol. 48, no. 3, pp. 382–396, Mar. 2003.
[164] D. Barth, O. Bournez, O. Boussaton, and J. Cohen, "Distributed learning of wardrop equilibria," in *Unconventional Computing*, Berlin, Heidelberg: Springer Berlin Heidelberg, 2008, pp. 19–32.
[165] S. Fischer, L. Olbrich, and B. Vöcking, "Approximating wardrop equilibria with finitely many agents," *Distributed Computing*, vol. 21, no. 2, pp. 129–139, Jul. 13, 2008.
[166] S. Fischer, H. Räcke, and B. Vöcking, "Fast convergence to wardrop equilibria by adaptive sampling methods," *SIAM Journal on Computing*, vol. 39, no. 8, pp. 3700–3735, 2010.
[167] S. Fischer and B. Vöcking, "Adaptive routing with stale information," *Theoretical Computer Science*, vol. 410, no. 36, pp. 3357–3371, Aug. 31, 2009.
[168] W. Mei and F. Bullo, "Lasalle invariance principle for discrete-time dynamical systems: A concise and self-contained tutorial," *arXiv preprint, arXiv:1710.03710*, Oct. 10, 2017.
[169] V. Sundarapandian, "An invariance principle for discrete-time nonlinear systems," *Applied Mathematics Letters*, vol. 16, no. 1, pp. 85–91, 2003.